Testing of CRP Supports for the Deep Underground Neutrino Experiment

By

Joshua A. Truchon

A dissertation submitted in partial fulfillment of

the requirements for the degree of

Master of Science

Mechanical Engineering

at the

UNIVERSITY OF WISCONSIN-MADISON

2023

Date of final oral examination: 11/03/2023

The dissertation is approved by the following members of the Preliminary Oral Committee:

Franklin K. Miller, Professor, Mechanical Engineering

Gregory F. Nellis, Professor, Mechanical Engineering

Dakotah Thompson, Assistant Professor, Mechanical Engineering

ABSTRACT

The Deep Underground Neutrino Experiment (DUNE) utilizes neutrino sensors that are submerged within liquid argon to measure the particle trails left by neutrinos. The sensors require specially designed supports to ensure they remain precisely positioned even after the thermal contraction of the sensors and the cryostat that occurs during cooldown. These supports must ensure that the fragile cryostat floor is protected, yet also allow the sensors themselves to slip in order to avoid any damage associated with stresses induced by thermal contraction. Further, the supports must ensure that the sensor position at the end of cooldown is at a predetermined location. These objectives are satisfied by utilizing an intermediate slip plane within the support itself that provides a lower coefficient of friction compared to the interface between the sensor support and the cryostat floor.

The design of these supports therefore requires knowledge of the static coefficient of friction for a variety of materials at cryogenic temperatures. It was found that the coefficient of friction associated with materials such as metals, ceramics, and polymers have all been studied very little at cryogenic temperatures. There is specifically not much data available relative to the static coefficient of friction associated with polymers at low temperature. Therefore, a test apparatus was developed that allowed the measurement of the cryogenic static coefficient of friction of various materials. The apparatus uses a linear screw to apply a measured force to a test sled contained in a low temperature, moisture-controlled environment. By measuring the maximum force which occurs just prior to motion, it is possible to infer the static coefficient of friction. The test sled contains three supports that have geometries consistent with the DUNE sensor supports but with interchangeable slip plane plates.

Using this test apparatus, a number of tests with different materials were carried out in order to identify a pair of material combinations with very different static coefficients of

friction that can be used for the membrane/support and slip plane interfaces. During these tests, it was observed that moisture significantly affects the coefficient of friction. Even when using an enclosure to minimize moisture from the atmosphere, inconsistent results were sometimes recorded for polymers; these were assumed to be due to moisture on the slip plates.

In conjunction with support design and testing, a device was built for placing the CRPs within the cryostat. This device required a special design to meet the requirements imposed by the DUNE project. The lifting device used tines to lift them to ensure that no damage was done to the edge and sides. The lifting device needed to have adjustable tines to account for different placement of supports and the significant amount of bending to the tines. This device successfully placed CRPs at DUNE's module zero test at CERN.

ACKNOWLEDGMENTS

Table of Contents

LIST OF TABLES

LIST OF FIGURES

LIST OF ABBREVIATIONS

CRP	Charged Readout Plane
DUNE	Deep Underground Neutrino Experiment
COF	Coefficient of Friction
CTE	Coefficient of Thermal Contraction
SD	Standard Deviation
APDL	Ansys Parametric Design Language

Chapter 1. DUNE Background

1.1. Understanding Matter Asymmetry

It is commonly accepted in the physics community that the Big Bang created an equal amount of matter and anti-matter. However, this may not be intuitive since the universe is dominated by matter. Scientists at Fermi National Accelerator Laboratory (Fermilab) believe that understanding the nature of neutrinos could potentially answer how matter asymmetry happens.

There are different types of neutrinos, and these types are referred to as flavors. These flavors are electron, muon, and tau. When a neutrino interacts with other particles, the reaction depends on the neutrino's flavor at the time of interaction. When an electron neutrino interacts with a particle, then an electron is produced from the interaction. The same applies to the other flavors and their namesake particle[1].

Even though there have been theories of the nature of neutrino oscillations only relatively recently has there been experimental data which have verified these theories. In 1957 Bruno Pontecorvo presented the theory that neutrinos have been predicted to oscillate between flavor states [2]. In 2015, the Nobel Prize in Physics was awarded to Takaaki Kajita and Arthur B. McDonald for experimentally discovering neutrino oscillations, proving neutrinos have mass[3]. Understanding the oscillation patterns of neutrinos could be significant to answering the matter asymmetry problem. If the oscillation ensemble of neutrinos and anti-neutrinos are not symmetric, this would prove CP-violation and provide a potential answer to matter asymmetry in the universe.

The Deep Underground Neutrino Experiment (DUNE) is an experiment that will help scientists better fundamentally understand the nature of neutrinos. DUNE is the first generation of experiments to attempt a precision measurement of the CP violation phase and neutrino mass

state. Using the data collected from this experiment the neutrino oscillation ensemble, as well as other important parameters will be discovered.

1.2. DUNE

DUNE will use a particle accelerator at Fermilab to create a beam of neutrinos and direct it toward detectors at the Sanford Underground Research Facility in Lead, South Dakota. Before traveling through 1300 km of earth, a detector close to the neutrino generator will provide a baseline data ensemble to compare to the far detector data. At the Sanford Underground Research Facility, multiple massive detectors will record the particle trails left by the neutrinos as they pass through the detector's liquid argon. A chain reaction propagating through the argon will be amplified with a charge field, ensuring the sensors can detect particle trails left by the passing neutrino. The particles, muon, and electrons, propagate differently, thus leaving differently shaped trails, which will be used to determine the neutrino's flavor at the intersection point. This data will allow scientists to create a statistical ensemble for the neutrino's flavors, allowing for a better understanding of the oscillation rate and other important parameters.

This cutting-edge detection method was tested and verified to work during Proto-DUNE at CERN. The drift detector, an iteration of the same technology, utilizes two horizontal sensor planes at the top and bottom of the massive cryostat. Each plane utilizes 80 Charge Readout Planes (CRP), which detect the electron trails after drifting through the liquid argon to the detector planes. Our research group has been tasked with designing supports for these highly fragile and critical components.

Chapter 2. Friction Testing

2.1. Friction Testing Relevance

While filling the cryostat with liquid argon, the cryostat membrane and the CRPs will have a significant thermal contraction. Corrugations in the cryostat membrane ensure that the membrane has sufficient flexibility to prevent strain from building during this cooldown. However, the CRPs will contract significantly. To ensure that this thermal contraction does not damage the cryostat membrane, the CRPs cannot slide on the membrane floor during this process; however, it is also critical that the CRPs remain in a known position after thermally equilibrating with the liquid argon.

The CRP support design allows for a controlled and predictable final position of the CRP, which is important to minimize the data processing required during neutrino detection. Three of the four CRP supports have an intermediate slip plane that utilizes a material combination with significantly lower frictional resistance (coefficient of friction) than the materials associated with the support to membrane interface, as shown in Figure 1.

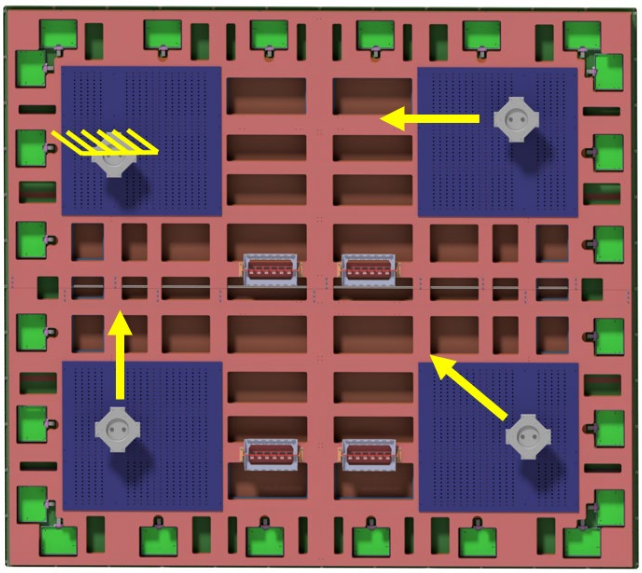

Figure 1: Underside of the CRP model with indicators to show the direction of thermal contraction and the fixed foot location.

The fourth CRP support does not include the slip plane; therefore, this support will remain fixed to the membrane, and the other three will move during the cooldown process. The selection of materials used at the slip plane and the support to membrane interface is important and not obvious. The tribology depends on several factors, and the coefficient of friction (COF) at low temperatures is not well-studied.

2.2. Support Design

Three important requirements constrain the design of the supports for the CRP. First, the support cannot damage the membrane floor during installation or while the CRP is thermally contracting. Second, the CRP must contract in a controlled, predictable manner. Third, the thermal contraction must not cause excessive forces that will damage the CRP. The support design developed to meet all these criteria supports the membrane interface and an intermediate slip plane, as shown in Figure 2. The support includes a mechanism for centering the support while positioning the CRP during installation. This centering mechanism guarantees the support of enough clearance for all thermal contractions.

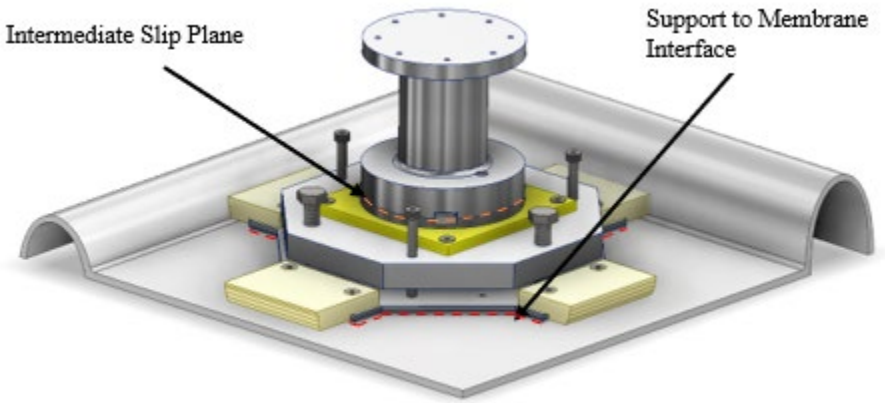

Figure 2:Special CRP support to ensure controlled positioning and controlled sliding during thermal expansion. The orange highlights the intermediate slip plane dashed line, and the support to membrane interface is highlighted with the red line.

The original design for the CRP supports utilized the support to membrane interface frictional resistance to fix the support. Materials would need to be tested to find the optimal difference in COF between the slip plane and support to membrane interface.

The goal of the intermediate slip plane is to ensure that sliding motion does not occur on the membrane floor to prevent any damage to the membrane floor due to thermal contraction. Materials with a lower COF are used for the intermediate slip plane compared to those used in the support to membrane interface to achieve the desired slip condition. The difference in COF between planes ensures that the friction forces on the membrane floor will be high enough that the metal footing will remain stationary (relative to the membrane) during the entire thermal contraction period. The membrane floor is made of stainless steel 316; therefore, all tests pertaining to the support to membrane interface were conducted with 16-gauge stainless steel 316 sheet metal.

A mechanism was designed to center the footpad to the slip plane, illustrated in Figure 4, ensuring that it is centered when lowered but has enough travel during contraction to prevent binding. This design uses four springs and conical positioning posts to center the footpad when no load is applied to the support (i.e., during lowering of the CRP into position). Once a load, which depends on the stiffness of the springs installed, is applied to the foot, the spring will expand, allowing for free movement of the slip planes. As the CRP structure thermally contracts, and the support slip plane moves the centering mechanism bolt will approach the edge of the clearance hole as seen in Figure 3. The clearance associated with the design is currently 10 mm in any direction, allowing for adequate travel from thermal contraction. The maximum estimation for thermal contraction expected is 6.2 mm.

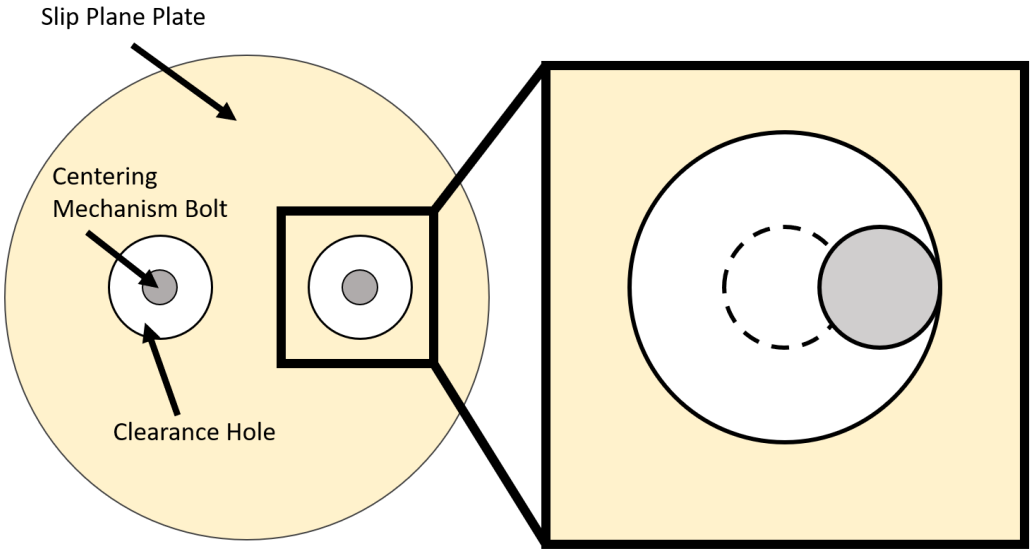

Figure 3: A diagram of the intermediate slip plane plate. On the right is an illustration of the center mechanism bolt at the extreme of the clearance hole.

The footpad design allows for the support clearance to be easily modified; this may be increased in future iterations to account for uncertainty in the placement of the CRP. This value was calculated using the farthest possible position for the supports that can be mounted to the CRP, 3.626 m, and the coefficient of thermal expansion from the National Institute of Standards and Technology[4]. It was assumed that due to the design of the CRP structure, which uses plates and c-channels, the warp direction would be a good model for the nature of the CRP contraction.

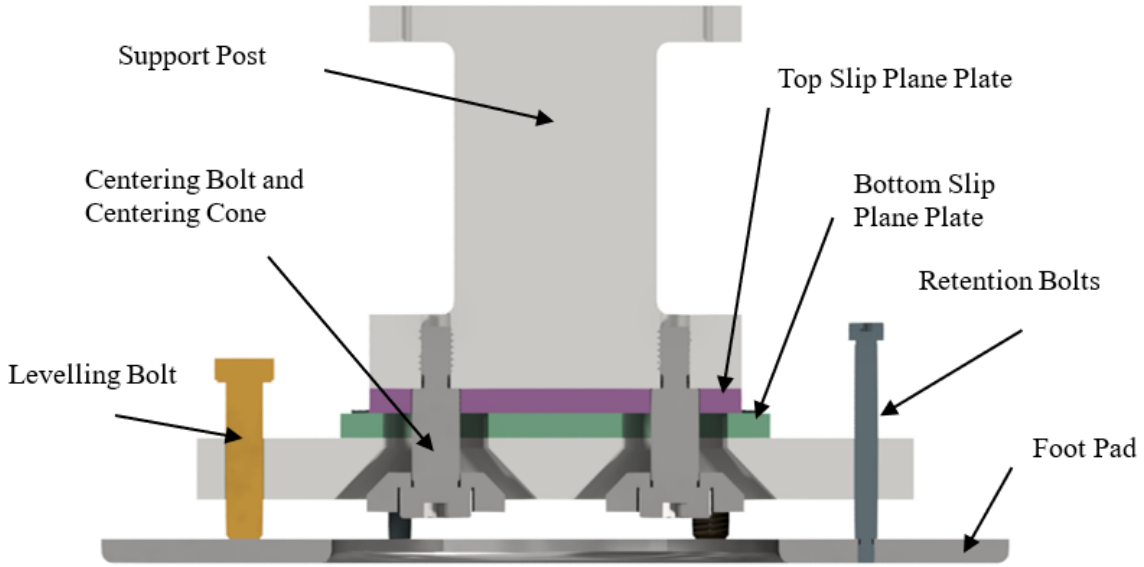

Figure 4:Cross section of support centering mechanism. The springs that open the intermediate slip plane when support is unloaded are not illustrated.

The footpad in contact with the membrane floor can be leveled without disassembly. Leveling is achieved using three jacking bolts, while springs are used to maintain proper assembly when unloaded. The ability for leveling and height adjustment is important to account for inconsistencies in the membrane floor.

2.3. Support Material Selection

Careful consideration of the materials used in the slip planes is needed to ensure that the CRP support functions appropriately. The coefficient of friction, strength, machinability, and coefficient of thermal contraction were all important while considering material selection.

Once the CRP is installed, the support design keeps the intermediate slip plane under a constant compressive load. Therefore, the selected materials must not creep at room temperature and change geometry significantly before cooldown. To satisfy this requirement, only ones with a glass transition temperature above room temperature were considered for further testing when choosing polymers.

Reduced temperature in polymers leads to changes in hardness, stiffness, and elastic modulus, affecting the cryogenic coefficient of friction[5]. Friction data collected at room

temperature may not reflect the behaviour at 77 K[6]. Also, tests carried out using dry surfaces may not reflect the coefficient of friction when submerged in liquid cryogen due to the presence of liquid cryogen[7]. In the DUNE project, the supports will be submerged in argon when most thermal contraction occurs. PEEK and nylon are used elsewhere on the CRPs and, therefore, have been approved for this application. It is important to ensure that the materials used do not negatively interfere with the overall scope of DUNE. Both polymers also fulfill the requirements mentioned above as well. Therefore, they were considered as a potential material for the intermediate slip plane.

As the literature suggests, the friction coefficient of metals is generally temperature-independent[8]. Using friction data at room temperature, different metals with a range of COF were selected, and then easy to machine and relatively affordable materials were prioritized. Of the materials, aluminum 6061 and stainless steel 316 were chosen for testing.

2.4. Test Equipment

The test equipment used to measure the friction coefficient is illustrated in Figure 5; it is comprised of a tub cryostat, linear motion device, test sled, load cell, and an enclosure.

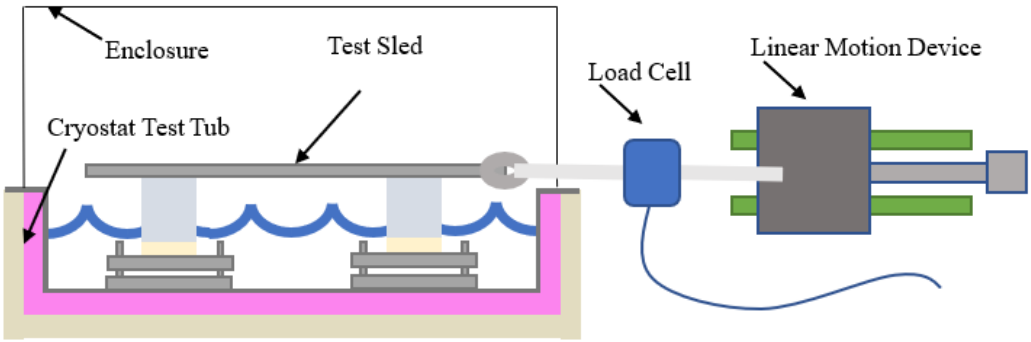

Figure 5: Schematic of test equipment used for friction testing.

The test enclosure is a tub cryostat, shown in Figure 6, made of 16-gauge 316 stainless steel insulated with polyethylene foam supported by a wooden structure. All seams are welded to make the tub liquid tight. The tub is designed to simulate DUNE's cryostat floor.

The test sled is a solid plate to which the supports described in the previous section can be attached and upon which reference weights can be stacked, see Figure 7. The sled has mounting locations on the front and back, allowing ropes to be attached for loading, and resetting the slip plane once the plate has reached the extremes of the slip plane clearance. The rope used for applying the load is made from nylon; nylon has sufficient elasticity to allow for a gradual increase in the force between the load cell and test sled during the displacement of the linear motion device, alleviating the need for any additional compliance.

Figure 6: 316 stainless steel sheet metal Cryostat tub.

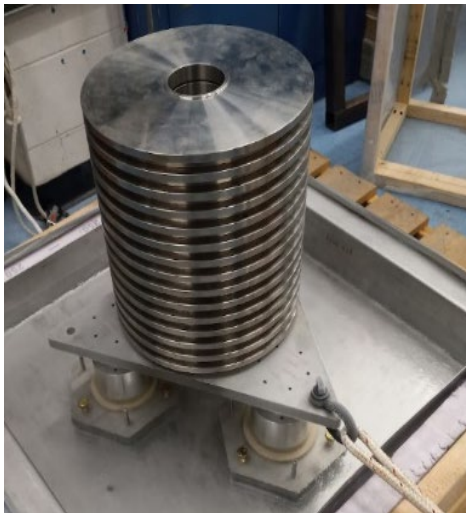

Figure 7: Test sled with reference weights before a test.

Test plates were made to assess different combinations of materials together. These plates are fixed to a foot plate that can be fixed in place using stopper blocks. This design allows the frictional force required to cause slip to be recorded without requiring the fabrication of different posts and feet.

A linear motion stage was used to apply a uniform and constant force. A ball screw moves a carriage linearly away from the test sled. The hand wheel turns the screw slowly to ensure a load reading can be identified and recorded during the slip. This device can be seen on the right side of Figure 8.

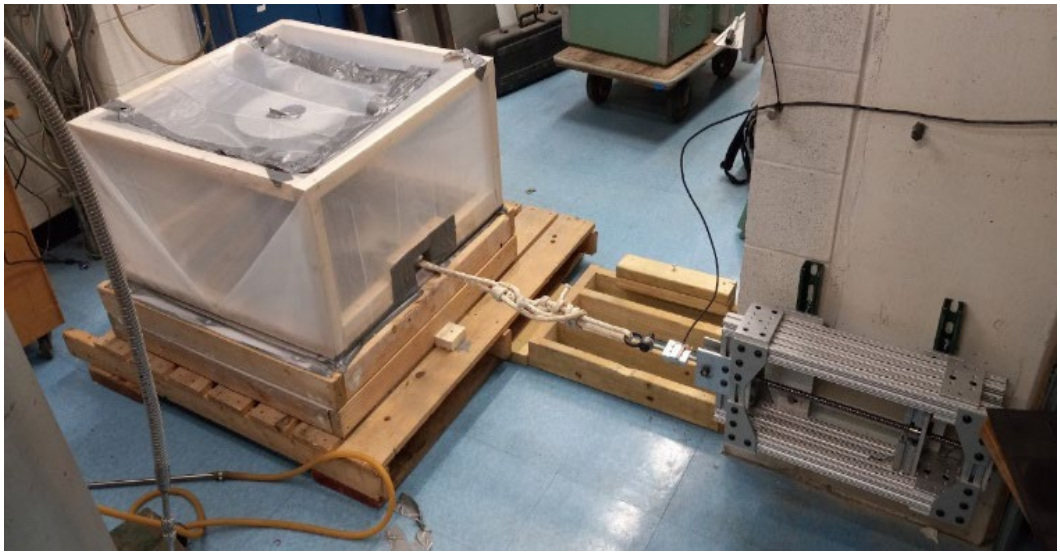

Figure 8: Entire test apparatus, including the enclosure.

To record the reactionary force from the friction, a load cell, Rice Lake weighing systems RL20000st 500lb, is installed between the linear motion device and the test sled. The nylon rope was used to connect the linear motion device and the test sled to ensure that gradual force was applied to the test sled. To record data, a National Instruments NI 9237 was used to measure the load cell analog output signal and digitize it for processing in the LabVIEW program.

During initial tests, moisture from the air condensed and led to solid impurities in the liquid nitrogen (LN2) that affected the friction results. In the DUNE environment, air will have been purged from the cryostat prior to the cooldown. Therefore, an enclosure was built to prevent this ice formation, and tests were conducted to determine the importance of these impurities. A nitrogen blanket prevented atmospheric moisture from affecting the friction tests. The nitrogen blanket uses a wooden structure covered in plastic sheets. The enclosure is purged of air before filling with LN2 to ensure that no moisture is frozen anywhere, which would affect the coefficient of friction. The bottom seams are sealed with weather stripping and duct tape.

2.5. Test Process

Several tests were performed to ensure all material combinations would function properly during the cooldown. Two tests were designed to isolate the intermediate slip plane from the support to membrane interface. The first test uses stopper blocks between the tub and footpad, which isolated the intermediate slip plane by ensuring the footpad was fixed in the slip direction. The intermediate slip plane was locked to test the support to membrane interface, isolating the slip to the support to membrane interface. All tests were performed in a climate-controlled building at temperatures of approximately 295 K.

A calibration test was performed to ensure that the test equipment was functioning properly. The calibration was done by hanging a known weight from the load cell to verify the force recorded by the data acquisition system. Loads from approximately 150 N to 2200 N were used, and a deviation of approximately 1 N was measured through the entire range of loads.

Preparation steps were performed before cooldown to ensure the tests were repeatable. The supports were leveled with the jacking bolt to provide consistent face pressure on the support to membrane interface. All mating surfaces that would be tested, membrane floor, support footing, and intermediate slip plane, were wiped with a clean, dry paper towel to clean and remove unwanted debris. Then, all of these surfaces were cleaned with acetone to remove any oils or contaminants.

The standard operating procedure used to ensure continuity between testers as well as from test to test is presented in Appendix 1.

2.6. Friction Test Results

It should be noted that these tests were meant to create a functional product for DUNE. This process resulted in a test matrix that was not complete. Testing for an individual material was concluded once a material was found to satisfy the requirements. Initial tests were repeated

several times to ensure that the testing process was consistent. It is important to note that the geometry of the support significantly affects the value of COF[9].

When calculating the COF for the intermediate slip plane, the weight of the support above the intermediate slip plane was used for the normal force calculation. It was initially thought that the dry room temperature tests would result in higher COF for PEEK compared to tests submerged in LN2. However, our tests showed this not to be the case. These nonintuitive results resulted in many additional tests to verify that the results were not due to the test process.

After receiving the nylon material for the slip plane plates, it was found that it had grooves on the surface related to the machining process. Surface imaging was performed to evaluate the magnitude of these machining grooves, as seen in Figure 9. Two test cases were performed with the nylon plates depending on the direction of motion and the groove direction. One case was performed with the grooves parallel to the motion, while the other was perpendicular.

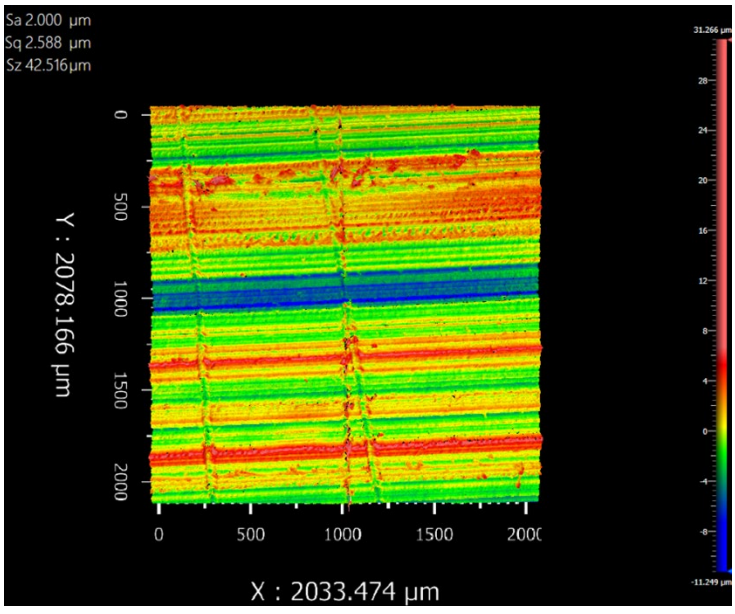

Figure 9: Surface roughness images of the machining grooves from a Zygo Newview 9000 3D optical surface profiler. Roughness values were as follows Sa 2.000 µm, Sq 2.588 µm, and Sz 42.516 µm.

The data from these tests were recorded in Table 1, and it should be noted that there is no significant difference in the mean COF observed between PEEK on PEEK and nylon on nylon 66. This realization resulted in eliminating nylon from consideration due to manufacturing imperfections. The standard deviation was calculated by taking the square root of the sum of squared differences between each data point and the sample mean, dividing by the sample size minus one.

Table 1: Test data from the isolation of the intermediate slip plane submerged in LN2 while enclosed. The = symbol represents the parallel test while the ⊥ represents perpendicular tests..

Material	Tests	Samples	Mean Static COF	Standard Deviation
PEEK on PEEK	3	83	0.27	0.017
Nylon 66 on nylon 66 =	2	21	0.26	0.054
Nylon 66 on Nylon 66 ⊥	2	21	0.35	0.182

When calculating the COF for the support to membrane interface, the weight of the entire support was used to calculate the normal force. All combinations of polymers tested resulted in a negligible difference in frictional resistance compared to the stainless steel on stainless steel result. The small difference in COF resulted in an effort to identify materials that provide a substantially larger frictional force for the support to membrane interface. Tests were conducted with aluminum foot pads on the stainless steel membrane that resulted in significantly higher frictional forces than those found for the intermediate slip plane. Data from the support to membrane interface tests can be seen in Table 2.

Table 2: Test data from the isolation of the support to membrane interface while submerged in LN2.

Material	Tests	Samples	Mean Static COF	Standard Deviation
Aluminum on Stainless Steel	7	97	0.34	0.017
Stainless Steel on Stainless Steel	3	97	0.20	0.006

During the initial testing, it was observed that there was a significant amount of moisture, which condensed and froze onto the test sled surface, which is illustrated in Figure 10. Due to concerns about additional friction forces that this moisture might cause, an enclosure

was designed and built to remove moisture from the LN2 testing environment, see Figure 8. Dry gaseous nitrogen is blown into the enclosure for at least 15 minutes to provide a nitrogen blanket to the system. Some tests were performed with a nitrogen purge of 24 hours. DUNE will utilize a purge cycle before filling the cryostat, so this process seems like the best method to replicate the final experiment conditions while minimizing moisture build up. Once the cryostat tub was filled with LN2, the boiling provided a positive pressure in the enclosure to prevent atmospheric air from entering the system.

Figure 10: Test without enclosure, resulting in ice buildup.

A grinding crunching sound was noticed during tests that had clear signs of moisture buildup in the LN2. These tests also resulted in significantly higher friction forces, as seen in Table 3. The presence of impurities in the cryogen significantly affects the friction forces. Due to the unpredictable and uncontrollable nature of these impurities, it is advised that little to no moisture is present in the cryostat while cooldown occurs for optimal performance of the supports.

Table 3: The static COF comparing the differences with and without an enclosure.

Material combination	Mean (SD) without encloser	Mean (SD) with encloser
Aluminum on Stainless Steel	0.44 (0.010)	0.34 (0.017)
Stainless Steel on Stainless Steel	0.23 (0.033)	0.20 (0.006)

During the testing of the polymers, the results recorded during 77 K tests were unexpectedly high compared to the room temperature tests. It is known that polymers change

hardness with decreased temperature [10]. It is also known that friction is a function of hardness for metals. The room temperature tests were also performed in a dry environment, whereas the 77 K test submerged the slip plane in LN2. The frictional forces recorded are static, and the lubrication properties of LN2 may not be as significant as in a dynamic system, but, as currently understood, the COF of a polymer should not be greater for the low temperature case. Table 4 shows that the measured COF for PEEK on PEEK did tend to increase substantially at cryogenic temperature.

Table 4: A comparison of room temperature tests to 77K for PEEK on PEEK.

	Temp	Test	Sample	Mean COF (SD)
PEEK on PEEK	295 K	3	45	0.216 (0.023)
	77 K	3	83	0.274 (0.017)

2.7. Membrane to Support Interface Results

The original design of the CRP support required that the membrane to support interface had sufficiently high enough frictional resistance to remain fixed. During testing, it was observed that the support was not operating properly. An iteration to the design was proposed to use the supports as a method to properly position the CRP while installing. This design would utilize the corrugation to fix the support footpad while also positioning the CRP, and this design can be seen in Figure 11. This change in design means that it is unnecessary for the membrane to support interface frictional forces to fix the footpad. This iteration of the design resulted in unfinished testing of the membrane to support interface. Data for the support to membrane interface will be in **Error! Reference source not found.**.

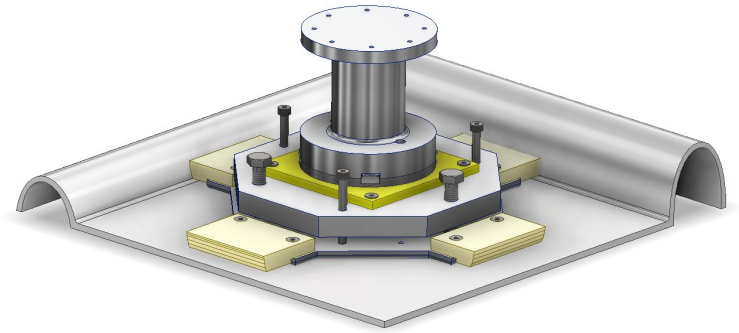

Figure 11: CAD model of the version 3 design with the fixed footpad design.

2.8. Intermediate Test Plane Results

The CRP consortium is interested in the amount of force that a single support will experience when a 255 kg CRP is thermally contracting to 87K. It is assumed that each support will have an approximately equal amount of normal force due to the gravitational force, which equates to approximately 625 N. The average COF of the three supports is calculated and then converted to frictional resistance using the 625N assumption. The following data is what each support would experience on the 255 kg CRP during thermal contraction.

A statistical analysis was performed on the data collected in the frictional tests. A normal distribution was assumed, and this can be seen in Figure 12.

Table 5: Results from tests of various material combinations of the intermediate slip plane at 77K submerged in LN2 with the use of an enclosure.

	Stainless on Stainless	PEEK on Stainless	PEEK on PEEK	Nylon on Nylon, Parallel	Nylon on Nylon, Perpendicular
Mean (N)	88.0	129.4	140..4	137.1	192.0
SD (N)	9.28	8.92	26.07	12.46	31.26
Count (-)	329	152	46	19	20
99.95 % CI (N)	(55.4, 120.6)	(97.6, 161.1)	(41.6, 314.6)	(84.9, 189.2)	(64.5, 319.4)

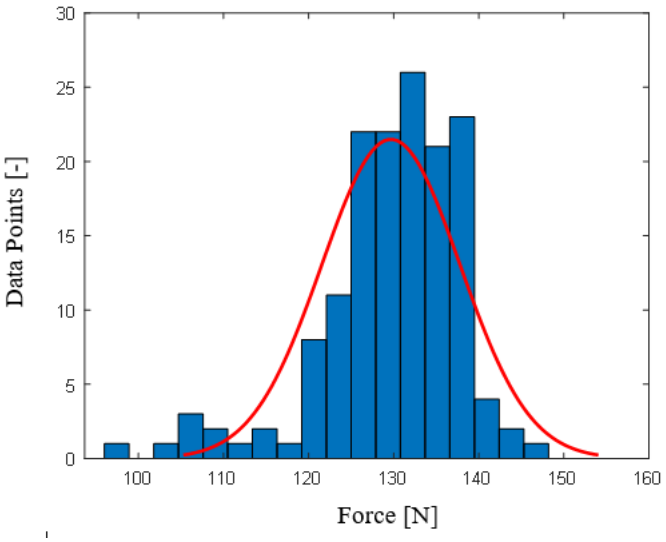

Figure 12: PEEK on Stainless Steel data with a normal distribution curve.

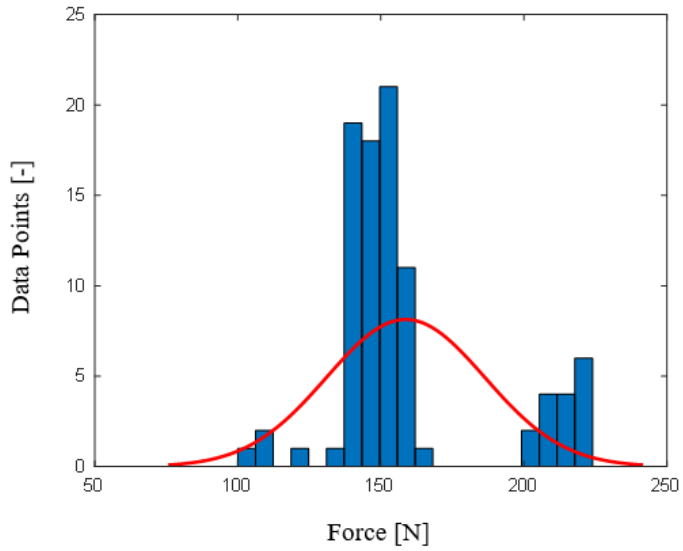

Figure 13: PEEK on PEEK data with a normal distribution curve.

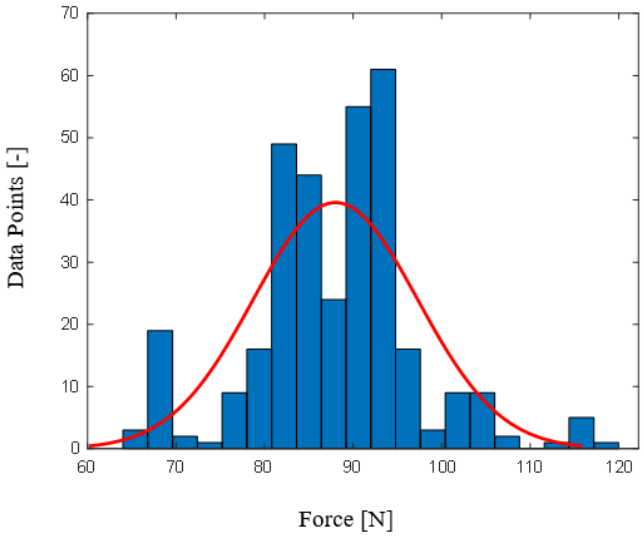

Figure 14: Stainless Steel on Stainless Steel data with a normal distribution curve.

There were two significant observations associated with the tests. First, moisture present in the cryogenic tests significantly affects the frictional forces. The presence of moisture increasing COF is intuitive, but it is believed that there could be similar effects associated with moisture retained within the polymer that causes an increase in friction when submerged within LN2.

Second, there was no significant benefit to using polymer, as seen in Figure 15. There is also concern that the static loading time of the polymer when all 80 CRP will change the COF of the polymer[11]. This slight deviation of COF led us to conclude that the best solution for our support would be to use stainless steel as the intermediate slip plane. Using stainless steel should provide a sufficiently low COF and a predictable result. The cost of materials is not significantly different between PEEK and stainless steel. Iteration to the support design is in process.

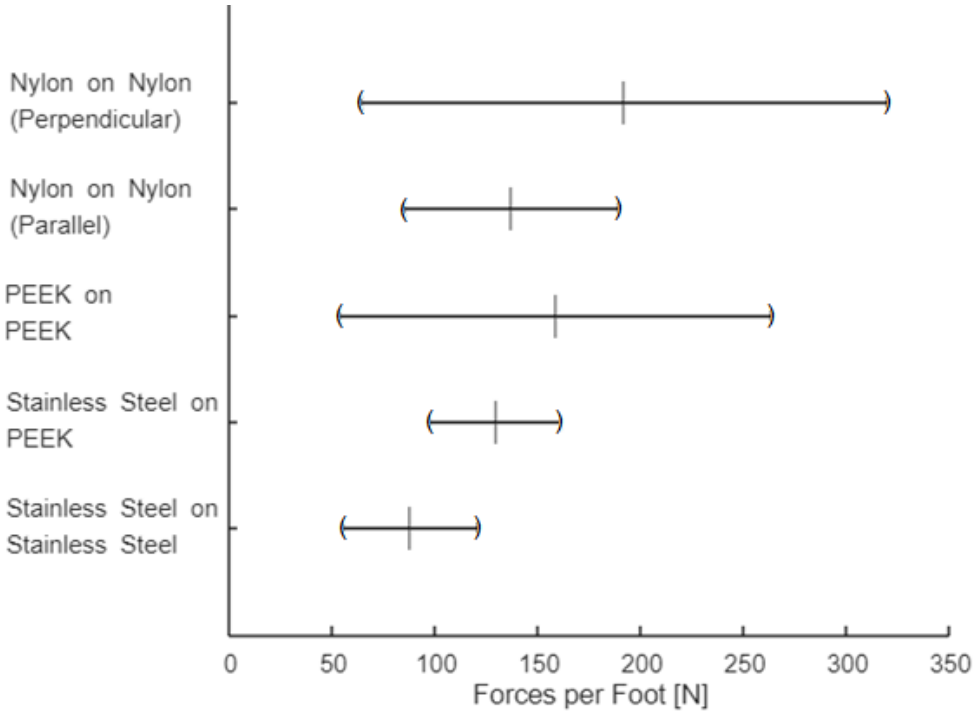

Figure 15:The 99.95% confidence interval for all of the data.

Chapter 3. Complex Model Analysis

3.1. Effect of Support Differences

During friction testing of the CRP supports, it was observed that the recorded COF varied significantly. The uncertainty in the testing system and procedure may contribute to the variance, but the geometry and differences from manufacturing is a significant factor of the variance[9]. Since there is no way to be sure that the three free supports will have exact slip plane COF, an ANSYS model of the effect was proposed. This model identifies all the forces caused by any differences between supports COF. After the stresses were identified, stress analysis was performed for the components with the highest potential for failure.

The support design performs three critical functions: protecting the CRP, protecting the membrane floor, and guaranteeing the final position of the CRP. As mentioned earlier, the slip plane will prevent excessive stresses in the CRP and excessive forces on the membrane floor. The bottom foot pad of the support has been designed to fit within the corrugations of the membrane floor, as seen in Figure 16, and Figure 17. This design constrains the support without the use of fasteners or welding.

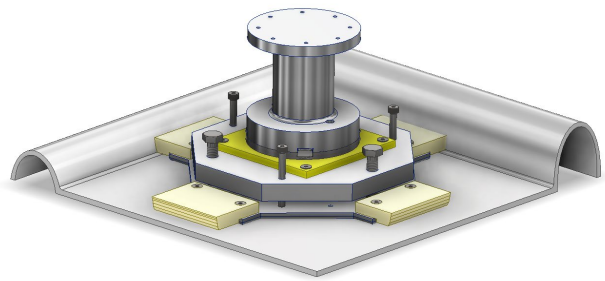

Figure 16: Illustration of the support fitting into the membrane floor. Two of the corrugations are removed for a better view.

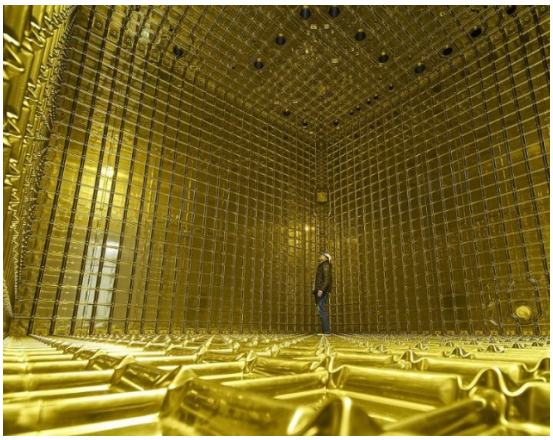

Figure 17: A smaller but similar design of the cryostat used for the far detector of DUNE.

This combination of the slip plane and footpad allows for the contraction of the CRP without movement on the fragile membrane floor. One of the supports will be fixed to prevent the CRP from contracting unpredictably. The fixed support provides a centralized point for the CRP to contract, ensuring it finishes its contraction in a known and predictable location; this idea is illustrated in Figure 18.

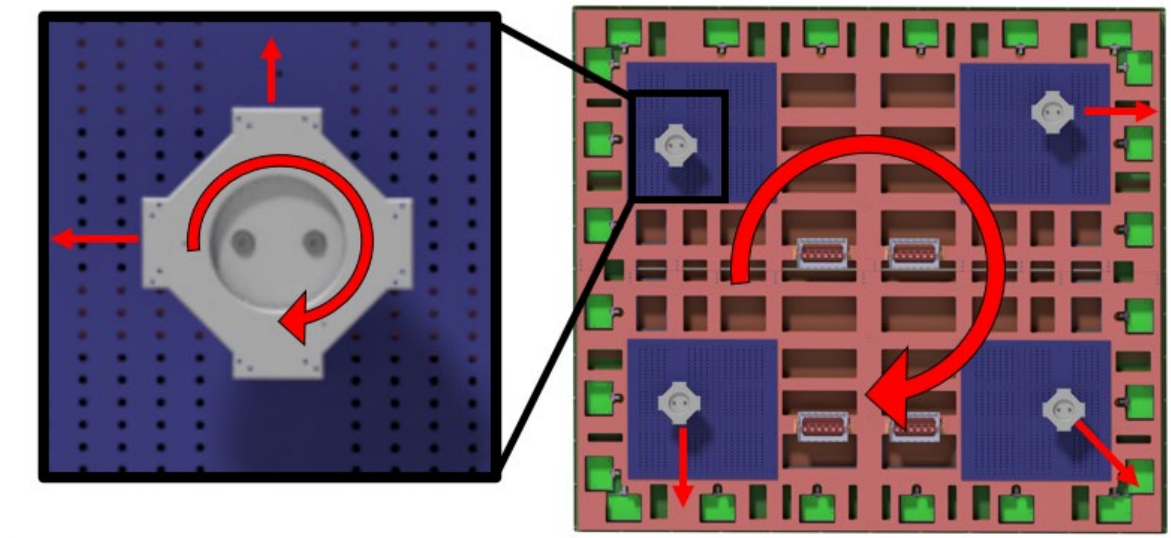

Figure 18: Visualization of how the fixed foot will provide a centralized point for the center of contraction. The red arrows represent the reactionary force due to the friction in the slip plane.

The slip plane of each support will have a different COF since it is impossible to manufacture and set up each support to guarantee the exact COF. This variance means that we must ensure no significant effect due to the difference in COF. There is concern that if the difference of COF causes shifting in the CRP, forces could be applied to the support, causing failure. Note that analyzing CRP structure is beyond this project's scope, and separate studies will be performed if there is concern.

3.2. Complex Model

A complex model was created to account for factors that were impossible to simulate in the friction testing, such as the geometry of the CRP, the thermal contraction of the CRP, and the effects of varied COF in the slip planes. A simplified version of the CAD model, see Figure

19, supplied by the CRP consortium, was used for this simulation. The CAD model consists of the electronics and the very complex structure of the CRP. Since the electronics, structure, and sensor face are not critical for this model, the simplified version consists only of the supports and a simple block to simulate the CRP structure, as seen in Figure 20. This simplification also absorbs the adapter plates.

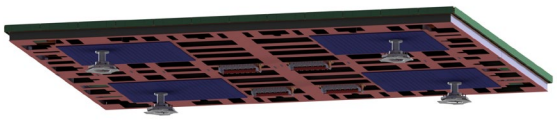

Figure 19: CAD model of CRP from DUNE CRP consortium.

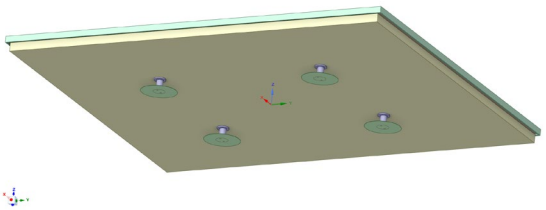

Figure 20: Simplified geometry for ANSYS mode

The geometry for the support was also simplified, see Figure 21. The point of interest for this simulation is the contact surface between the slip plane plates. The foot pad was neglected, as well as all the hardware. It is assumed that any deflection by the hardware is minimal and insignificant. The exact geometry of the support post was used to ensure that any deflection in the post could be calculated.

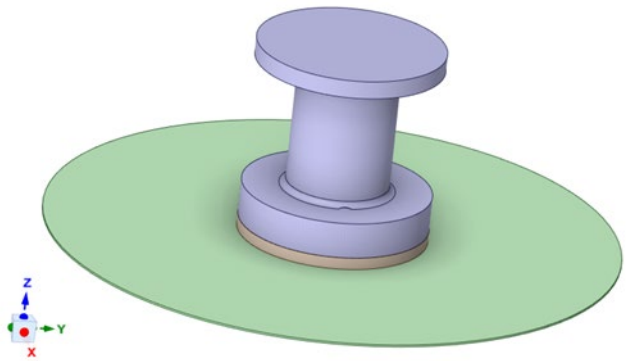

Figure 21: Simplified geometry for the CRP support for complex ANSYS model.

The location of supports varies due to the cryostat corrugations and the requirement that the bottom CRPs and top CRPs must align perfectly. For this model, the support posts are positioned on the CRP structure to test the most extreme configuration. This configuration

minimizes the distance between supports on the narrow side while maximizing the distance on the wide side. This configuration is the conservative assumption that can result in the most significant effect from the difference in COF.

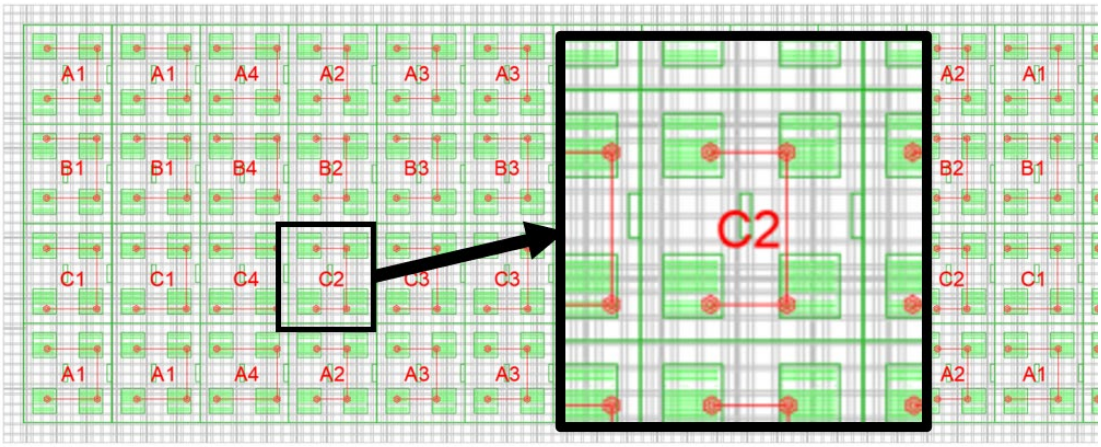

Figure 22: The floor plan for the far detector CRP layout. Highlighted is an example of the support configuration code.

The CRP structure is primarily made from FR-4/G-10 composite. It is important to note that, like many other composites, FR-4/G-10 is polytropic, making thermal contraction calculations difficult. Luckily, the geometry of the CRP structure allows for an isotropic assumption for the overall structure. The structure is designed with c-channels and thin plates. The layup of the structure positions the c-channels and plates so that the fiber direction of the composite dominates the overall length of the x, y, and z directions, as seen in Figure 23.

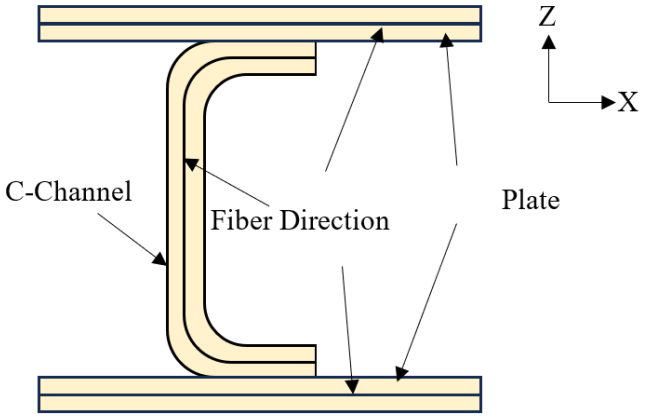

Figure 23: A visualization of the cross-section of the FR-4/G-10 weave layup. This illustrates how the weave properties dominate a significant portion of all directions. This is only a cross-section of the z-y plane, but the same would hold for the y-x plane.

The coefficient of thermal contraction (CTE) of FR-4/G-10 is 9.90 μm/m in the flow direction (parallel to fibers) and 11.9 μm/m transverse to flow (perpendicular to fivers)[12]. This means that overall, it can be assumed that the structure of the CRP will contract uniformly in all directions with a CTE of 9.90 μm/m. In this model, a custom isotropic material was created with the same CTE of FR-4/G-10 flow direction. Since the only force acting on the structure of the CRP will be gravity, the strength properties of the custom material were ignored. The support post material selected was 6061 aluminum alloy from the ANSYS database. The material selected for the top and bottom slip plane plates is 316 stainless steel from the ANSYS database.

A finer mesh, 0.05 m, was used with no localizations during this model's early iterations. That version became very computationally demanding and created excessively long runtimes. An iteration of simulations was created to test to find the largest mesh size without a significant loss in information. This process increased the model's efficiency without losing significant information. A very coarse mesh, 0.25 m, was used for the CRP structure, and finer localized mesh was used for the supports, top slip plate, and bottom slip plate. This is possible

because the only significant information calculated with CRP structure is deflection due to thermal contraction.

The top and bottom slip plane mesh size was set to 0.01 m. This size was selected to increase the number of nodes within the contact surface without creating excessively long runtimes. Simulations were done with finer mesh sizes, which did not significantly affect the model outcome. The support post used a mesh of 0.005 m. This mesh size allows for a significant increase in efficacy without losing information in the model.

The post is fixed to the CRP structure with a bonded contact connection with the top plane of the support post, as seen in

Figure 24. The frictional contact connection is located at the slip plane surface, as shown in Figure 25. The top slip plane plate is fixed to the post with a bonded contact connection. The plane of this connection can be seen in Figure 26 and Figure 27. This connection mates the contact surfaces, ensuring the components are rigidly fixed. This assumption can be made because the hardware will not strain significantly with the frictional forces from the slip plane.

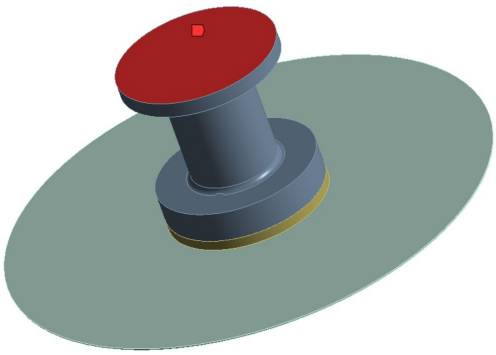

Figure 24: The plane on the support post used to fix the CRP structure.

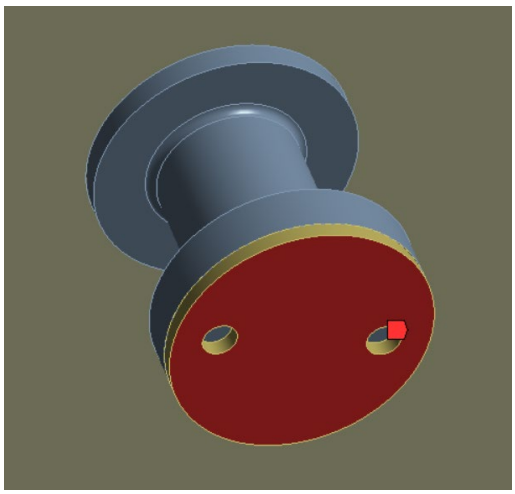

Figure 25: The plane on the top slip plane plate used for frictional contact on the bottom slip plane.

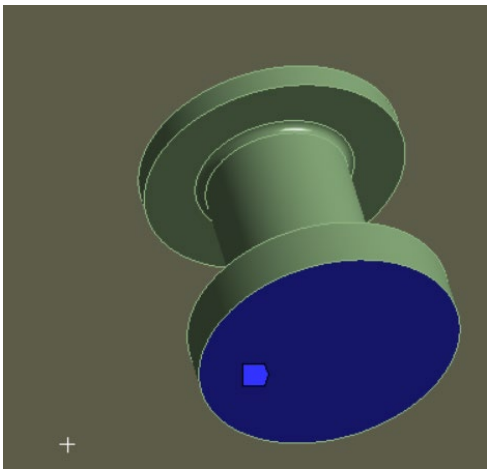

Figure 26: The plane on the support post fixed to the top slip plane plate.

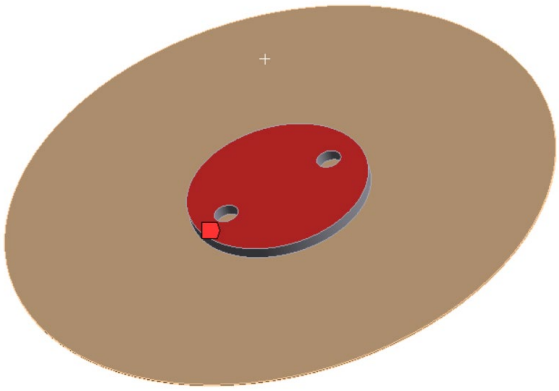

Figure 27: The plane on the top slip plane plate fixed to the support post.

The bottom slip plate is fixed in space with respect to the global coordinate system using a fixed support feature. The foot pad design is fixed within the corrugations of the membrane floor. The installation truss, as seen in Figure 28, will support the CRP when connecting cables to the electronic components. The installation truss also allows for feet leveling when the exact CRP load deflects the membrane floor. The leveling allows the assumption that the foot pad will parallel the posts and the slip plane will be fixed in the z-direction.

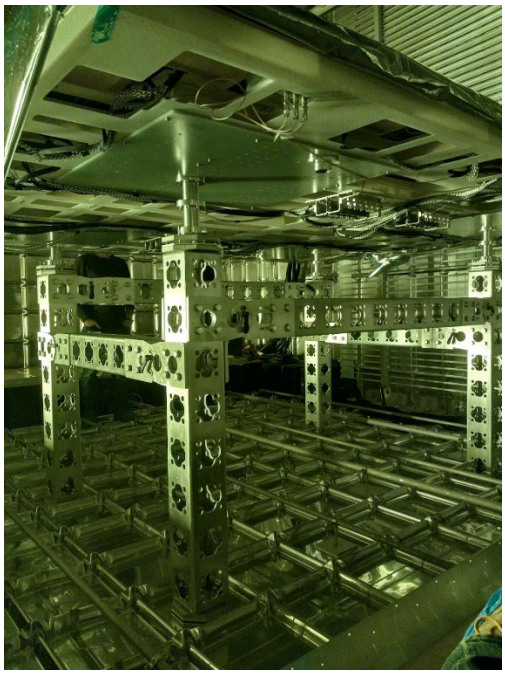

Figure 28: The installation truss used to support the CRP while connecting the cables. The levelling procedure also utilizes the installation truss to ensure the floor has similar deflection to when the CRP is installed.

Each CRP will have three supports with a slip plane, while one must be fixed to ensure that the center of contraction has a reliable and known location. The supports with the planes utilize separate frictional contact connections with separate variables for the COF. This feature enables the ability to create a parametric study to be performed by varying the values of COF for each support's slip plane. A rough connection was used to ensure that the fixed support cannot slip yet allows for the top slip plane plate's contact surface to partially or entirely be removed from the bottom slip plane plate's contact surface.

When an object transfers from static frictional resistance to dynamic, it is typical that there is a significant difference. This phenomenon can be seen in the test data in Figure 29. The transition from static to dynamic COF is critical in this model, yet ANSYS does not have a simple organic method for inputting this transition. An Ansys Parametric Design Language (APDL) command was added to the frictional connection to support this feature. This APDL command transitions the COF at a designated time. This time was selected by running the

model and finding where the slip occurs. It was attempted to run the APDL with a velocity condition to change COF when a slip occurred, but this resulted in excessive run times that resulted in run time errors in the model. The CRP will contract in a quasi-static condition, which will result in very small increments of slip. The main concern of this model is to identify what happens at an individual slip increment, assuming that there will not be enough velocity to maintain a dynamic COF for the entire contraction. By using this time method to initiate slip, a single transition occurs and then can be the point of focus when analyzing the data.

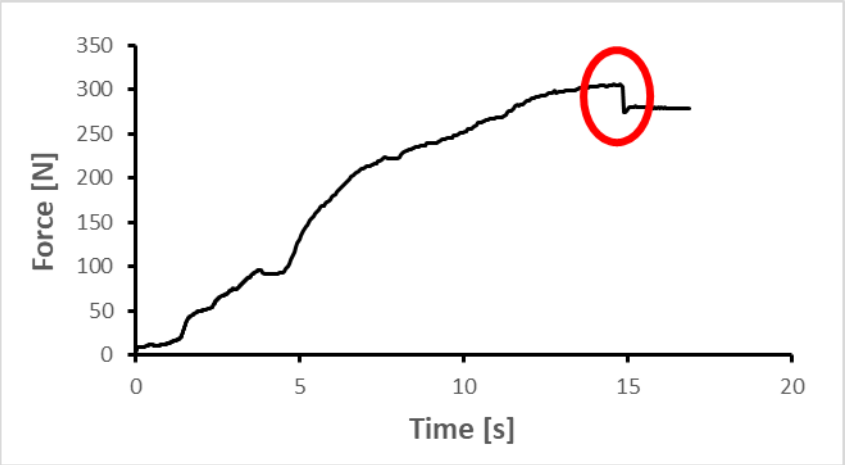

Figure 29: This plot shows the results of a friction test. Highlighted with a circle is the slip phenomenon the slip plane experiences when transitioning from static to dynamic COF.

The value of this transition was from the two extremes of the test data from a COF of 0.3 to 0.1. This transition would result in a drop of 400 N. While testing, the typical drop that was observed was from 30-50 N. By using the extreme COF values calculated from the friction tests, an extremely conservative estimation of the torque created on the fixed foot was found in this model.

Two significant forces are imposed on the supports: gravity and thermal contraction. The gravitational force is simulated by imposing a dispersed normal force on the top of the CRP. The simplified geometry that is used for the simplification of the model creates an unrealistic mass compared to the actual CRP structure. The thermal contraction is created by

creating a modified FR-4 material in which the CTE is isotropic and will contract similar to the actual CRP while remaining relatively simplified.

This model has three phases: the initialization, thermal contraction, and equilibrium phase. The initialization and equilibrium phases are before and after the thermal contraction of the CRP structure, respectively. These phases are to verify that the model starts and finishes at rest. The initialization and equilibrium phases are five seconds long. The thermal contraction phase is 95 seconds long, which was deemed to simulate a relatively low enough heat transfer rate to assume a quasi-static model. Models with longer thermal contraction phases were tested with no significant change to the data. In the thermal contraction phase, the CRP structure has a thermal condition in which the structure's temperature will change from 295.15 K to 87K, which causes the supports to contract a maximum of 5.7 mm between the farthest two supports. This is similar to the estimations that were made for the fiction testing of 6.2 mm for the maximum displacement between two supports.

The initial time step is 1 second. The max time step is set to 10 seconds. The minimum time step is 0.1 seconds. These values allow adequate steps to create convergence without losing efficiency in the overall model.

Large deflection must be activated in the solver controls. The complex geometry of the model creates the need to account for changes in stiffness and stresses due to deflection. Using large deflections accounts for that deflection and appropriately adjusts for it every time step.

A transient structural model was used because it was deemed necessary to have a time-history analysis of the post positions as the thermal contraction shrunk the CRP structure. As the locations of the post-change, the moment arm will change, affecting the torque on the fixed post. It is assumed that the acceleration of the post is insignificant during the thermal

contraction. This model used Quasi-Static application-based analysis settings to account for this assumption.

To analyse the final rotation of the CRP, a remote point is created. The top face of the CRP structure is used as this point, which is important to identify the final position of the CRP after thermal contraction.

3.3. Results

There were concerns that the collective forces would become excessive on the fixed support. The force taken on the fixed support was calculated with the slip planes set to the high extremes found during friction testing. The COF value of 0.2192, which is the extreme end of the 99.95% confidence interval, provided an overall force of 315.5 N. This value will be analysed by the CRP consortium.

The model was run with varying values for the COF to see how the CRP would be affected by the differing COFs; the values and results can be seen in Table 6. This study showed that there will be no significant torsional effect from the differing COF of supports.

Table 6: Table of torque values from an iteration of runs of the model with different values of COF. The symbol (->) signifies the change from static to dynamic coefficient of friction.

Test Run	Post 1	Post 2	Post 3	Post 4	Max Torque [N-M]
1	Low	Low	0.2192 -> 0.20	Fixed	1.08
2	Low	Low	0.2192 -> 0.15	Fixed	0.79
3	Low	Low	0.2192 -> 0.1056	Fixed	0.76
4	Low	Low	0.2192	Fixed	0.62
5	High	High	0.2192 -> 0.20	Fixed	0.86
6	High	High	0.2192 -> 0.15	Fixed	0.88
7	High	High	0.2192 -> 0.1056	Fixed	0.87
8	High	High	0.2192	Fixed	1.13
9	0.2192 -> 0.2	High	High	Fixed	0.86
10	0.2192 -> 0.15	High	High	Fixed	0.80
11	0.2192 -> 0.1056	High	High	Fixed	0.73
12	0.2192 -> 0.2	Low	Low	Fixed	0.86
13	0.2192 -> 0.15	Low	Low	Fixed	0.80
14	0.2192 -> 0.1056	Low	Low	Fixed	0.79
15	0.2192 -> 0.15	Low	High	Fixed	1.46
16	0.2192 -> 0.15	High	Low	Fixed	1.01
17	Low	High	0.2192 -> 0.15	Fixed	0.72
18	High	Low	0.2192 -> 0.15	Fixed	0.87
19	Low	0.2192 -> 0.15	High	Fixed	0.29

20	High	0.2192 -> 0.15	Low	Fixed	0.38
21	Low	0.2192 -> 0.15	Low	Fixed	0.37
22	High	0.2192 -> 0.15	High	Fixed	0.72

Once the parametric study was completed, it was concluded that the greatest torque observed in the study was 1.46 N-m. This study also analyzed the effect that differing COF at each support would have on the fixed foot. There was no significant increase in torsional forces based on the difference in COF.

3.4. Analyzing Weak Points

After modelling the potential for rotational forces on the fixed support, it is natural to identify the overall support's safety factor. Two components were identified to have the highest potential to fail due to a potential torsional effect of the CRP. Those components are the bolts that fasten the support onto the adapter plate on the CRP structure and the retention bolts on the footpad of the support.

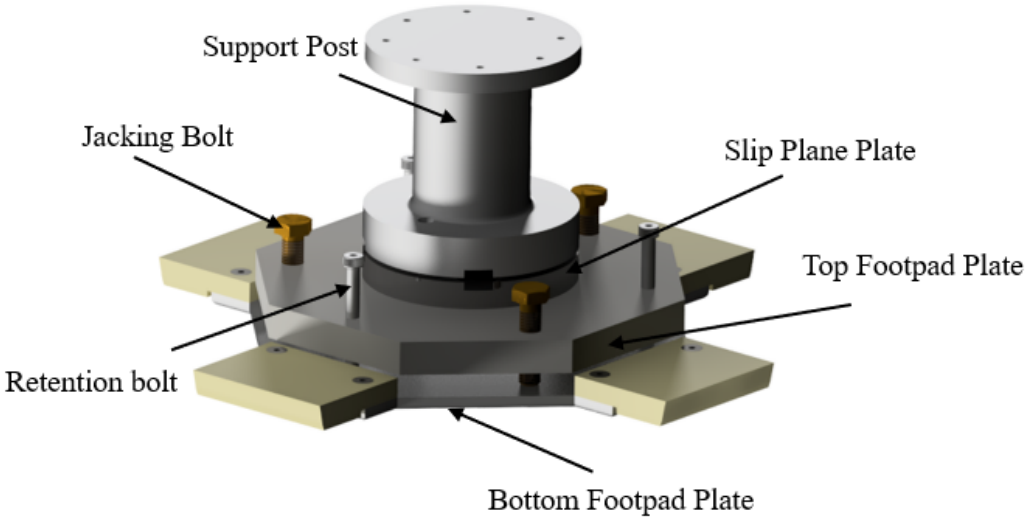

Figure 30:Rendering of the CAD model used to create a simplified model to analyze the mounting bolts and retention bolts.

3.5. Analyzation of mounting bolts

The support is fastened to the CRP's adapter plate with eight M3 stainless steel bolts. The support post has eight through holes for these bolts in a circular pattern with a diameter of 80 mm, as seen in Figure 31.

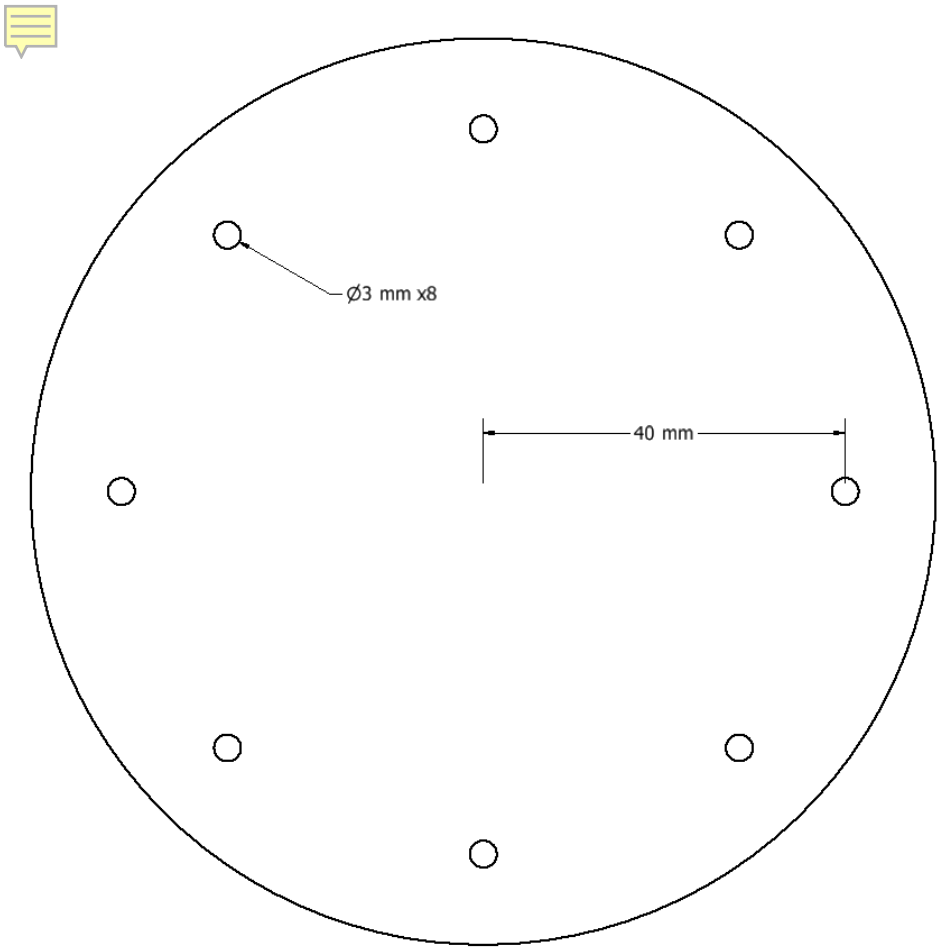

Figure 31: Circular pattern of bolt holes at the support post's top.

A simple force calculation can be used to derive the greatest amount of force that a single bolt can experience before it fails. This calculation assumes that two bolts will receive the load since a single bolt would not have adequate constraints to create a static situation. The moment being applied to the bolts is from the center of the post, resulting in the moment arm being 40 mm. The ultimate shear stress of stainless steel was derived using 50% of the value of the tensile strength provided by the supplier, McMaster-Carr[13] [14].

This calculation neglects any frictional forces between the post and the CRP, creating a more conservative calculation. Spring washers are used which minimize the effects of thermal contraction to ensure they do not loosen during cooldown.

The calculations for this analysis can be seen in Appendix 2. The final calculation has a value of 55.5 N-m on the post for a single bolt. Since there must be two bolts in contact for a moment to create a fulcrum point, a value of 110.5 N-m would cause failure of the CRP fasting bolts.

3.6. Retention bolts Analysis

The retention bolts for the foot pads will have a bending moment on them if any torque is applied to the support; a free body diagram is illustrated in Figure 32.

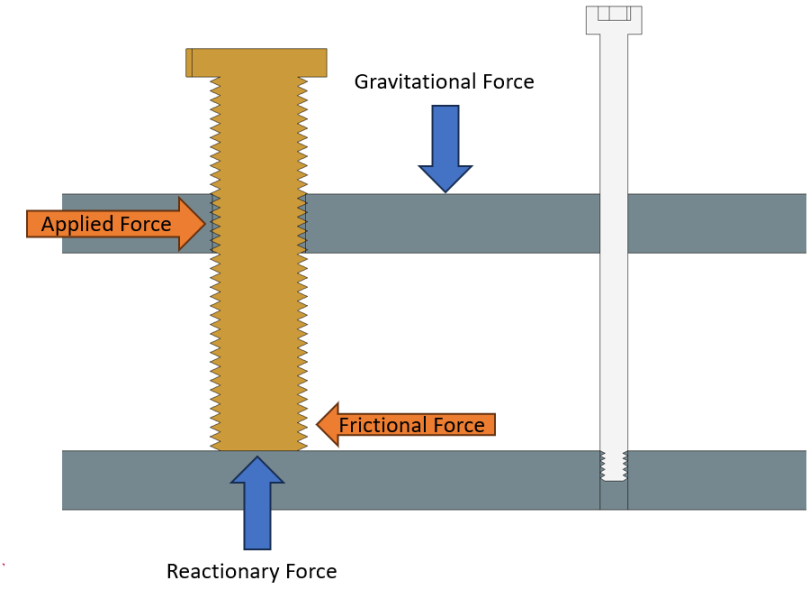

Figure 32: FBD to visualize forces for the stress calculation of the retention bolts.

The maximum stress in the bolt was calculated using a beam bending calculation with the greatest distance the footpad plates can be separated, as seen in Figure 33. When the jacking

bolts are fully extended, the distance between plates is 21 mm. This value creates the greatest bending moment on the retention bolt, creating the worst-case scenario.

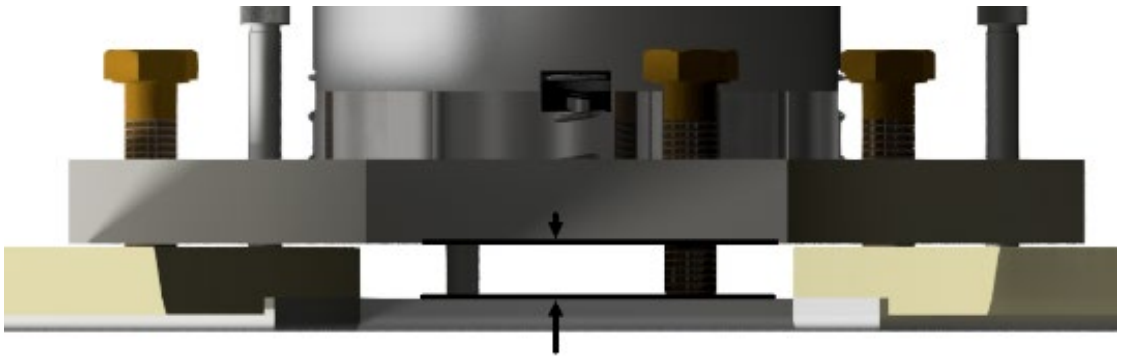

Figure 33: The distance dimension between the bottom footpad plate and the top footpad plate.

The jacking bolts will provide a frictional force. A conservative assumption was made that this force would be the same as the values recorded in our frictional test with the same material. This assumption is conservative because the geometry of the jacking bolt is much different than the friction tests. The frictional tests used flat plates where the screw has a significant edge, and scoring is made on the foot pad plate made during leveling.

When doing a simplified analysis of the retention bolts, the calculations showed that a maximum torque of 61 N-m would cause failure, see Appendix 2. This calculation assumes that jacking bolts have a constant frictional force. This assumption is not conservative and should not be made.

Once the initial calculation was performed, a complex model was created in ANSYS to account for the factors that the above calculations could not. The geometry used for this model was from the CAD model for the support design. This model was then simplified to remove unnecessary complexity in the model. The center mechanism was removed due to the assumption that the center mechanism bolts would not fail before the retention bolts. The centering mechanism bolts are much larger, as the moment arm is much smaller. This model

combines the support post, spacer, and top foot pad plate into a singular ridge body. The fixed support uses a spacer to account for the height of the slip plates.

The geometry for the retention bolts and jacking bolts was created using the CAD model supplied by the supplier, McMaster. They were then simplified to remove the threads to remove complexity. Since the threads were removed, the amount of material is less than the actual bolts, resulting in a more conservative estimate than reality.

The bottom plate for the foot pad is fixed in space due to the assumption that the membrane floor corrugations will mechanically constrain the plate. All locations with threads were fixed using a fixed contact connection.

The retention bolts used for the footpad are 18-8 stainless steel shoulder bolts. The supplier, McMaster-Carr, states that these bolts have a tensile strength of 70,000 psi or 483 MPa[14]. In this model, 304 stainless steel was used from MATWEB.com material library that had been uploaded into ANSYS]. The material properties of 304 stainless steel in MATWEB.com matched the McMaster-Carr data sheet[15].

The jacking bolts per the supplier, McMaster-Carr, meet ISO 4017 standards and have a tensile strength of about 110,000 psi, which equates to 765 MPa. ANSYS has structural steel with an ultimate tensile strength of 561 MPa in the default material database. This structural steel was used since the jacking bolts are not the focus of this study, and the lower value will provide a conservative estimate.

As mentioned earlier, the post and plate were combined into a single solid object. This object is significantly stronger than the hardware and is assumed to have minimal impact on the results. A general material, structural steel, was selected for this object.

An evenly distributed force was applied to the top of the post of 545 N to simulate the normal force due to gravity. This value was calculated by taking a 220 kg CRP structure and

distributing the load between all four supports. This value would equal the weight of the CRP evenly distributed between the four supports.

A frictional contact connection was created to account for the frictional force between the bottom plate of the foot pad and the jacking bolt. The COF used for this was 0.3, which, as mentioned earlier, is a conservative estimation due to the geometric restrictions.

For the first iteration of this model, an arbitrary torque input was added to this model about the z-axis on the post, as seen in Figure 34. Once a value was found, the torque was calculated, and the model was rerun to verify results to ensure confidence in case the stress buildup was not linear. This force ramped from zero to the final value. The maximum amount of force from the ANSYS model was 25.25 N-m, which is the failure point for the retention bolts. This value is significantly higher than any force that is expected.

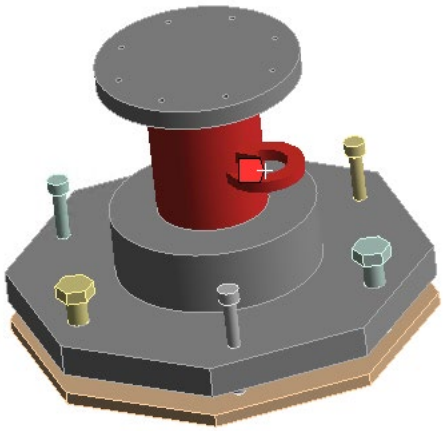

Figure 34: The simplified model used in ANSYS with an arrow illustrating the direction of torque applied to the post.

Since there was a model created and with a simple modification to the force input to a linear force from the CRP contraction from the top of the CRP, the failure point of the bolts was found to be 525 N, which is the most frictional resistance that the support can withstand before the retention bolts fail, which is significantly higher than any amount of force we are expecting. For example, during testing, the maximum estimated amount of force expected is

316 N, which means that with the worst-case scenario created in the model, there will still be a safety factor of 2.62.

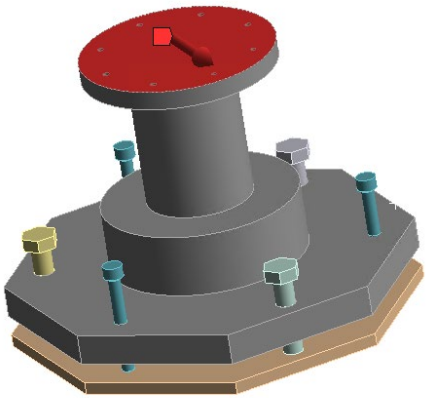

Figure 35: The simplified model used in ANSYS with an arrow illustrating the direction of force from the thermal contraction of the CRP structure.

After performing the first simulation of this model, using the stresses in the retention bolt, the torque input was modified to find the point of failure. The conclusion is that with very conservative assumptions, the failure of the retention bolts would appear at 25.25 N-m.

3.7. Complex Model Conclusion

After creating the model to test the potential of the rotation, it was concluded that if there is any rotation, it would be insignificant to damage the supports. The amount of force during contraction that would result due to the rotation of the CRP is minimal and insignificant. The collective force on the fix foot due the the slip condition is significant but not alarming. If the consortium feels that there needs to be greater safety factor value then larger bolts can be used but are not deemed necessary at this time.

Chapter 4. Lifting Device

4.1. Lifting Device Design

The University of Wisconsin-Madison was tasked with designing and building a mechanism for placing the CRP properly. The original design of DUNE only utilized a single suspended plane of CRPs, which resulted in many significant engineering obstacles in creating a lifting device, see Figure 36. The first iteration of the prototype was used to successfully install two CRPs for DUNE's module zero at CERN.

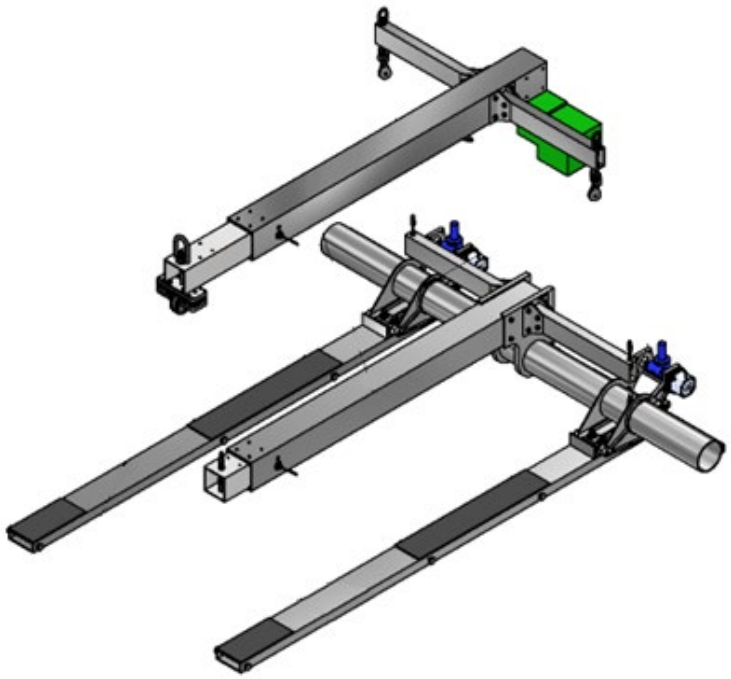

Figure 36: The CRP lifting device used for placing CRPs. Not shown is the cabling system that hold the bottom tine carriage to the top structure of the device.

The CRPs and cryostat membrane are mission critical. If the membrane or CRP is damaged while installing the CRPs, even slightly, it could result in significant setbacks or potential failure of the entire experiment. The electronics on the CRP will be tested at room temperature, but any damage that passes the room temperature test but is significant to be

exacerbated during cool down would result in blind spots in the sensors, which is unacceptable and requires great care to ensure that the CRP can be placed with extreme control.

The design of the CRP also requires that the top plane does not get scratched or dented. This design could result in the sensor working improperly. To ensure that the sensor top is not damaged, the DUNE CRP consortium required that the lifting device only contact the CRP from underneath the CRP structure. The underside of the CRP has important electronics and cabling, as seen in Figure 37, which require careful positioning of the tines.

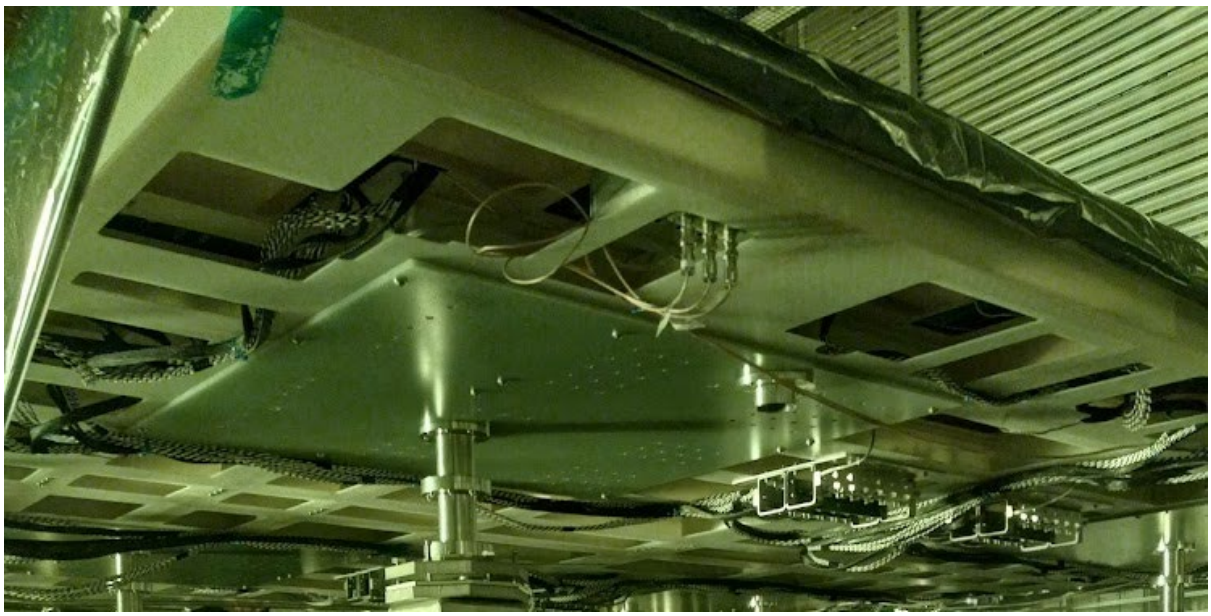

Figure 37: The electronics and CRP underside.

The cryostat utilizes a membrane floor with corrugations, see Figure 38. These designs add complications during the CRP placement. The distance between planes is a critical dimension, and this means that the required height of the CRP is fixed. This results in fixed space under the CRP of 60 mm from the bottom of the CRP to the top of the corrugation. When designing the tines strong enough to withstand the 255 kg of the CRP, the greatest thickness was less than 60 mm, which is relatively small for the amount of bending deflection. The width of the tines was also restricted by the placement of electronics and cabling under the CRP. A

special mechanism was designed to manually rotate the tines to account for the bending of the tines which could not be avoided due to the constraints on the tine dimension

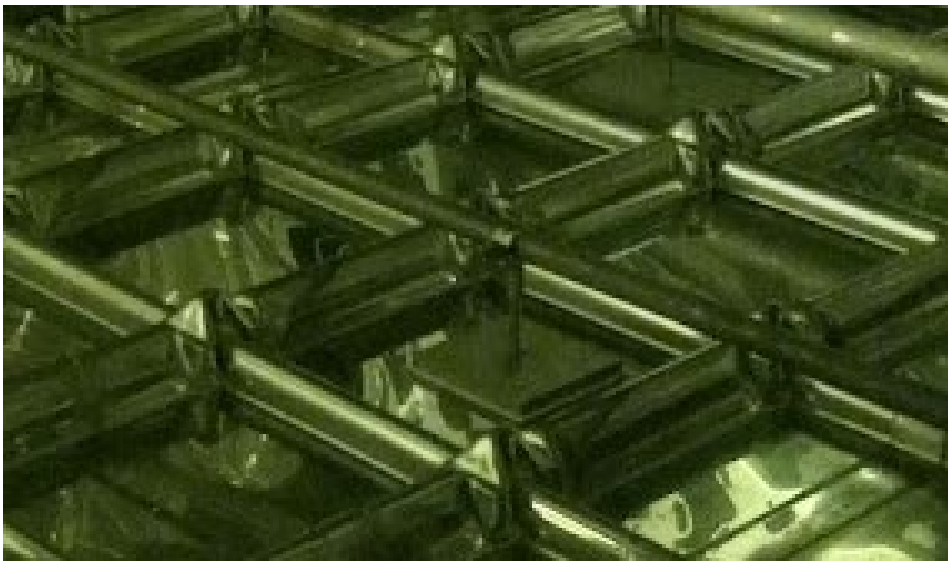

Figure 38: A similar cryostat with the same corrugated membrane design.

The spacing of the corrugations is not consistent with the location of the center of the CRP. To ensure that the CRP supports are placed in the center of a corrugation square, multiple different feet locations are required. The varied support locations create a requirement for the tines system to have the ability to adjust for different widths of the supports.

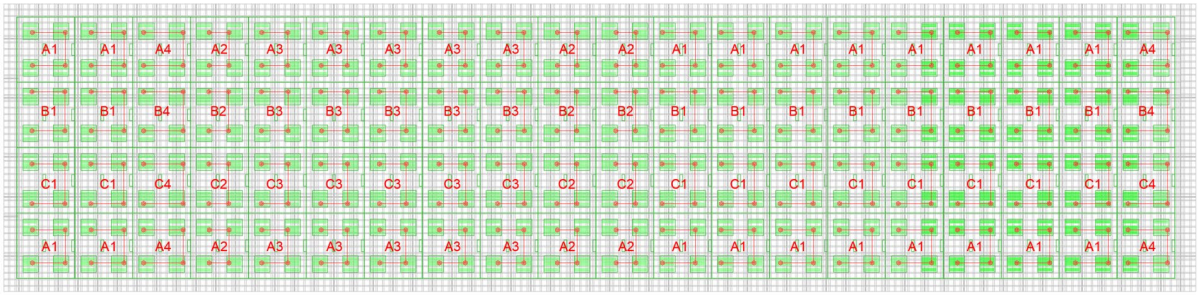

Figure 39: The layout of the far detector with all 80 bottom CRPs. Each letter and number combination signifies a different required support spacing.

To protect the cryostat membrane, a false floor is placed on top of the membrane for protection during the installation of the CRPs. The false floor is simply wood pillars and plywood panels, as seen in Figure 40. The crane that will be used to install the CRP must use the false floor during installation. Once the CRP is placed on the membrane floor, the tine

system cannot be removed from under the CRP since the false floor with the crane will trap the tines since the false floor sits higher than the bottom of the tine system. The time is required to be removed from the lifting system once the CRP is in place; then, the lifting system, crane, and false floor can be removed. Once there is no false floor boxing in the tines, the tines can then be retrieved.

Figure 40: The false floor that will be used to protect the membrane floor.

The design of the detector requires the CRPs to be positioned within 5mm from each other, which is an extremely difficult task since the CRP is 255 kg with dimensions of 3m x 3.4m. Since the CRP is large and heavy, it is extremely important to control it at all times yet must ensure that the CRP has the ability to move in very small increments.

The entrance to the cryostat is only 1.5 m wide, which creates a requirement for the lifting system to be easily disassembled and assembled, ensuring that it can be brought in and out of the cryostat. The relatively narrow entrance requires the crane that will be used for the lifting system to be within 1.5 m wide. The cranes that fit this requirement have a relatively low lifting capacity, creating a requirement for the lifting device and CRP to weigh less than 500 kg combined.

4.2. Mock CRP and Functionality Testing

After assembling the lifting device, it was required that a mock CRP was designed and built to test the lifting capacity and functionality of the lifting device. This mock CRP was rigid like an actual CRP as well as the same dimensions. Extra mass was added to the CRP to ensure that the lifting device could lift 150% of the CRP weight. It must be noted that the next iterations will be designed for 300% of the CRP weight to ensure safety requirements will be met for US and European standards. The mock CRP was made from plywood and polystyrene foam. Steel slotted strut channel was used to add mass and create a ridged structure, which can be seen in Figure 41.

Figure 41: The mock CRP and the lifting device during functionality testing.

4.3. Stress Analysis

Stress analysis was done on every critical component to ensure that the lifting device was safe and functional. This analysis was then verified and used to certify the capabilities before use at module zero at CERN; see Appendix 3 for the stress analysis documents.

4.4. Operation Procedure

A procedure document was created to ensure that the lifting device was safe. This document was used by safety personnel to verify that the lifting device would not create unnecessary risks. This procedure document was then verified and used to certify the capabilities before use at module zero at CERN; see Appendix 4 for the stress analysis documents.

References

[1] M. Sajjad Athar, A. Fatima, and S. K. Singh, “Neutrinos and their interactions with matter,” *Prog. Part. Nucl. Phys.*, vol. 129, p. 104019, Mar. 2023, doi: 10.1016/j.ppnp.2022.104019.

[2] B. Pontecorvo, “MESONIUM AND ANTIMESONIUM,” *Zhur Eksptl Teor. Fiz*, vol. Vol: 33, Aug. 1957, Accessed: Oct. 27, 2023. [Online]. Available: https://www.osti.gov/biblio/4343073

[3] “The Nobel Prize in Physics 2015,” NobelPrize.org. [Online]. Available: https://www.nobelprize.org/uploads/2017/09/advanced-physicsprize2015.pdf

[4] NIST, “Material Properties: G-10 CR (Fiberglass Epoxy).” Accessed: Jun. 21, 2023. [Online]. Available: https://trc.nist.gov/cryogenics/materials/G-10%20CR%20Fiberglass%20Epoxy/G10CRFiberglassEpoxy_rev.htm

[5] T. Osswald and G. Menges, *Material Science of Polymers for Engineers*, Third. Hanser Publications, 2012.

[6] Z. Sápi and R. Butler, “Properties of cryogenic and low temperature composite materials – A review,” *Cryogenics*, vol. 111, p. 103190, Oct. 2020, doi: 10.1016/j.cryogenics.2020.103190.

[7] Z. Zhang, P. Klein, G. Theiler, and W. Hubner, “Sliding performance of polymer composites in liquid hydrogen and liquid nitrogen,” *J. Mater. Sci.*, vol. 39, pp. 2989–2995, May 2004, doi: https://doi.org/10.1023/B:JMSC.0000025824.18291.f0.

[8] R. A. Burton, J. A. Russell, and P. M. Ku, “Metallic friction at cryogenic temperatures,” *Httpsdoiorg1010160043-16486290181-3*, vol. 5, no. 1, pp. 60–68, Feb. 1962, doi: https://doi.org/10.1016/0043-1648(62)90181-3.

[9] “Standard Guide for Measuring and Reporting Friction Coefficients.” Jul. 2018.

[10] Q. Wang, F. Zheng, and T. Wang, “Tribological properties of polymers PI, PTFE and PEEK at cryogenic temperature in vacuum,” *Cryogenics*, vol. 75, pp. 19–25, Apr. 2016.

[11] A. Ptak, “Effect of loading time on the static friction polymer-metal sliding pairs at low temperature,” *24th Int. Conf. Eng. Mech. 2018*, pp. 693–696, May 2018, doi: 10.21495/91-8-693.

[12] “G-10 Fiberglass Epoxy Laminate Sheet.” Accessed: Oct. 27, 2023. [Online]. Available: https://www.matweb.com/search/datasheet_print.aspx?matguid=8337b2d050d44da1b8a9a5e61b0d5f85

[13] J. Shigley and C. Mischke, *Mechanical Engineering Design*, Fifth.

[14] “18-8 Stainless Steel Socket Head Screws,” mcmaster.com. Accessed: Oct. 27, 2023. [Online]. Available: https://www.mcmaster.com/90751A114/

[15] “304 Stainless Steel.” Accessed: Oct. 27, 2023. [Online]. Available: https://www.matweb.com/search/DataSheet.aspx?MatGUID=abc4415b0f8b490387e3c922237098da

Appendix 1: Test Procedures

Calibrating load cell

1 Verify load cells calibration with hanging fixture and ref weights.

2 Hang Load cell from the crane.

3 Ensure that the LabView program is running and receiving a signal from the load cell.

4 Fix test weight device to load cell.

5 Lift the device so that it's completely clear of the floor.

6 Run LabVIEW with a 0-correction value to find the uncalibrated mean force of the test device.

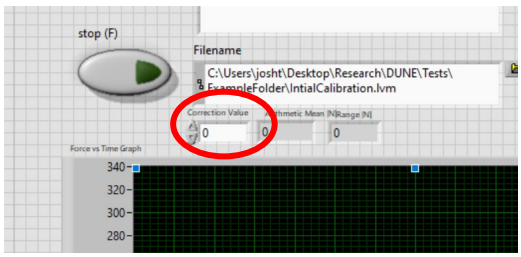

7 Use the Arithmetic mean found in the previous step as the correction value.

Note: When changing the correction value, ensure that the current value is set to default before running the program.

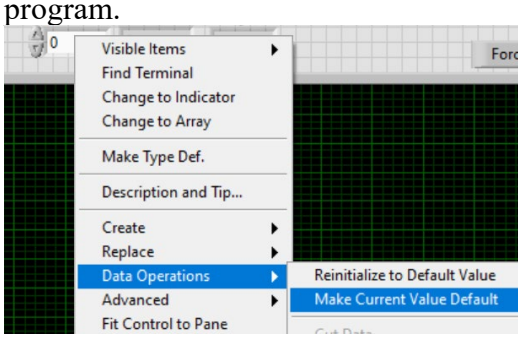

8 Run the LabView program to ensure that the mean value now reads near 0 N

9 Run test with about 100N.

a. Put one known reference weight on the test device.

b. Run the test for at least 30 seconds.

10 Verify force recorded as mean value correlates with the known force applied by reference weight.
11 Retest the previous test by increasing one reference weight at a time.

Set up of testing equipment

1 Zero load cell
   a. With no load apple to load cell run the LabView program for at least 30 seconds.
   b. Make the current mean value default for the correction value.
   c. Rerun LabView Program to ensure that the mean value is ± a one newton.
      a. If the value does not satisfy requirements then re-zero load cell.

Note: When changing the correction value, ensure that the current value is set to default before running the program.

   d. Verify the gap from the base plate to the foot plate for uniformity.

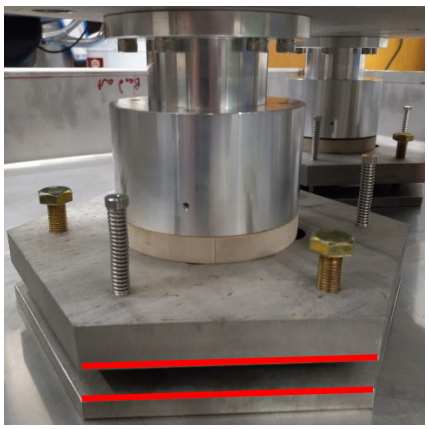

2 Ensure that the supports are centered on the feet plate and that the sled has ability to slip forward.

3 Apply the desired load to the sled.
4 Ensure load is excellent enough to overcome springs.

5 Check the slip plane plate for the entire contact surface.
   a. If the slip plane plate and aluminum support have a visible gap, adjust leveling screws until there is no gap.

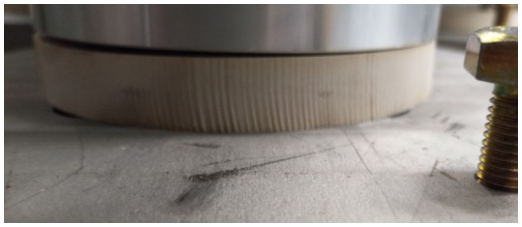

6 Check leveling screws for uniform torque on each foot.

7 Connect the rope to the load cell and sled.

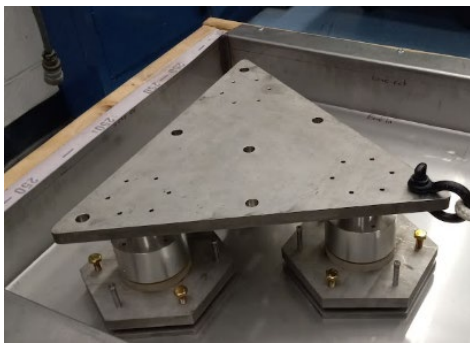

Note: Ensure that the ropes are not catching on the encloser or tub.

8 Close encloser and ensure that the front rope and reset ropes are attached.

9 Filling procedures (For the room temperature test, ignore steps 17-19.)
10 Insert dry nitrogen gas line. Purge process for 30 mins.
11 fill the tub- with liquid nitrogen until the fluid level is above the plastic disk. Wait for a steady-state; more liquid nitrogen may need to be added to ensure the level is maintained above the plastic disk.

Operating Tests

1 Turn the knob until there is a slip.
   a. The knob should be turned at a rate of 1 turn per 10 seconds.
   b. Connect the backside rope.

2 Rest sled with backside rope (Need second rope).
3 Disconnect the backside rope.
4 Repeat.

Data Processing

1 Save data files into the folder with the MATLAB program
2 Ensure MATLAB code correct date of tests modified.
3 Ensure MATLAB file has folder name set to mother folder, which contains all data files.
4 Run the MATLAB program
5 Copy Static and Dynamic arrays into Excel
6 Calculate COF with normal force applied and resistive frictional force.
7 Create an average and extreme graph for each test criteria.

Appendix 2: Calculations

Calculation for the Shear on the support mounting bolts

The mounting bolts that hold the support to the CRP may experience a rotational effect during cooldown. The consortium wants to understand what the failure point of these bolts will be. There are 8 bolts that hold the support to the CRP. It is assumed that if there is a rotation two bolts will be engaged to create a fulcrum point. Using these assumptions, a bolt and plate calculation was used. The minimal diameter of the bolt was used to ensure no stress concentration would complicate the calculation, as well as assuming the most conservative case.

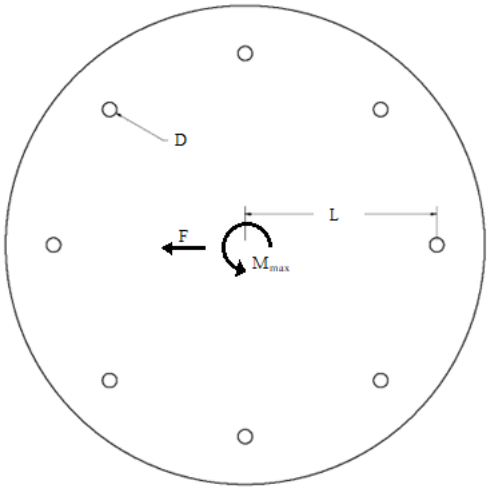

Diameter (D)	0.003	m
Moment Arm (L)	0.04	m
Frictional Force (F)	316	N
Ultimate Strength (σ_{ult})	70,000 [1]	psi
Ultimate Shear Stress (τ)	$241x10^6$	Pa
Cross Sectional Area of Bolt (A)	$7.07x10^{-6}$	m^2
Max Force Allowable Force (F_{max})	1704	N
Max Moment per bolt (M_{max})	55.5	N-m

Equation 1 $\boldsymbol{\tau = \sigma * 0.5 * \frac{1x10^6[Pa]}{145[psi]} = 241x10^6\,[Pa]}$

Equation 2 $\boldsymbol{A = \frac{\pi D^2}{4}}$

Equation 3 $\boldsymbol{F_{max} = \tau * A}$

Equation 4 $\boldsymbol{\Sigma M_z: M_{max} + (L * F_{max})) = 0}$

Equation 5 $M_{max} = L(F_{max} - F)$

Calculation of load to reach failure for retention bolts on the support

To ensure that the support can withstand the loads applied to it during cooldown failure points were analysed. The retention bolt that retains the bottom footpad plate to the top footpad plate has the highest likelihood of failure. The calculation for this assumes that the bolt will act as a cantilever beam and the jacking bolt will provide a resistance due to friction. The value used for the frictional force of the jacking bolt is .3, which is what was found during friction testing with similar materials. This value should be extremely conservative because the geometry of the bolt should create greater forces.

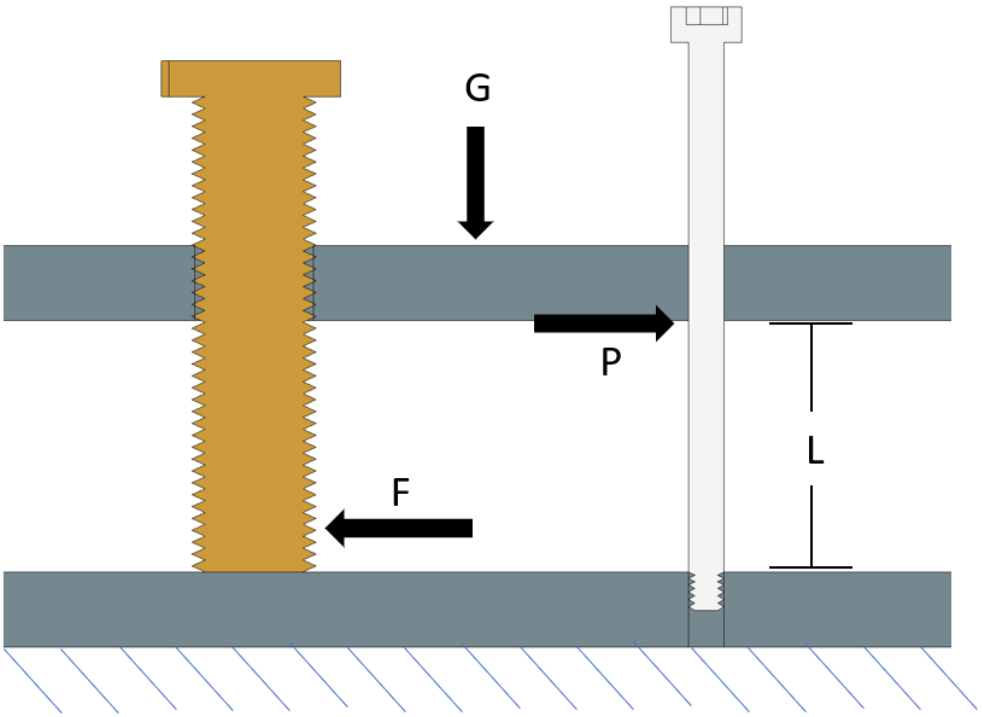

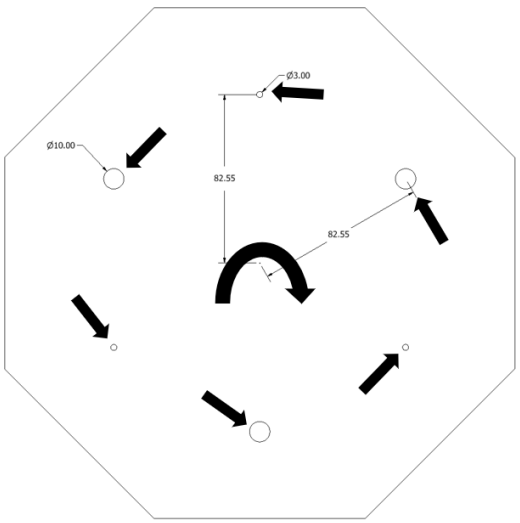

CRP Mass (m)	225	kg
Gravitational Force (G)	625	N
Coefficient of Friction (μ)	0.3	-
Moment Arm (L)	0.021	m
Diameter of Retention Bolt (D)	0.003	m
Ultimate Strength (σ_{ult})	70,000	psi
Frictional Force (F)	316	N
Moment of Inertia (I)	3.98×10^{-12}	m^4
Force Acting on Bolt (P_{max})	30.4	N

Equation 6 $\boldsymbol{F = \frac{m}{4} * 9.81 * \mu}$

Equation 7 $\boldsymbol{I = \pi \frac{D^4}{64}}$

Equation 8 $\boldsymbol{P_{max} = \frac{\sigma_{ult} * I * D}{2 * L}}$

Equation 9 $\boldsymbol{M_{max} = L_M(3(P + F))}$

Moment Arm Length (m)	0.083	m
Frictional Force (F)	316	N
Force Acting on Bolt (P_{max})	30.4	N
Maximum Allowable Moment (M_{max})	61	N-m

Appendix 3: Lifting Device Stress Analysis

CRP Lifting Device Stress Analysis

1 Introduction

1.1 General Summary of Document

This document presents the analysis of forces and stresses which will be acting on the CRP Lifting Device during the installation of the CRP (Charge Readout Plane). The analysis in this document demonstrates that the CRP Lifting Device is safe and will fuction as intended.

1.2 Design Code: ASME BTH-1-2017

The components within this application follow ASME BTH-1-2017 *Design of Below-the-Hook Lifting Devices*. According to this standard this assembly is classified as a "Design Category A" and "Service Class 0" device. The following section of this report verify that these classifications are met.

1.3 Safety Factors

In accordance with ASME BTH-1-2017 para. 3-1.3.1, a Design Category A lifter has a nominal design factor of 2.0 for yielding or buckling and 2.40 for limit states of fracture and for connection design.

1.4 Project Requirements

The CRP lifting device described in this report must be able to be attached to a crane, used to pick up a fully assembled CRP, and used to install a CRP with percision.

1.5 A note on design weights

The design weight of the bottom CRPs has not yet been finalized. As of 24 February 2023 the weights of CRP5 and CRP4 were estimated at 255 kg. Since the exact weight of the CRP was not known when designing the lifting system, a conservative estimate of 300 kg for the weight of the CRP was assumed. All calculations in this report assume a CRP weight of 255 kg.

1.6 General description of Sub-Sections

SUB-SECTIONS		
SECTION	*QTY*	*SECTION NOMENTCLATURE*
A	*1*	*Tines and Tine Supports*
B	*1*	*Spreader Beam*
C	*1*	*Carriage Boom*
*D**	*1*	*Cable System*
*E**	*1*	*Block and Tackle Assembly*

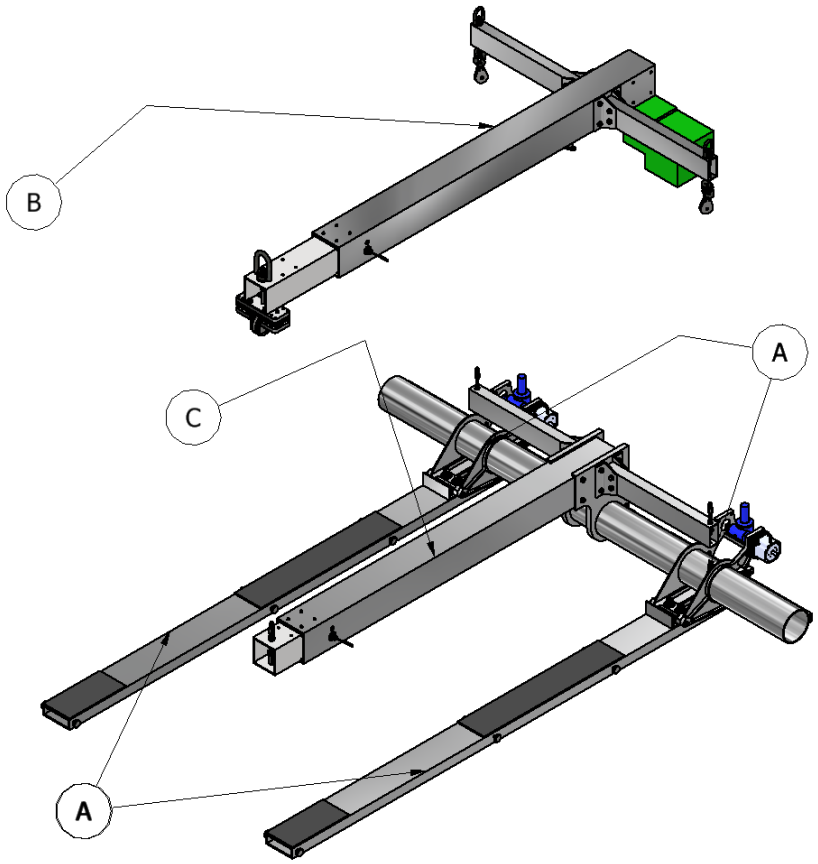

Figure 42: Illustrated Parts Breakdown for bottom CRP lifting device.

2 General Force Analysis

2.1 Loading

This lifting device is designed to be used in a slow and controlled manner. The applied load has therefore been modelled as static with a gravity vector positioned at the center of mass acting as its force contributer. Two load cases will be considered, corresponding to a single lift point and double lift point.

2.2 Mass of all components below the hook while in use

The total mass of all components under the hook is **442 kg**. All assemblies are labeled in Table 7. A CRP mass of 255 kg was used for all analyses in this document. All safety factors calculated in this report do not include the additional factor of safety that is associated with the use of 150% CRP mass. This means all safety factors are conservative.

Table 7: Mass of all CRP lifting device components.

Component Name	***Mass [kg]***
Tines	*22.5 (each)*
Carriage Boom	*50*
Spreader Beam	*70*
Tine Straps	*11 (each)*
CRP	*255*
Total Mass	***442***

2.3 Load Case 1: Single lift point

In the single lift point configuration, three lengths of chain and lifting straps are used to lift from each eye bolt to a point directly above the center of mass of the unit with the CRP installed. Each lifting strap will apply a force vector from the lifting point to the attachment point, as illustrated in Figure 2
Figure 243. Due to the process of installing a CRP, the center of mass may move depending on the location of the CRP relative to the lifting device. Since all three lifting straps are attached the same point, the CRP lifting device in this configuration will redistribute the load between the different lifting points.

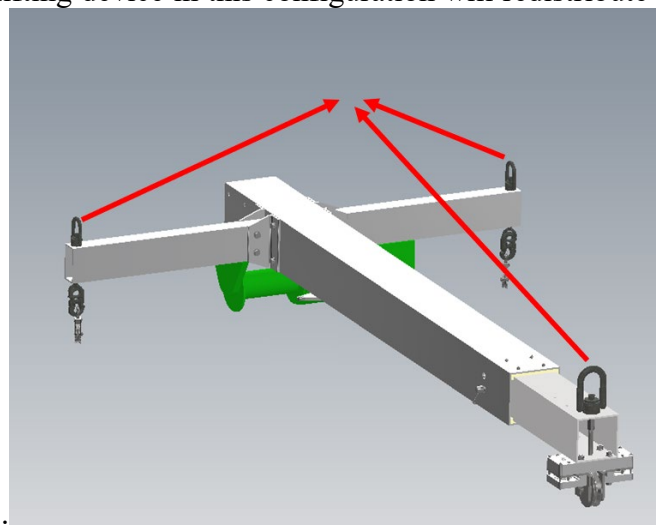

Figure 243: Force vectors from chains and straps attached to single lift point.

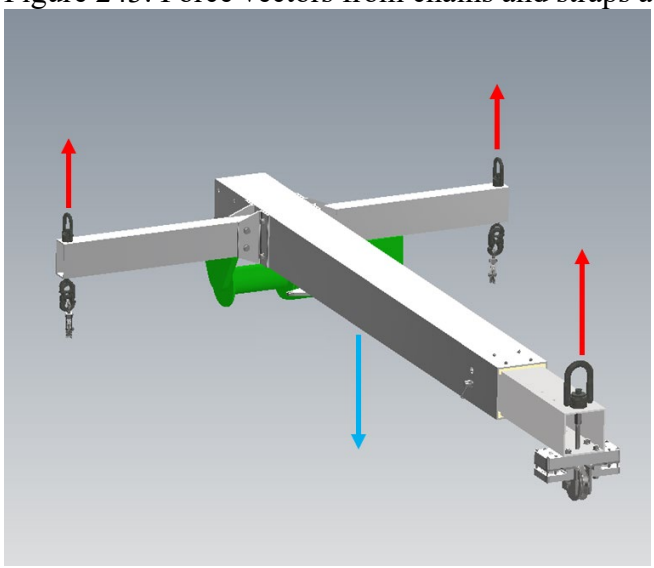

Figure 344: Force vectors in an extreme case where each vector represents the entire weight of the system.

For ease of calculations the most extreme scenario is used. This scenario for load case 1 is that the weight of the device is being lifted from an individual point, and that the center of mass is directly below that lifting point. This would result in a force of **4336 N** due to the mass of the system. All masses have been recorded in Table 7: Mass of all CRP lifting device components. The extreme case would then assume this entire force on all three lifting points at the same time as seen in

. This makes the position of the center of mass irrelevant and therefore there is no need to calculate the angle of the force vector for every center of mass possibility.

2.4 Load Case 2: Dual lift points

In load case 2, the CRP lifting device will be lifted from the front and the rear from two different lift points. Each lifting strap will apply a force vector to the lifting point, as illustrated in Figure 45. Depending on the angle of the lifting device and the center of mass, the forces associated with each lift point may vary. Using the same logic as for load case 1, the extreme case will be assumed. This results in the same result as load case one. For all following calculation **4336 N** will be assumed for all forces on the spreader beam lifting points.

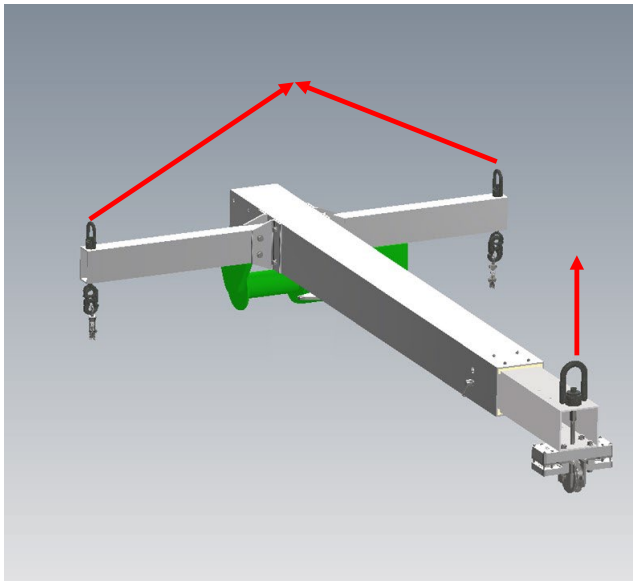

Figure 45: Force vectors from chains and straps attacked to two lift points.

2.5 Spreader Beam to Carriage Boom Analysis

The lower carriage boom is attached to the upper spreader beam by cables. While suspended under the spreader beam the carriage boom will act as a pendulum. The mass of all components below the spreader beam is 4336 N. While under load case 1, a dual pendulum is formed and this will result in the weight being equally distributed between the the three cables connecting the spreader beam to the carraiage boom. Under load case 2, the center of mass has the potential to vary. To avoid complex calculations, the extreme senerio associated with the center of mass being under the cables will be assumed. For the following calculations **4336 N** will be assumed for all forces on the cables connecting the spreader beam to the carrige boom, as seen in Figure 46.

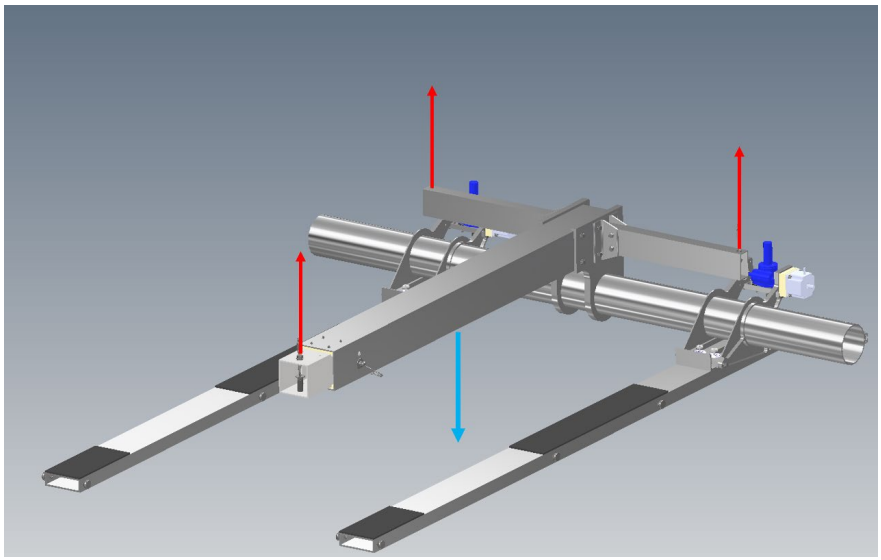

Figure 46: Most extreme case where each force vector equals the weight of everything below the spreader beam.

3 Materials and Hardware

Table 8: Materials and material properties used within this analysis. All values for metals were obtained from the material manufacturer.

Material	***Tensile Yield Strength (MPa)***	***Modulus of Elasticity (GPa)***	***Part Index from IPB***
6061-T6 Aluminum	*276*	*310*	*B.8,B.10,B.12,C.4,C.6,C.7,C.13*
Hardened 4140 Chromoly Steel	*685*	*140*	*E.3*
1566 carbon Steel	*517.1**		*B.9.a, E.1, E.4*
1144 Carbon Steel	*420*		*B.11,C.8*
Grade 5 Bolts	*827**		*B.15*
Class 8.8 Bolts	*640**		*B.1, B.9.a, B.13,C.11,C.12*

4 Tines

Deflection of the Aluminum tines was modelled in FEA using beam elements and contact between the aluminum beam and rigidly modelled CRP adapter plates and tine support. The tines are elastically modeled as 6061-T6 Aluminum rectangular tube, whose properties are given in Table 28. The incline of the tines was varied from 0 to 5 degrees, pivoting about a point representing the pivot of the tine supports.

The tines are modeled using 88 beam elements. The beam elements are defined by the rectangular tube cross-section of the tines, which is 152.4 mm wide, 50.8 mm tall, with a 6.35 mm thick wall. See inset of Figure 47. The tine beam is bonded to the rigid tine support plate. Adapter plates are modeled as rigid body subsections which contact the tine. Note that figure graphics appear to show the tine support and adapter plate sections intersecting the tine beam.

This is a graphical artifact, as the tine is made of 1D line elements, thus the plates contact the centerline of the tine, not the graphically generated tine preview.

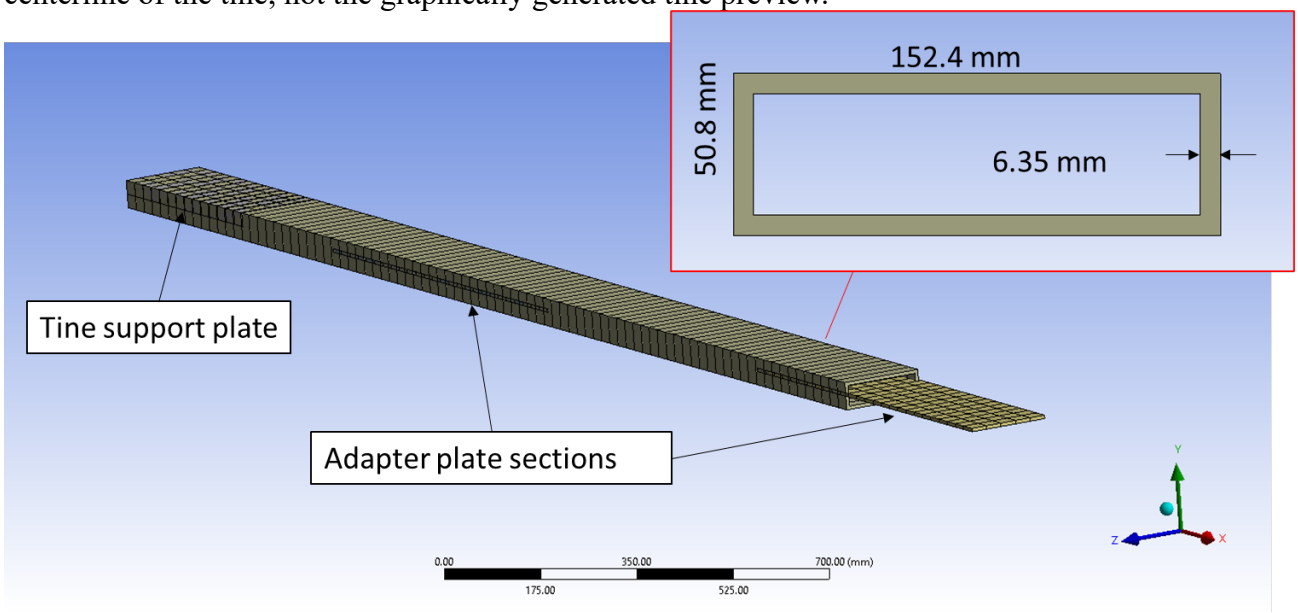

Figure 47: Mesh for the tine loading model. The tines are defined by beam elements with a cross-section shown in the insert.

4.1 Loading

A variety of loadings were applied to the tines, representing CRP weights up to 455 kg.
A 305 kg load was taken as the representative load case. This applies 1500N to each of the tines. This is applied to the tine model as a 1500N load spread across the rigid adapter plate sections, shown as load A in Figure 48. Applied as a downward force on the adapter plates, the force remains down as the adapter plate translate and rotate in space as one rigid assembly. This allows the adapter plates to push the tine downward and rotate to match the droop of the tine.

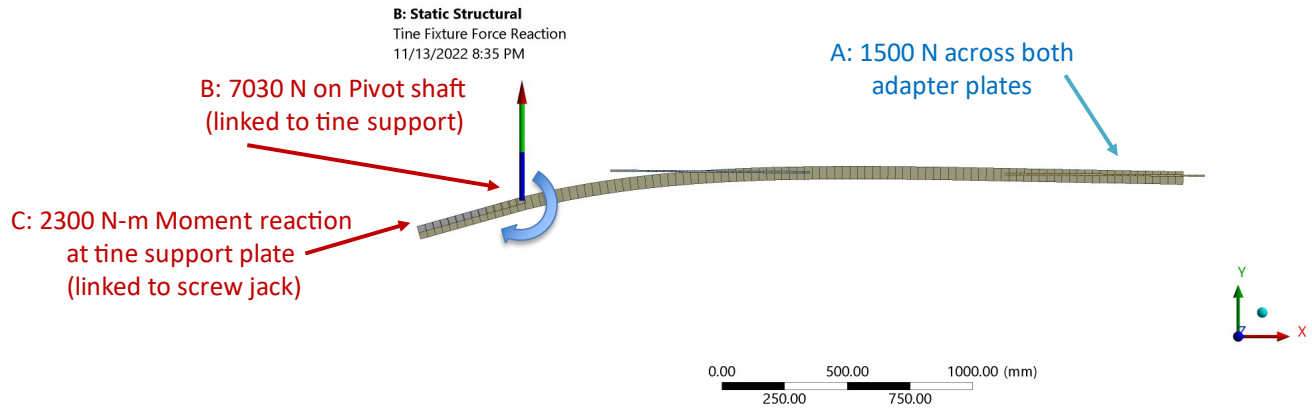

Figure 48: Forces and supports on the tine model for a 305 kg CRP load

Displacement of the tine is fixed but rotation is free at the point of the pivot shaft, support B. The reaction here is 7030 N. A 2300 N-m moment about the pivot is resisted at the end of the tine support plate, where the screw jack is connected to the support plate, see support C. The forces on the tine support fastening components are calculated from these loads:

- *Angle adjustment jack, 5530 N (1243 lbf) on connecting wheel*
- *Pivot shaft, 3515 N (790 lbf) in single shear on each side of shaft*
- *At cross bar key, 28536 N (6415 lbf) in double shear*
- *On each of the 2 ball-lock fasteners, 3293 N (740 lbf)*

4.2 Treatment of Contact between Tines and the CRP

4.3 Ball Locks

Two ball locks are used to clamp the tine support plate to the tine. The ball locks use a back mount bushing inside the tine, see Figure 49, that anchors the ball locks. When the ball lock is torqued to 35 in-lbs the balls will expand into the back mount bushing and provide 13.3 kN of holding force. Each tine support has two ball locks equating to a total of 26.6 kN of holding force.

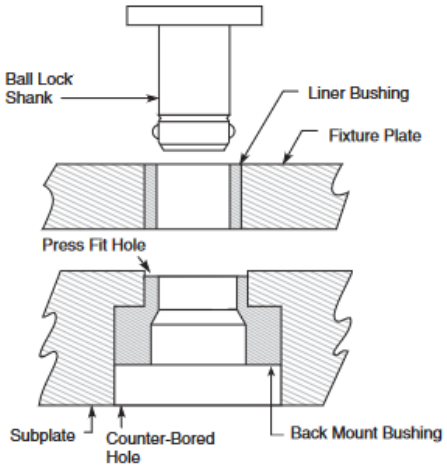

Figure 49: Ball lock for clamping the tine support to the tine.

4.4 Contact

Varying contact of the adapter plates with the bending tine is considered. A friction contact region between the adapter plates and tine is defined with a coefficient of friction of 0.3. This allows the bending tine to separate from the adapter plate, creating a gap at the near end of the tine. Load is redistributed forward to parts of the tine still in contact with the adapter plate.

4.5 Stress in the Tine

The tine loading model was run at a variety of tine incline angles and CRP loads. The largest load considered was 2230 N through the adapter plates, corresponding to a 455 kg CRP (170% of the 255 kg design weight). This resulted in a maximum combined stress of 84.8 MPa, a factor of 2.8 less than the 240 MPa yield stress of 6061-T6 Aluminum. This meets the 2.0 design factor required in ASME BTH-1-2017 para. 3-1.3.1. The maximum combined stress within elements of the beam is show in Figure 9, this is the combination of bending and normal stress in the beam.

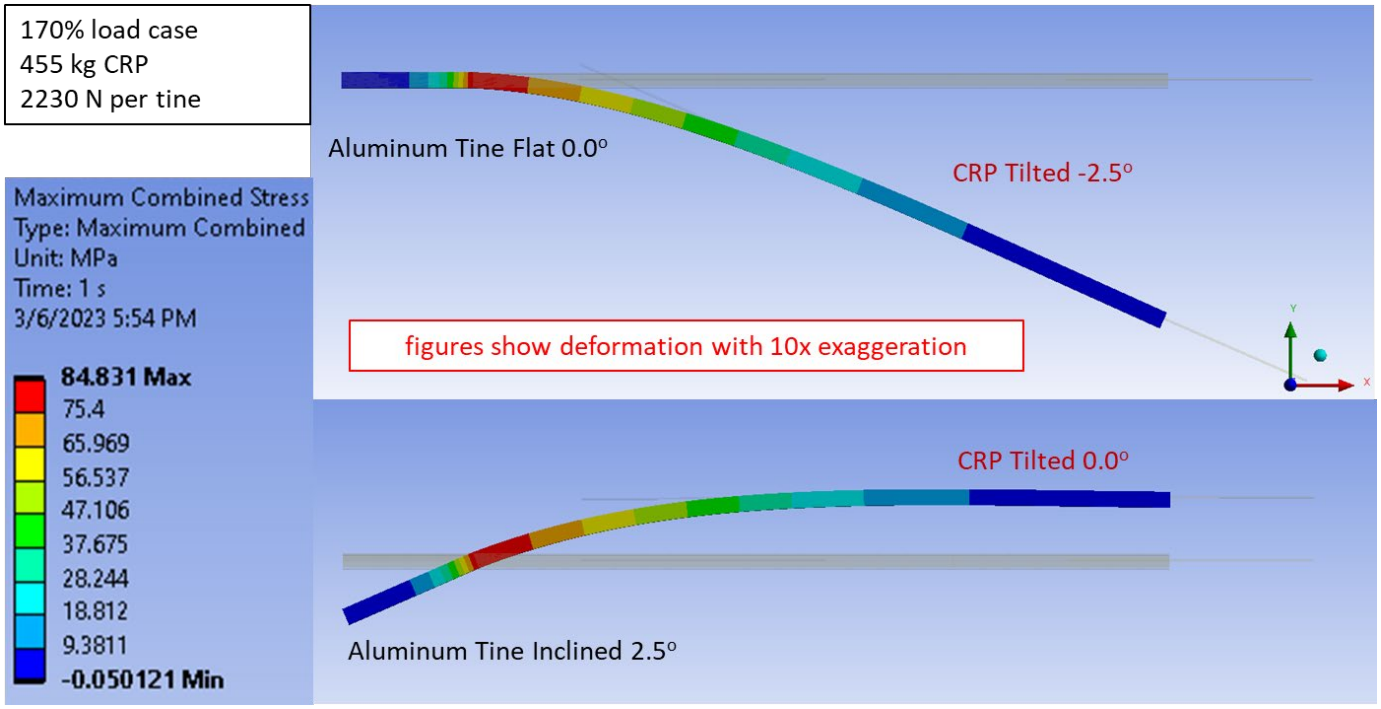

Figure 50: Stress in tine beam for 455 kg CRP load case. (top) stress and deflection of the tine when the tine support has 0º incline, (bottom) stress and deflection when the tine support has 2.5ºincline,

The maximum stress is located in the tine section spaning between the tine support plate and the first point of contact with the adapter plate. Maximum stress remains relatively the same as tine angle increases. Variation of tine angle from 0-5 degrees doesn't shift the weight of the CRP enough to create a noticible drop in tine stress. Incline of the tine support allows the CRP to be held level with 0º of tilt.

4.6 Ball locks

The tines are attached to the tine support plate with two 20 mm diameter Jergens Ball lock quick clamping fasteners.

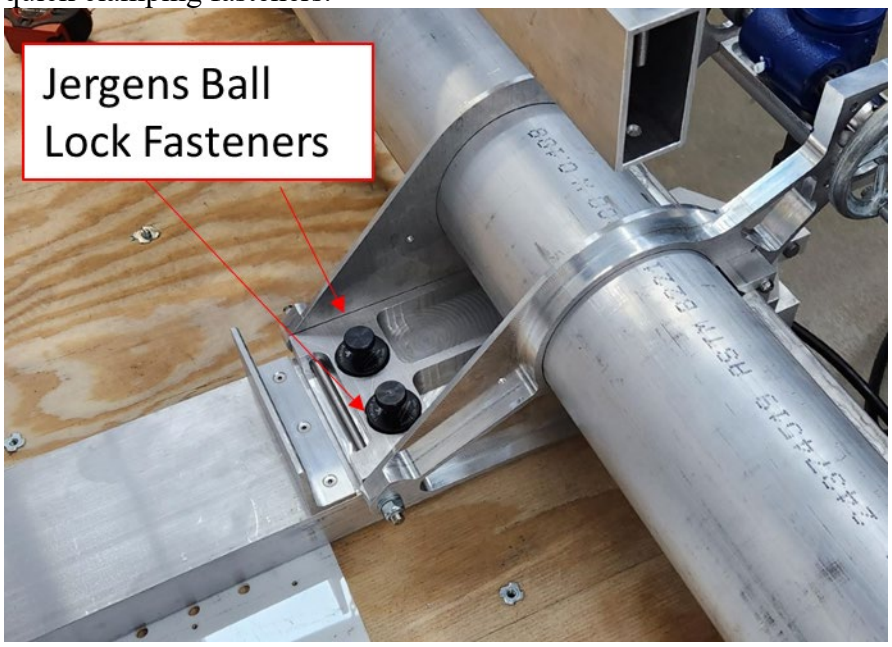

Figure 51: Two 20mm diameter Jergens Ball lock fasteners attach the tines to the tine support plate

When tightened to the recommended torque each of these fasteners clamps the tine to the support plate. The manufacturere gives the following recommended and maximum tightening torque and corresponding clamping loads in Table 3.

Table 9:Clamping load of 20mm diameter Jergens Ball Lock Fasteners

	Screw Torque		Clamping Force	
	ft/lbs	N-m	lbf	N
recommended	3	4.1	2250	10008
maximum	4	5.4	3000	13345

When tightened to the recommended 4.1 N-m torque, the ball lock fasteners hold a clamping force 3.04 times greater than the 3293 N load applied to each fastener by a 305 kg CRP. The 2.0 design factor required in ASME BTH-1-2017 para. 3-1.3.1 is met.

5 Tine Incline Adjustment Jack

The angle of the tines is adjusted by extending a screw jack. The jack pushes on the tine support plate at a position 438.15 mm behind the tine support pivot point. From the tine analysis, Section 4.1, the jack pushes on the tine support plate with 5530 N, counteracting the 2300 N-m moment applied by the tines. This is for a 305 kg CRP load on the tines.

The screw jack pushes down on a -2.5° angled plate through a 62mm steel wheel. The wheel and angled plate allow the contact point to roll back as the tine plate changes incline. The wheel is attached to the rod of the screw jack using a clevis rod end. The jack is fully retracted at 0º of tine incline, extending past its housing by 29.2 mm. This 0º position is shown at left in Figure 52. In this position the jack can be backed off of the tine support plate, and load is transferred to a steel square tube stop which surrounds the mechanism. This stop is a fail-safe in case the screw jack rod were to buckle and fail. The stop prevents the tine support from declining past 0º.

As the jack is operated its extension increases, reaching 67.4 mm at the 5º limit of incline, see right side of Figure 52. As the tines are inclined past 0°, the stop is no longer in contact and the screw jack rod and wheel bear the full force. Once the desired incline is reached, a spacer block can be inserted in the gap between the stop and screw jack plate, and the load can then be taken off the screw jack and put back on the stop.

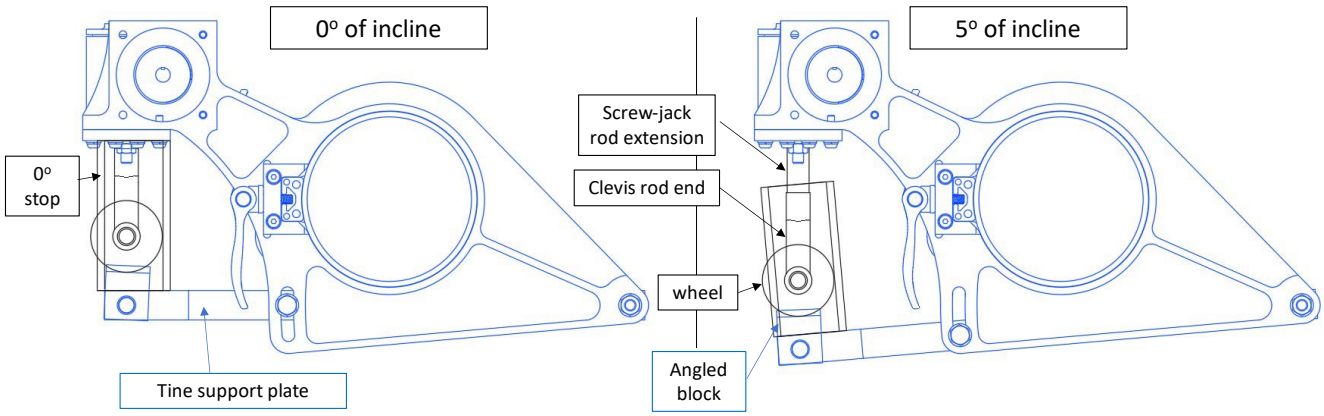

Figure 52: Operation of the screw jack in adjusting the tine support plate angle. (left) at 0° of incline, force is transferred through the tube stop.

5.1 Loading

At 102% CRP load, 260 kg, the force on the screw jack is nominally 4623 N. This is applied to the screw-jack rod as a combination of an axial on-center load and a perpendicular load at the clevis end, see Figure 11Figure 53
Figure 243. This creates a combined buckling and beam bending problem which is best modeled using FEA.

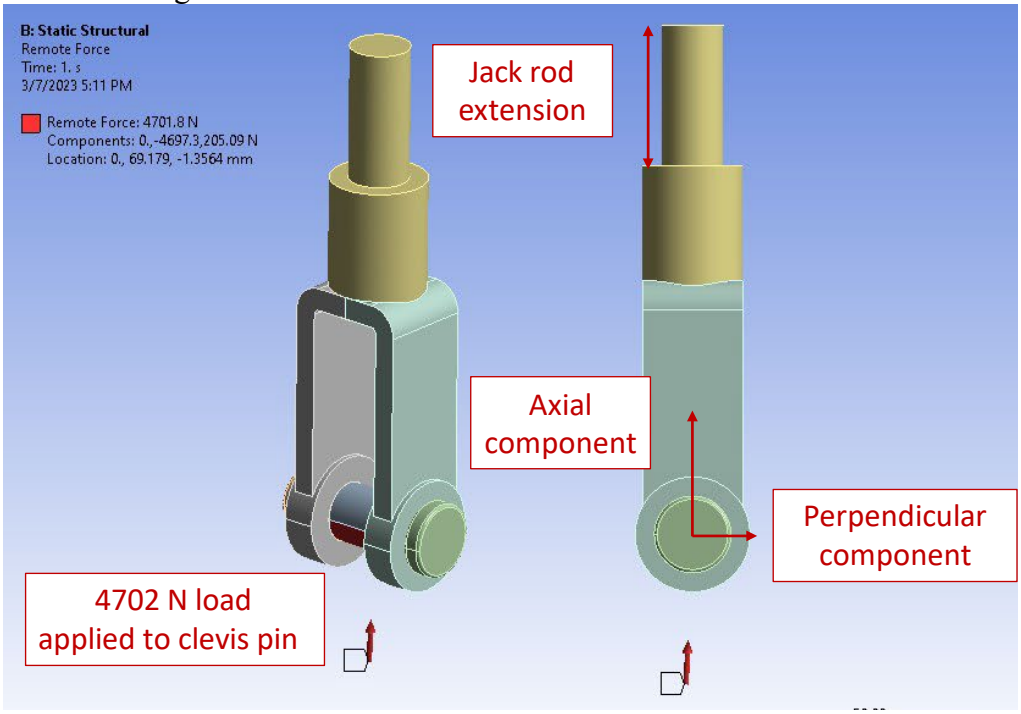

Figure 53: Load on the screw jack rod and clevis rod end; (left) geometry of the model, (right) applied force has axial and perpendicular components.

The screw jack-rod is a ¾-6 ACME threaded rod made out of 1018 Cold Drawn Steel. As the rod is threaded, only the 12.75 mm diameter core of the rod is considered in the model. Elastic properties for the cold drawn steel are used in the FEA model, see Table 2 for properties. The clevis rod end is also modeled as cold drawn steel.

As the incline of the tine support changes, the direction of the load on the screw jack rod changes. The angle block which the wheel contacts creates a -2.5º off center force when the tine support is at 0º inlcine. As incline is increased to 2.5º, the angle of the force decreases to 0º. As incline angle increases past 2.5º to 5º the angle of the force increases to +2.5º. The axial and perpendicular forces on the screw jack rod change through this travel and are summarized in Table 10. Perpendicular force is greatest at 0º and 5º of incline, and 0 at 2.5° of incline.

5.2 Stress in the screw jack

The screw-jack and clevis rod end are modeled using a large deflection analysis. This is more thorough than a standard elastic FEA model, as it captures the changing geometry and position of the clevis-rod end as it is loaded. As the screw-jack rod bends, the clevis rod end and the location of applied force shift to an off axis position. Standard elastic analyses would not capture this shift, while a non-linear large deflection analysis does.

Stress is highest at the root of the screw-jack rod and concentrated on the side of the rod that sees combined axial compression and bending forces. This concentration is shown for the 0α incline case in Figure 54, here the maximum equivalent von Mises stress is 130 MPa.

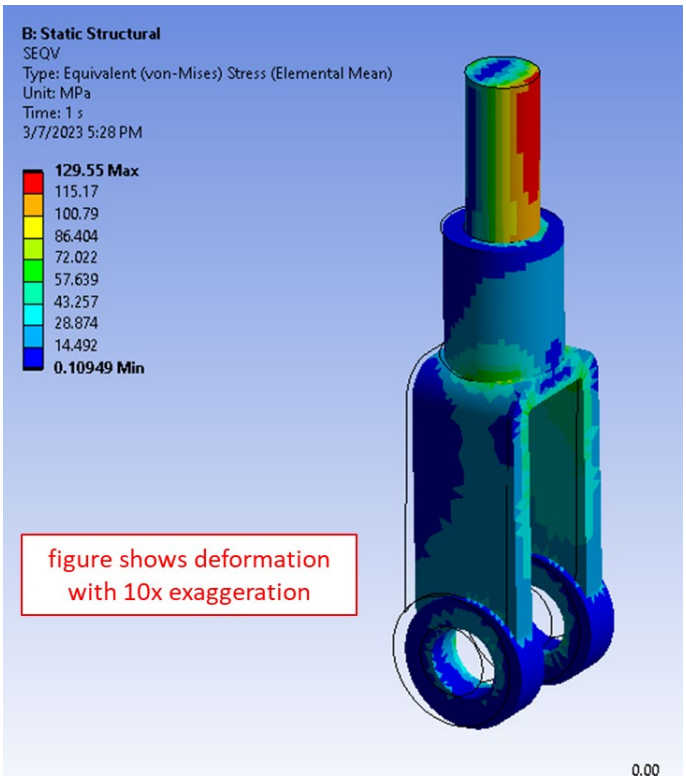

Figure 54: Von Mises equivalent stress in the screw jack rod and clevis rod end

A yield saftey factor for the loading is determined from the maximum equivalent stress, which occurs at one end of the base of the screw jack rod, and the yield stress of cold drawn 1018 steel from which the screw jack rod is made. The yield stress of the 1018 cold drawn steel rod is 370 MPa. Thus the yield saftey factor is calculated as,

$$SF_{yield} = \frac{370MPa}{\sigma_{eqv}}$$

Yield safety factors were determined for three cases of tine support incline angle.

Table 10: Extension, Forces, and Yield Safety Factor of the screw jack at various tine support angles when the system is loaded with a 260 kg CRP.

angle of tine support plate	Extension of Screw-jack		axial force on screw-jack		perpendicular force on screw-jack		Yield Safety Factor
deg	in	m	lbf	N	lbf	N	-
0	1.148	29.2	-1056	-4697	-46	-205	2.86
2.5	1.902	48.3	-1057	-4702	0	0	5.64
5	2.654	67.4	-1056	-4697	46	205	2.01

Yield safety factor is lowest, at 2.01, when the screw-jack rod is at it's furthest extension in the 5° position. This meets the 2.0 design factor required in ASME BTH-1-2017 para. 3-1.3.1.

6 Beam Spreader

6.1 Analysis of all load bearing components in Beam Spreader

All force analysis for the beam spreader assembly assume that a force of 4336 N is acting at the three lift points opposite of the gravity vector direction. Any component that attaches to the beam spreader and the boom carraige is assumed to have a force of 3649 N perpendicular to each attachment point.

B. Spreader Beam

PARTS LIST							
ITEM	*QTY*	*PART NOMENCLATURE*	*LOAD BEARING*	*ITEM*	*QTY*	*PART NOMENCLATURE*	*LOAD BEARING*
1	*4*	*Bolts*	*X*	*10*	*1*	*Beam, Internal Adjustment*	*X*
-	*4*	*Nuts*	*X*	*11*	*1*	*Pin, Positioning*	*X*
2	*1*	*Hoist Ring, Front*	*X*	*12*	*1*	*Beam, Main*	*X*
3	*2*	*Bearing*		*13*	*8*	*Bolts*	*X*
4	*8*	*Bolts*		*-*	*8*	*Nuts*	*X*
-	*8*	*Nuts*		*14*	*8*	*Bolts*	
5	*2*	*Pulley Assembly, Side*	*X*	*-*	*8*	*Nuts*	
6	*2*	*Pulley Link, Side*	*X*	*15*	*1*	*Winch, Cable*	*X*
7	*2*	*Hoist Ring, Rear*	*X*	*-*	*4*	*Bolts*	*X*
8	*2*	*Spreader Bars*	*X*	*-*	*4*	*Nuts*	*X*
9	*1*	*Pulley Assembly, Front*	*X*				

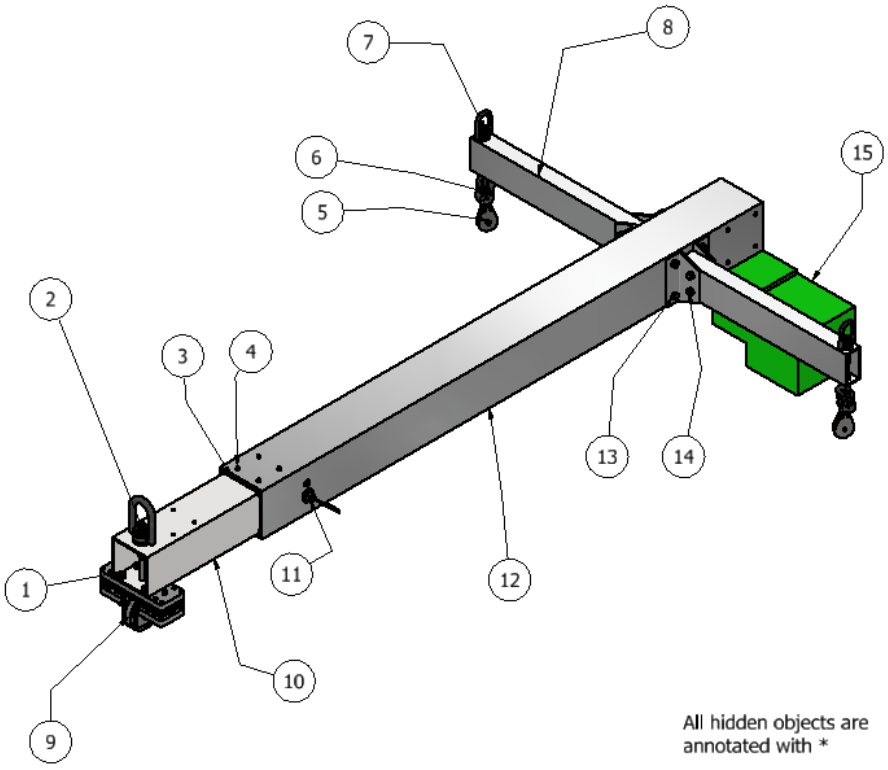

Figure 55: Individual parts breakdown of beam spreader.

B.1- Bolts and Nuts for front pully assemble

See cabling section for analysis.

B.2- Front Hoist Ring

This 6-1/8" hoist ring, PN2994T91, has a manufacturing vertical load capacity of 2500 lbs (1134 kg) and is rated for lifting at angles from 90° vertical to 30°. As lifting angle decreases, the vertical lift capacity of the hoist ring decreases with angle α from the horizontal,

$$Vertical\ Capacity = 1134\ kg * \sin(\alpha)$$

The vertical lift capacity of the hoist ring is given for various angles in Table 11.

Table 11: Vertical lift capacity of front hoist ring at various lift angles

Angle of lifting strap, α, in deg	Vertical lift capacity, in kg
90	1134
80	1117
70	1066
60	982
50	869
45	802
40	729
30	567

The front hoist is safe for lifting the full 255 kg weight of the CRP at angles down to 30° from the horizontal, as the manufacturer rated vertical lift capacity is not exceeded.

B.5- Front Pulley Assembly

See cabling section for analysis.

B.6-Side Pulley Link

See cabling section for analysis.

B.7- Rear Hoist rings for Lifting

This 3/8"hoist ring, PN2994T63, has a maunfaturing vertical load capacity of 1000 lbs (453 kg) and is rated for lifting at angles from 90° vertical to 30°. As lifting angle decreases, the vertical lift capacity of the hoist ring decreases with angle α from the horizontal,

$$Vertical\ Capacity = 453\ kg * \sin(\alpha)$$

The vertical lift capacity of the hoist ring is given for various angles in Table 12.

Table 12: Vertical lift capacity of rear hoist rings at various lift angles

Angle of lifting strap, α, in deg	Vertical lift capacity, in kg
90	453
80	446
70	426
60	392
50	347
45	320
40	291
30	227

Each back hoist is safe for lifting the full 255 kg weight of the CRP at angle down to 40° from the horizontal, as the manufacturer rated vertical lift capacity is not exceeded at these angles. At hoist angles below 40° from the horizontal, the hoist rated load is exceeded. The back hoist rings should not be rigged with chains, straps, or other lifting attachments at angles below 40° from the horizontal.

B.8-Spreader Bars

The spreader bars are symmetric and have identical forces acting on each beam. They can be modeled as a cantilever beam fixed at the main beam. The geometry of the spreader bar, see Figure 56, has an area moment of inertia of $5.04 \times 10^{-6}\ m^4$ and this results in a maximum

stress of 26.64 MPa at the base of the spreader bar when a force of 4336 N is applied to it, see figure Figure 57. This results in a safety factor that is higher than 2 and satisfies the requirement of ASME BTH-1-2017 para. 3-1.3.1.

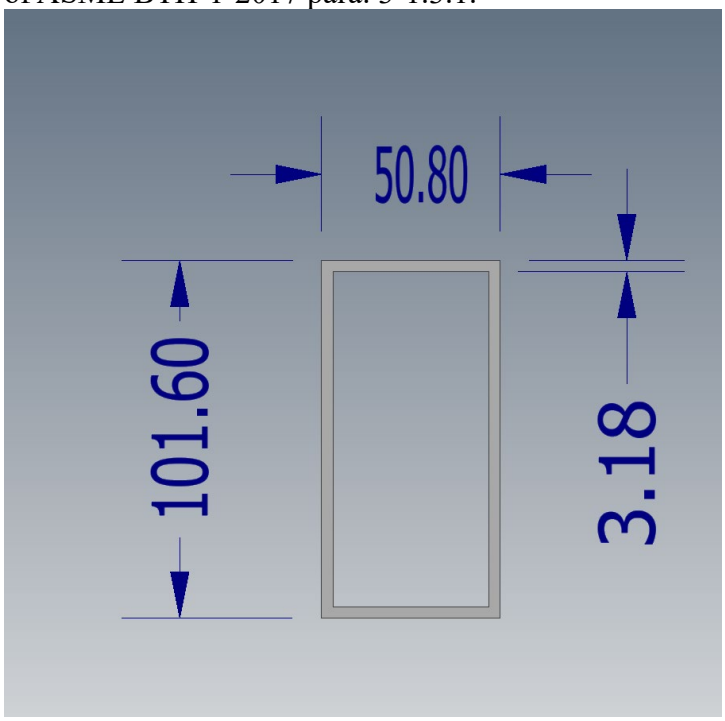

Figure 56: Cross sectional geometry of spreader bars, all dimensions are in units of millimeters.

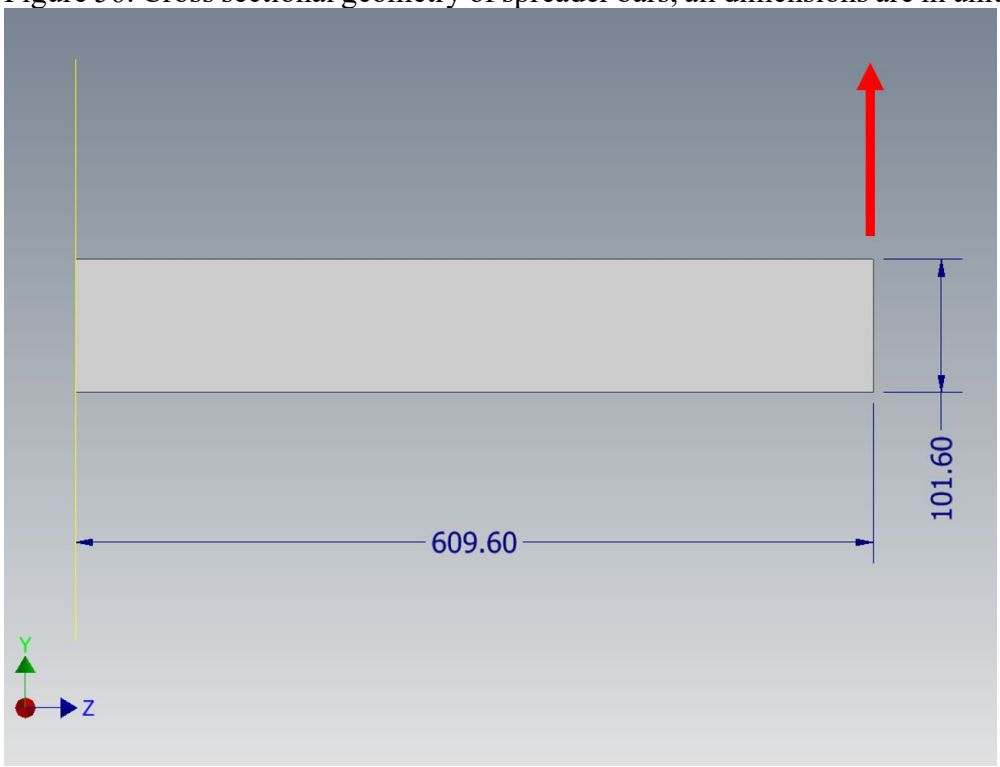

Figure 57: Beam bending force diagram for spreader bars.

B.9- Front Pulley Assembly

See the cabling section for analysis.

B.10-Internal Adjustment Beam

The internal adjustment beam for the spreader beam can be modeled as a cantilever beam fixed at the cross beam extending 0.572 m. The area moment of inertia of $1.52x10^{-5}$ m^4, see Figure 58, and will experience a maximum stress of 10.35 MPa at the base of the internal adjustment beam. This results in a safety factor higher than 2, which satisfies the requirement of ASME BTH-1-2017 para. 3-1.3.1.

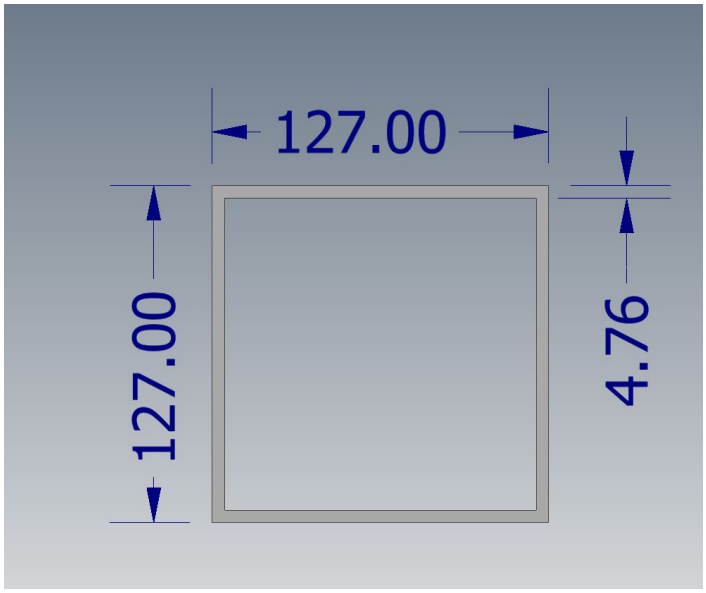

Figure 58: Cross sectional geometry of the internal adjustment beam, all dimensions are in units of millimetres.

B.11-Postioning Pin

The positioning pin holding the internal adjustment beam and the main beam in position will experience shear if there is any horizontal load applied to the internal adjustment beam as shown in Figure 59. The extreme case of the potential load that could be applied to the adjustment pin occurs if the weight of the entire system is applied using a force that is perpendicular to the pin being 4336 N. This amount of force being applied to the internal adjustable beam will create 15.21 MPa of shear stress on the pin. This pin is made from 1144 carbon steel. The shear force that this pin will experience results in a safety factor greater than 2 which satisfies the requirement of ASME BTH-1-2017 para. 3-1.3.1.

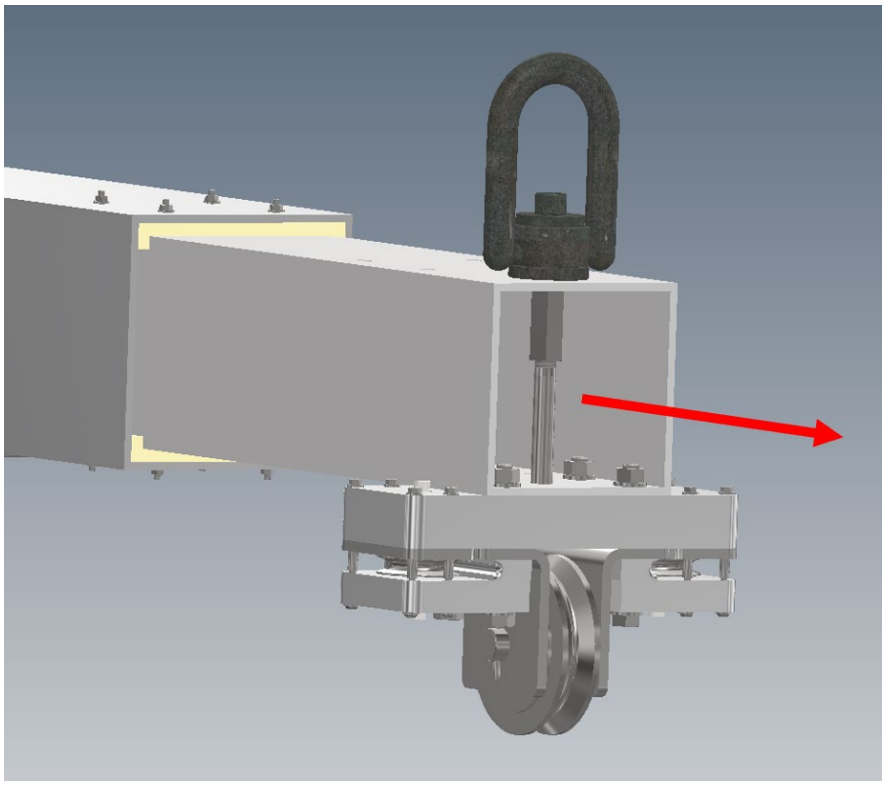

Figure 59: Force applied to position pin.

B.12- Main Beam

The main beam can be modelled as a cantilever beam fixed at the cross beam, see Figure 60. The area moment of inertia of $1.023 \times 10^{-5}\ \mathrm{m}^4$, see Figure 61, and will experience a maximum stress of 68.91 MPa at the base of the main beam. This results in a safety factor higher than 2, which satisfies the requirement of ASME BTH-1-2017 para. 3-1.3.1.

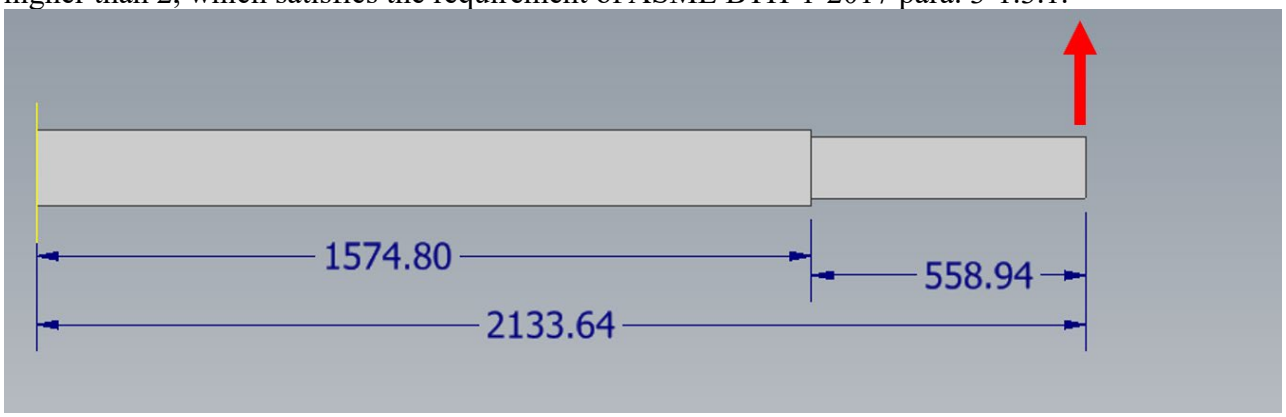

Figure 60:Beam bending force diagram for main beam.

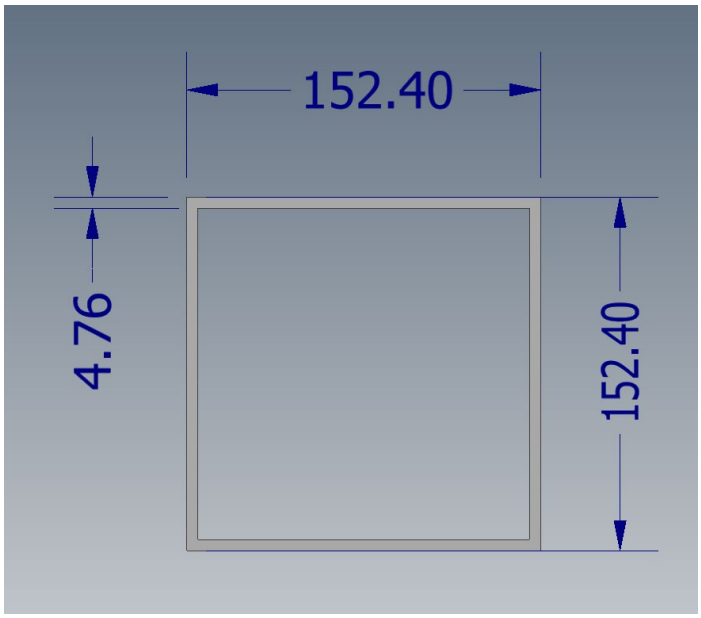

Figure 61:Cross sectional geometry of main beam.

B.13-Bolts and Nuts for Spreader Bars

The spreader arm has four M10 grade 8.8 bolts which are symetrically placed, see Figure 62. The force transferred to the spreader bars from the cable system will result in a moment at the top of the bracket illistrated in Figure 63. This moment can then be assumed to be located at the center of symmetry and held in static equilibrum by the two pairs of bolts. The sum of moments about the axis of pivot forces on each bolt can be calculated. The maximum force that any of these bolts would experience is 15.9 kN resulting in a stress of 202.9 MPa. This results in a safety factor of 2.0 or greater which satisfies the requirement of ASME BTH-1-2017 para. 3-1.3.1.

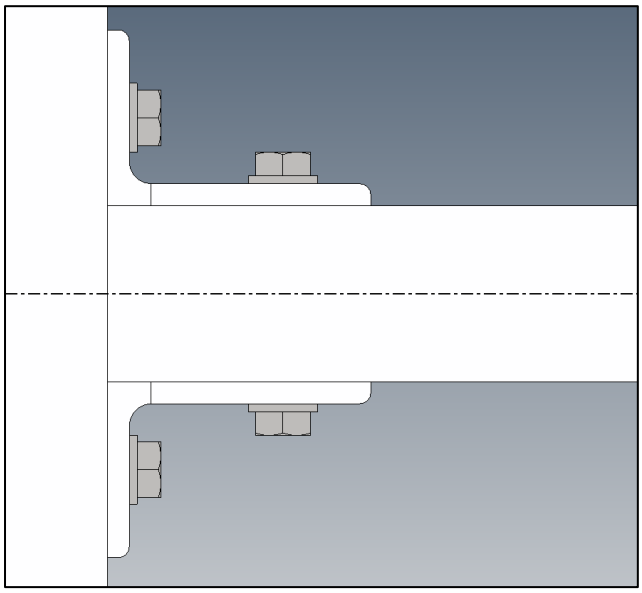

Figure 62: Top-down view of cross spreader bar bolt pattern, showing the symmetry.

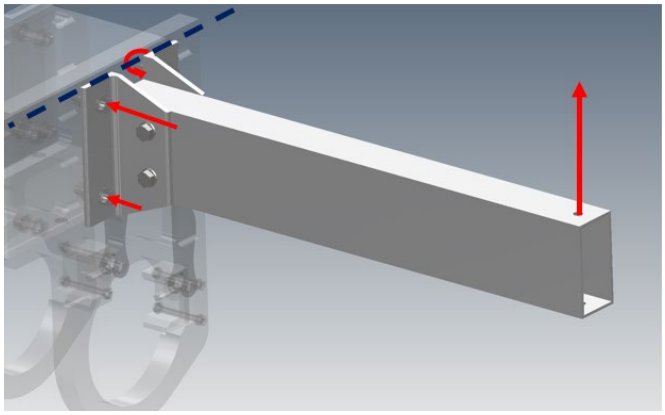

Figure 63: Beam bending force diagram for bolts on spreader bars.

B.14-Wench and mounting bolts

See the cabling section for analysis.

7 Boom Carriage

7.1 Analysis of all load bearing components in Boom Carriage.

All force analysis for the boom carrige assembly assumes that a force of 3649 N is acting at the three lift points opposite the gravity vector direction.

C. Boom Carriage

PART LIST							
ITEM	*QTY*	*PART NOMENCLATURE*	*LOAD BEARING*	*ITEM*	*QTY*	*PART NOMENCLATURE*	*LOAD BEARING*
1	*1*	*Lifting Point, Front*	*X*	*9*	*8*	*Bolts*	
2	*2*	*Bearing*		*10*	*2*	*Support, Crossbar*	*X*
3	*8*	*Nuts*		*11*	*4*	*Bolts*	*X*
4	*1*	*Beam, Main*	*X*	*-*	*1*	*Nuts*	
5	*2*	*Lifting Point, Rear*	*X*	*12*	*8*	*Bolt*	*X*
6	*2*	*Spreader Bars*	*X*	*-*	*1*	*Nuts*	
7	*1*	*Beam, Internal Adjustment Beam*	*X*	*13*	*1*	*Crossbeam*	*X*
8	*1*	*Pin, Postioning*	*X*	*14*	*4*	*Nuts*	*X*

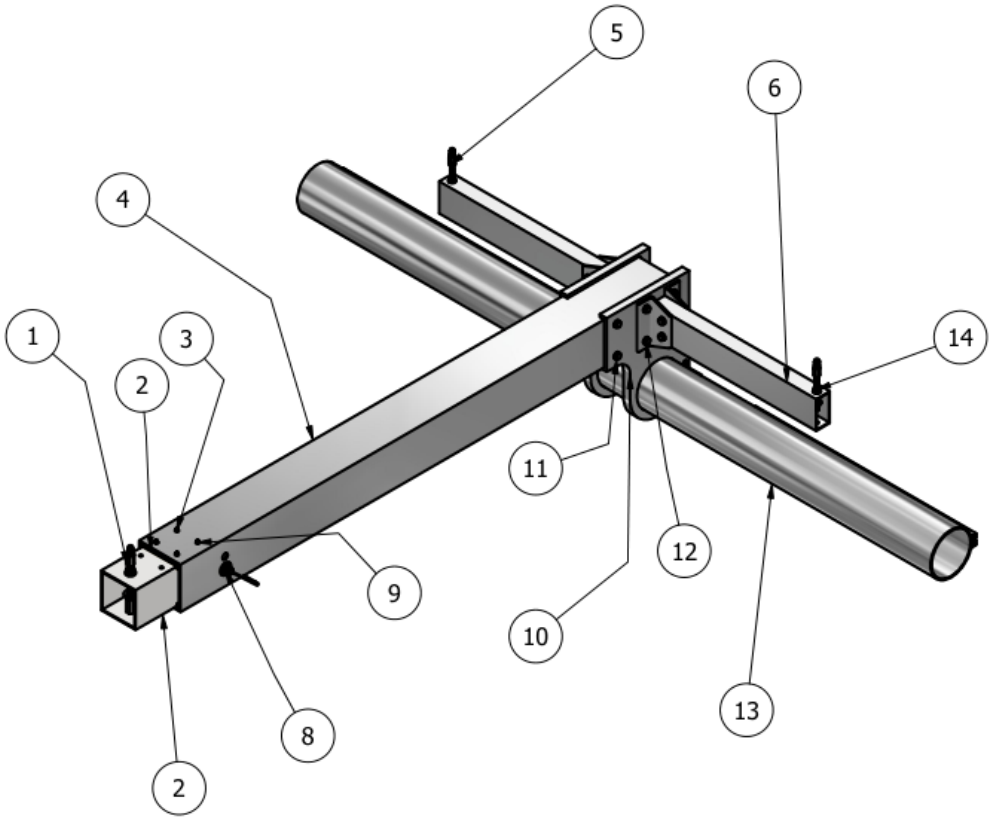

All hidden objects are annotated with *

C.1- Front Lifting Point

See the cabling section for analysis.

C.4- Main Beam

The main beam can be modelled as a cantilever beam fixed at the cross beam, illustrated by Figure 65. The geometry from Figure 64 was used to calculate the area moment of inertia of 1.023×10^{-5} m^4. Using these values, the beam will experience a maximum stress of 59.28 MPa at the base of the main beam. This results in a safety factor higher than 2, which satisfies the requirement of ASME BTH-1-2017 para. 3-1.3.1.

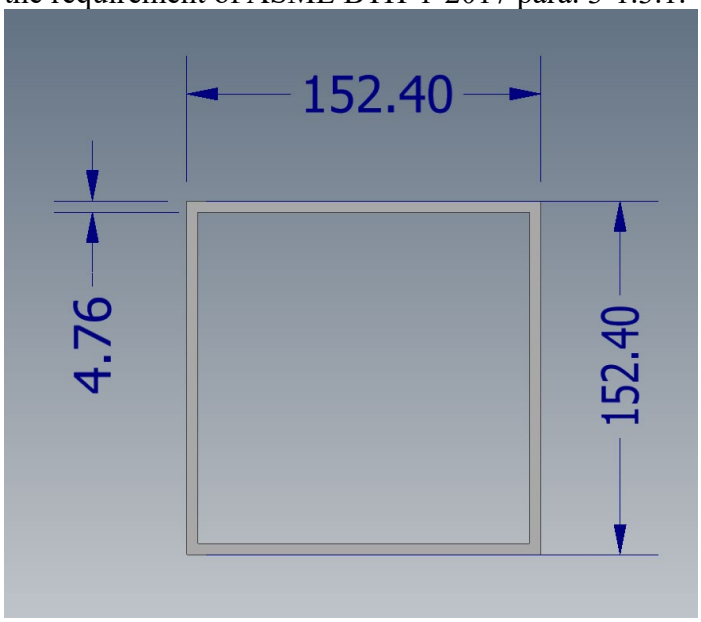

Figure 64: Cross sectional geometry of main beam, all dimensions are in units of millimetres.

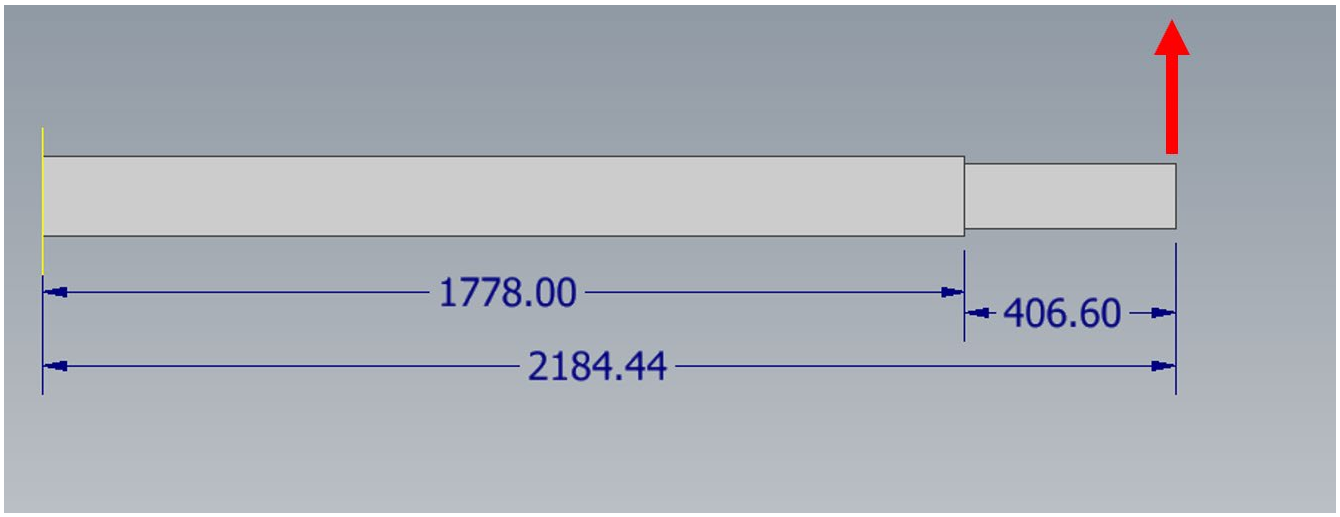

Figure 65:Beam bending force diagram for main beam.

C.5- Rear Lifting Points

See cabling section for analysis.

C.6-Spreader Bars

The spreader bars are symmetric and have identical forces acting on each beam. They can be modeled as a cantilever beam fixed at the main beam extending 0. 0.610 [m]. The area moment of inertia of $5.041x10^{-6}\ m^4$ and maximum stress of 22.42 MPa at the base of the spreader

bars was calculated. This results in a safety factor higher than 2, which satisfies the requirement of ASME BTH-1-2017 para. 3-1.3.1.

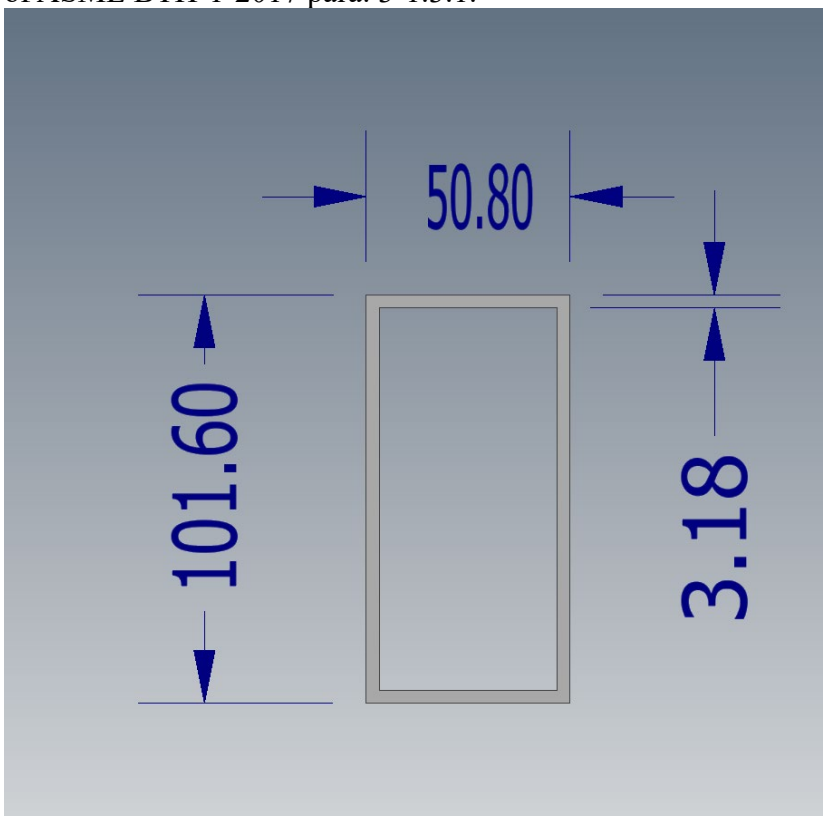

Figure 66:Cross sectional geometry of spreader bars, all dimensions are in units of millimetres.

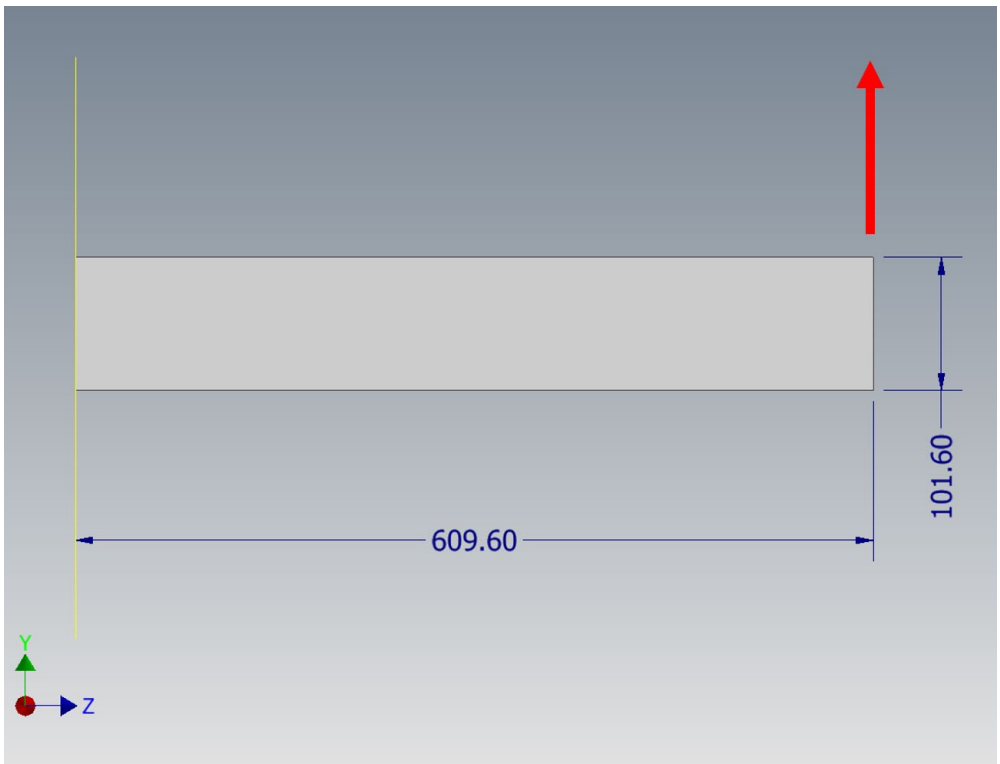

Figure 67:Beam bending force diagram for spreader bars, all dimensions are in millimetres.

C.7-Internal Adjustment Beam

The internal adjustment beam for the spreader beam can be modeled as a cantilever beam fixed at the cross beam extending 0.714 m. The area moment of inertia of $1.52x10^{-5}$ m^4, see Figure 68, and will experience a maximum stress of 11.4 MPa at the base of the internal adjustment beam. This results in a safety factor higher than 2, which satisfies the requirement of ASME BTH-1-2017 para. 3-1.3.1.

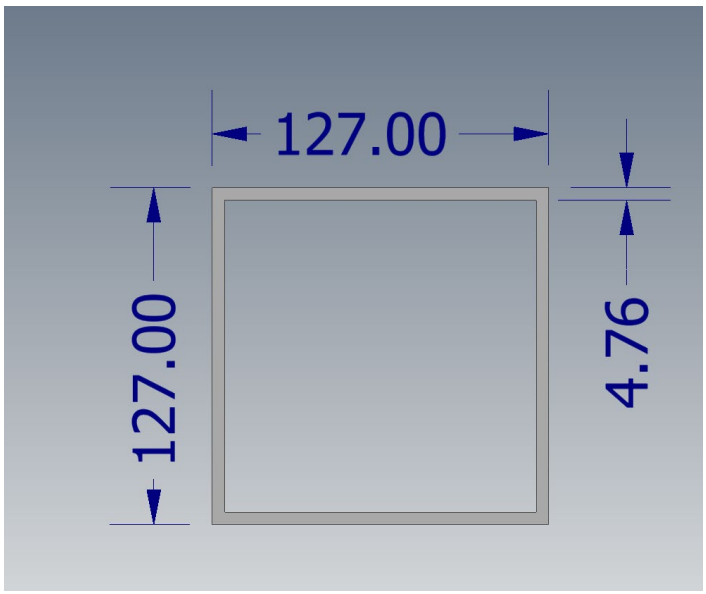

Figure 68:Cross sectional geometry of internal adjustment beam, all dimensions are in units of millimetres.

C.8-Postion Pin

The positioning pin holding the internal adjustment beam and the main beam in position will experience shear if there is any horizontal load applied to the internal adjustment beam as shown in Figure 69. The extreme case of the potential load that could be applied to the adjustment pin occurs if the weight of the entire system is applied using a force that is perpendicular to the pin being 4336.02 N. This amount of force being applied to the internal adjustable beam will create 15.21 MPa of shear stress on the pin. This pin is made from 1144 carbon steel. The shear force that this pin will experience results in a safety factor greater than 2 which satisfies the requirement of ASME BTH-1-2017 para. 3-1.3.1.

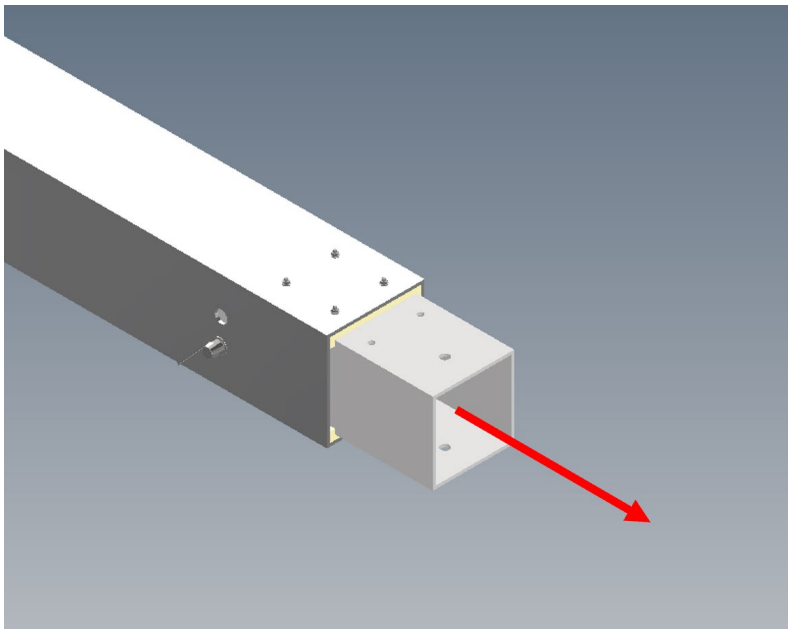

Figure 69:Force applied to position pin.

C.10 Cross Bar Support

The cross bar supports are evaluated using FEA methods as described in Section 8. A minimum yield safety factor of 2.97 was found for a CRP loading of 305 kg, see Figure 76. This results in a safety factor of 2.0 or greater which satisfies the requirement of ASME BTH-1-2017 para. 3-1.3.1.

C.11-Bolts and Nuts for Crossbeam Support

All bolts for the crossbeem support are M10 grade 8.8. These bolts will experience a shear stress of 70.2 MPa assuming the extreme case that the force found in section 2 is applied entirely to a single bolt. This results in a safety factor of 2.0 or greater which satisfies the requirement of ASME BTH-1-2017 para. 3-1.3.1.

C.12-Bolts and Nuts for Spreader Bars

The spreader arm has four M10 grade 8.8 bolts which are symetrically placed. The force transferred to the spreader bars from the cable system will result in a moment at the top of the bracket illustrated in Figure 70. This moment can then be assumed to be located at the center of symmetry and held in static equilibrum by the two pairs of bolts. The maximum force that any of these bolts would experience is 15.9 kN resulting in a stress of 202.9 MPa. This results in a safety factor of 2.0 or greater which satisfies the requirement of ASME BTH-1-2017 para. 3-1.3.1.

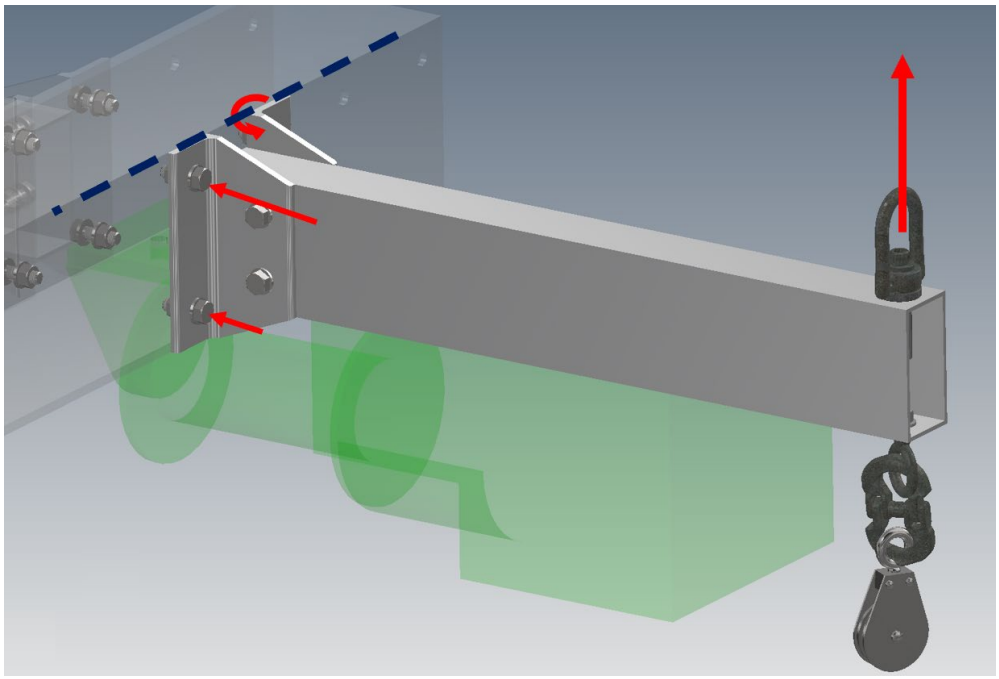

Figure 70: Beam bending force diagram for bolts on spreader bars.

C.13-Cross bar

Loading on the cross bar was modeled in greater detail using FEA, as described in Section 8. This model captured greater detail of the t-slot key and weld that are part of the cross bar, as well as the contact interaction between the cross bar, cross bar support, and tine supports. A minimum yield safety factor of 1.83 was found for a CRP loading of 305 kg, see Figure 77. Correcting for the lighter 255 kg CRP, a safety factor of 2.19 is achieved for 100% CRP load. This results in a safety factor of 2.0 or greater which satisfies the requirement of ASME BTH-1-2017 para. 3-1.3.1.

C.15 Bolts and Nuts for Crossbeam

This bolts are not load bearing due to the weld between beam and bracket. These bolts are a product of design iteration and should be ignored for stress analysis.

8 Crossbar, crossbar support, and tine supports

The tubular crossbar, crossbar support, and tine supports straps were modeled as a full 3D FEA assembly. Half symmetry about the center of the crossbar is taken. The tine straps are modeled at their widest position, as this creates the greatest bending moment on the crossbar. The tines, screwjack mechanism, and boom are considered in separate analyses. All components are modeled as elastic 6061-T6 Aluminum with properties given in Table 7.

8.1 Loading

Loading on the Crossbar is a combination of torque and deadweight loading that is transferred from the loaded tines, as well as gravity on the entire assembly. The loading was assumed to be a 305 kg CRP, which represents 120% of the current 255 kg CRP weight.

The boundary condition loadings and supports applied to the model are shown in Figure 71. A 305 kg CRP was found to exert 3515 N of force on each side of the tine support pivot shaft, totaling 7073 N on the pivot shaft, shown as load A. Each tine is prevented from rotating by a screwjack linkage at the back of the tine support. The load on the tine support throught the screw jack is 5530 N. This is represented as a distributed pinball load, shown as load B. The carriage boom is not modeled, but rather assumed to provide a fixed support for the crossbar support, shown as support C. Symmetry about the center of the carriage is achieved by using a frictionless support at the center of the crossbar, shown as support D. Gravity acts on all components in the model, shown as load E.

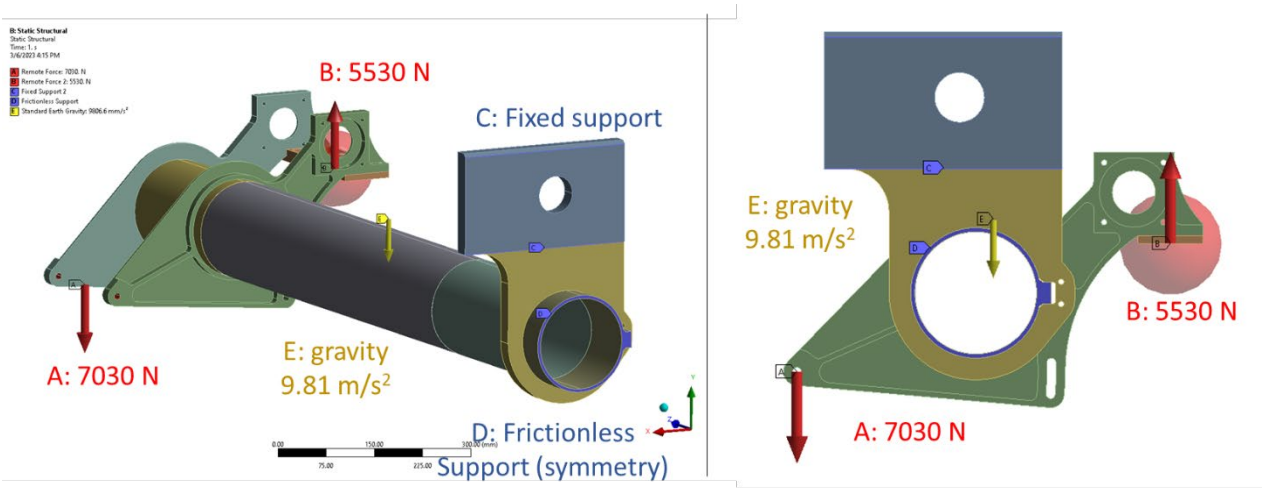

Figure 71: Loadings and Supports on model of crossbar and supports. (left) isometric view (right) side view showing opposing forces on A: the tine support pivot point, and B: the screw jack mounting plate.

8.2 Contact

The crossbar is not rigidly bonded to the crossbar support or to the tine supports. The supports slide over the crossbar and its t-slot key. Load is transferred to the crossbar through the contact between the crossbar and these supports. This contact is modeled as a frictional contact region, with a coefficient of friction of 0.3 when the surfaces are in contact.

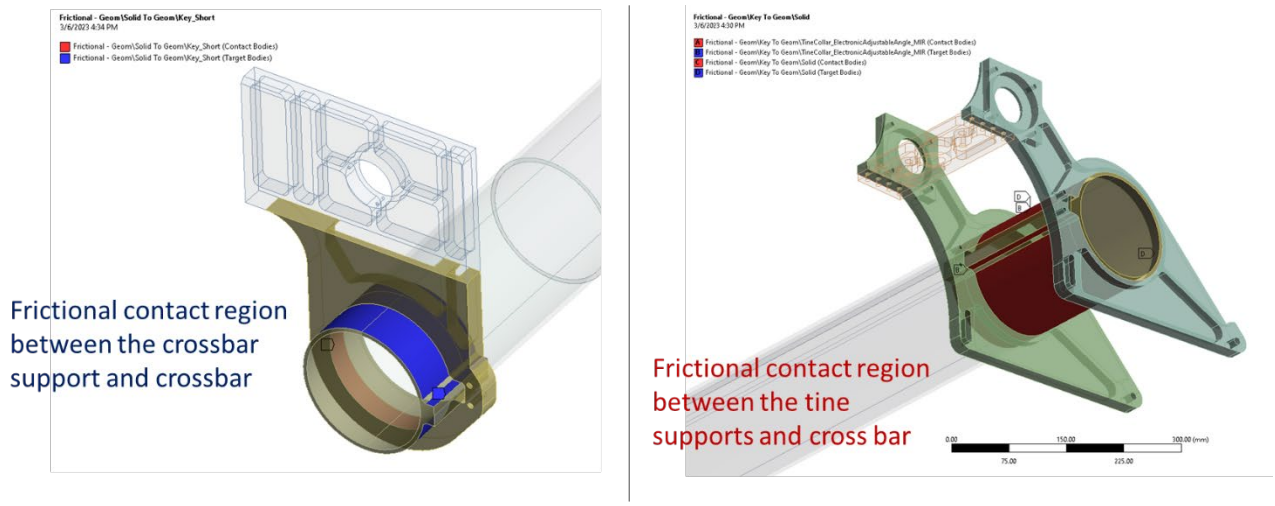

Figure 72: Frictional contact regions between the crossbar and supports.

8.3 Mesh

The model is meshed as full solids consiting of tetrahedral and hexahedral elements. A more refined mesh is used near the contact regions in order to capture the contact between the crossbar and the supports. A total of 295471 elements are used in the model.

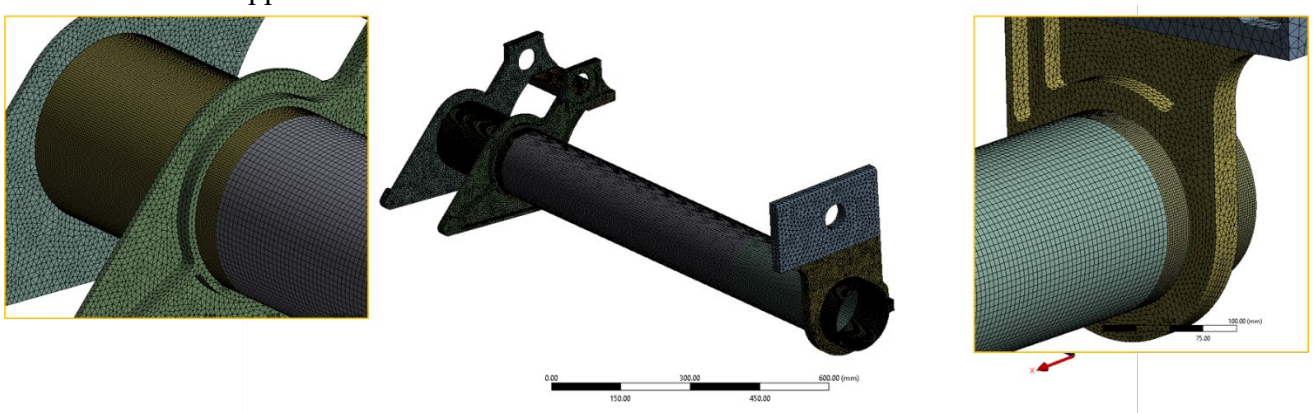

Figure 73: Mesh of the Crossbar and supports model. (left and right) refinement of the crossbar mesh near contact regions.

Use of hex elements throughout the crossbar results in a better distrubution of high quality elements. The coarsest hex elements are sized to capture the 4.76 mm wall thickness. In refined regions the mesh size is decrease so that 3 hex elements span the wall thickness.

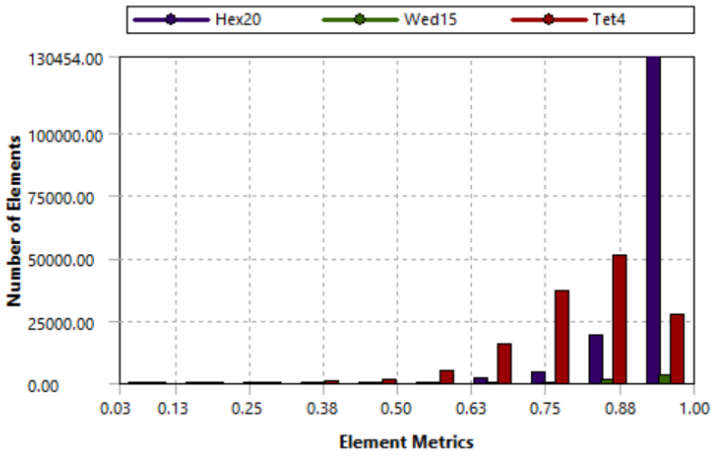

Figure 74: Element quality within the mesh.

8.4 Deformation and Stress

Deformation is a combination of deflection from bending of the crossbar and rotation of the tine supports as the crossbar is put under torsion. Maximum deflection of 6 mm occurs at pivot point of the outside tine support, see Figure 75.

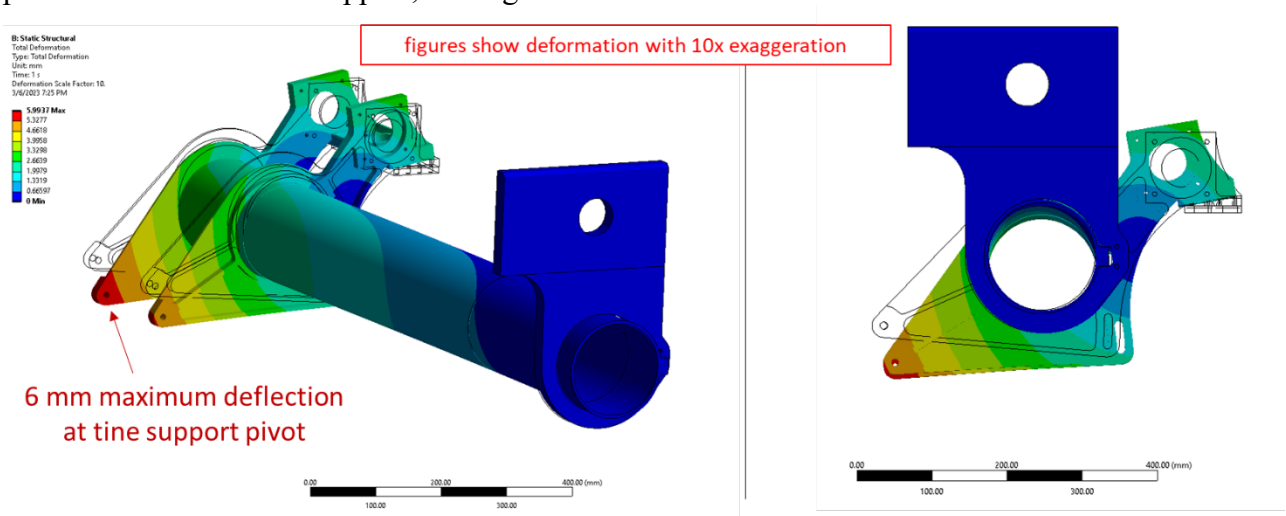

Figure 75: Deflection of crossbar and supports. Undeformed wireframe is shown.

Stress in the supports is well below the 240 MPa yield stress of 6061-T6 Aluminum. The yield stress safety factor is determined by dividing the material yield limit by the equivalent von-mises stress within the elements.

$$SF = \frac{\sigma_Y}{\sigma_{eqv}}$$

Safetry factors withing the tine supports and crossbar supports range from 2.97 to 3.87. as shown in Figure 76.

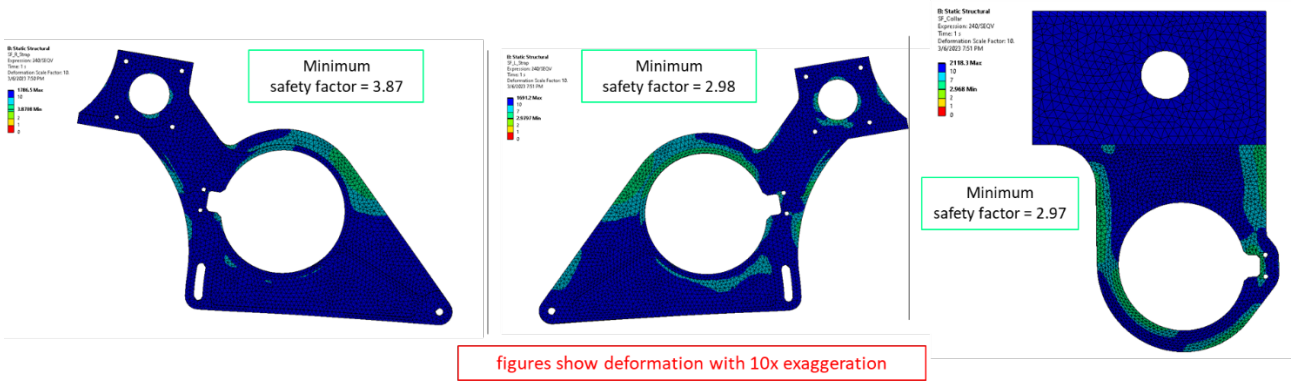

Figure 76: Stress in supports, shown as a yield safety factor. (left) outer tine support, highest stress is in top of strap, at bottom of keyway, and in back webbing. (middle) inner tine support has higher stress than outer tine support. (right) crossbar support has highest stress in keyway and straps that link to the boom.

Stress in the crossbar is concentrated over points of contact with the supports. A minimum yield safety factor of 1.83 occurs at the keyway where the crossbar contacts the crossbar support. The stress is elevated at the surface of the key and in the weld which joings the key to the round tube.

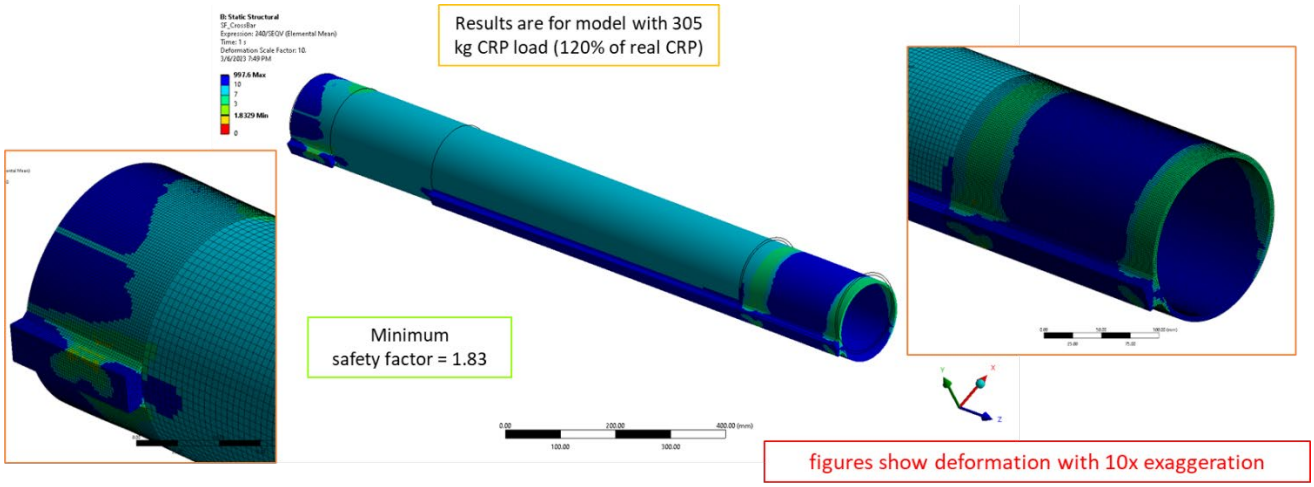

Figure 77: Cress in the cross bar, shown as a yield safety factor. (left) t-slot keyway and welds near the cross-bar support have the highest stress and lowest safety factor. (right) t-slot keyway and welds near the tine supports have highest stress where the tine supports contact the round tube.

Note that this 1.83 safety factor is for a CRP loading of 305 kg. As this is an elastic model, stress scales with load. Thus correcting for the lighter 255 kg CRP, a safety factor of 2.19 is achieved for 100% CRP load. This meets the 2.0 design factor required in ASME BTH-1-2017 para. 3-1.3.1.

9 Cabling and Pulley System

9.1 Cable Stress analysis

A cable system is used to attaching the spreader beam and carraige boom. There are four cables, as seen in Figure 78, with two of them being identical with respect to forces.

D. Cable System

PARTS LIST			
ITEM	*QTY*	*PART NOMENCLATURE*	*LOAD BEARING*
1	*1*	*Cable, Front*	*X*
2	*2*	*Cable, Side*	*X*
3	*1*	*Cable, Back*	*X*

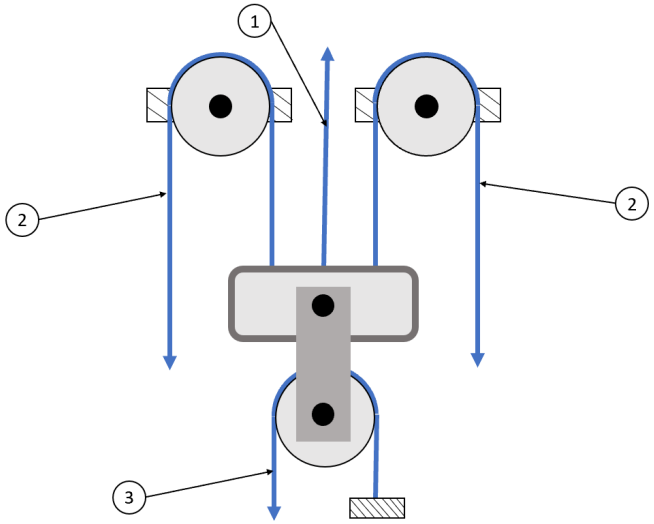

Figure 78: Illustration of the general cable layout.

D.1- Front Cable

The manufacturer rating for the ¼-inch 6x19 galvanized steel wire rope is 1360 lbs, or 6049 N. Under the extreme scenario in which all the weight under the spreader beam is held up only by the front cable a force of 3649 N would be experienced by the front cable. This is less than the manufacturer rating.

D.2-Side Cables

During operation the spreader beam will be perpendicular to the gravity vector. The CRP and tines are also required to be realitivley equidistant from the center axis fo the carriage boom. Due to these requiremnts it can be assumed that the location of center of mass may move forward and backward but will always remain in the center of the carraige boom. To account for every potenical location of center of mass it will be assumed that all the weight below the spreader is equally shared by the back two cables.

The manufacturer rating for the 3/16-inch 6x31 galvanized steel wire rope is 800 lbs, or 3559 N. Under the extreme scenario in which all the weight under the spreader beam is held up only by the back cables a force of 1825 N would be experienced by each side cable. This is less than the manufacturer rating.

D.3-Back cable

The manufacturer rating for the ¼-inch 6x19 galvanized steel wire rope is 1360 lbs, or 6049 N. When lifting the cariage all the cables will have a resultant force acting on the block and tackle. The back cable will experienced half of the force from the block, resulting in a force of 1825 N. This is less than the manufacturer rating.

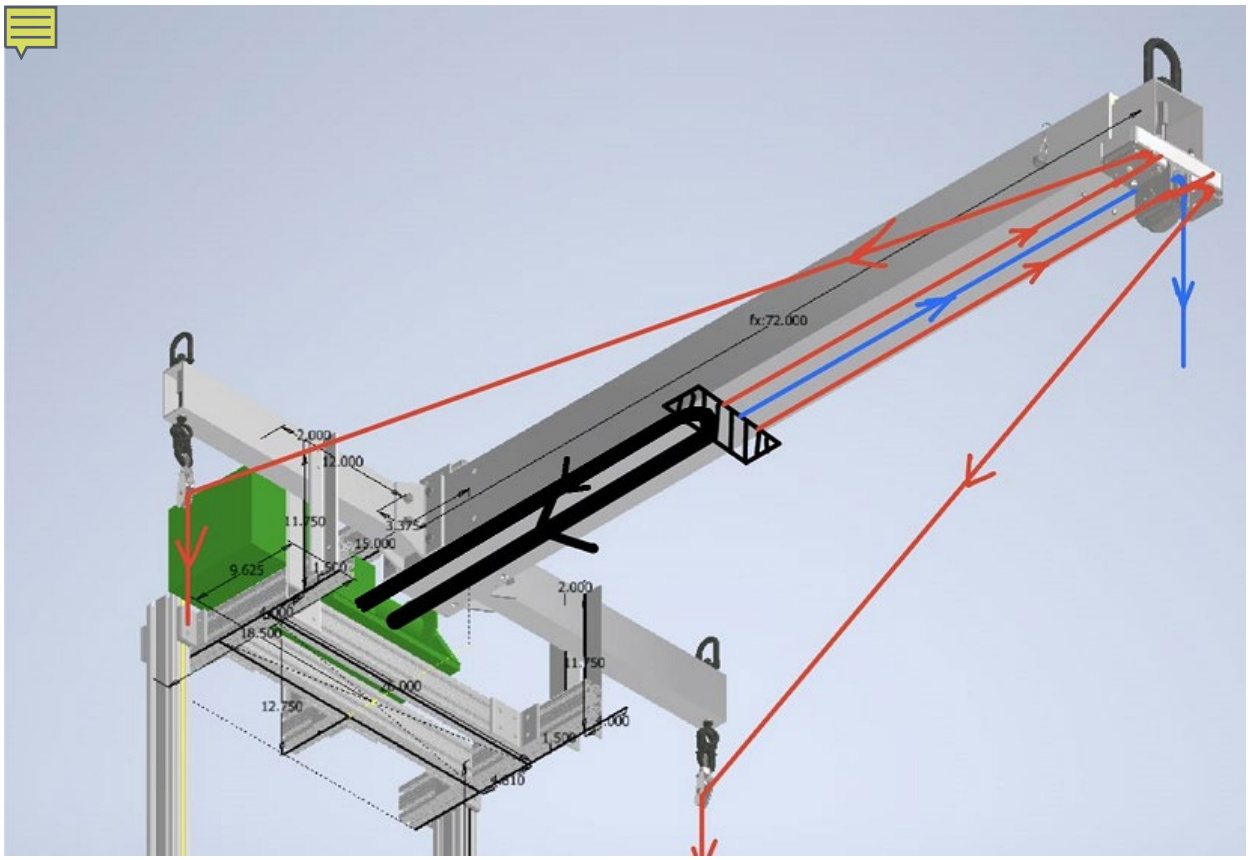

Figure 79: Cartoon showing the layout of the cable runs.

B.9 Front Pulley Assembly

PARTS LIST			
ITEM	*QTY*	*PART NOMENCLATURE*	*LOAD BEARING*
a	*2*	*Pin, Front Side Pulley*	*X*
b	*4*	*Bolts, M10*	*X*
c	*1*	*Pulley, Front Main*	*X*
d	*2*	*Pulley, Front Side*	*X*
e	*1*	*Front Cable crimp*	*X*
f	*1*	*Hook, Front*	*X*
g	*1*	*Eyebolt, Shoulder*	*X*

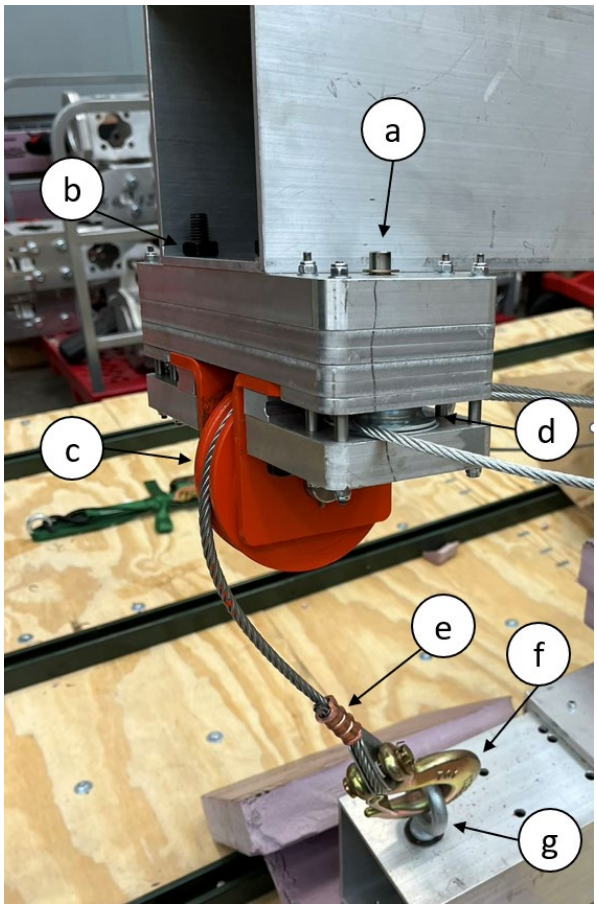

Figure 80: Individual parts breakdown of the front pulley assembly

B.9.a Front Pulley Pin

The front pulley pins are manufacuted from 3/8 inch 1566 carbon steel. The significant stress experienced by this pin will result from the force of the side cables resulting in double shear on the pin. This will result in shear stress on this pin calculated to 20.2 [MPa]. When considering minnimum yield strength of 1566 carbon steel, 517 [MPa] , the saftey factor would be above 2, and would satisfy the requirement of ASME BTH-1-2017 para. 3-1.3.1.

B.9.b-Bolts for front pully assemble

There are 4 grade 8.8 M10 bolts holding the front pully onto the front of the spreader beam. The stress within each bolt would be 13.8 [MPa]. This stress is signifcantly lower then the rated yield strength of a grade 8.8 M10 and would satisfy the requirement of ASME BTH-1-2017 para. 3-1.3.1.

B.9.c – Front Pulley

The front pulley has a manufacuter rating of 3500 lbs, or 15.6 [kN], under the extreame condition of all the weight of the lifting device was held by this front pulley would be 4336 N. This is less than the manufacuter rating.

B.9.d- Front Side Pulleys

The front side pulleys have a manufacuter rating of 1000 lbs, or 4448 N. This pulley redirects the side cables resulting in twice the force present in the cable.Assuming the extreame case

where both lengths of the cable are in the same direction, the front side pulley would expereince a force of be 3649 N. This is less than the manufacuter rating.

B.9.e-1/4 inches Cable crimp

The 1/4 cable crimps are rated for 100% of the rope's capacity per the manufacture. Because the cable has satisfed the requirements the crimps will as well.

B.9.f-Hook, Front

The front hook has a manufacuter rating of 6600 lbs, or 29.4 kN. This hook connects the front cable to the carrige. The forces presented by the front cable will go through to the hook and will expereince a force of 3649 N. This is less than the manufacuter rating.

B.9.g- Shoulder Eyebolt

The front shoulder eyebolt has a manufacuter rating of 2600 lbs, or 11.6 kN. This eyebolt is where the front hook connects the front cable to the carrige. The forces presented by the front cable will be through to the hook to the eyebolt, due to this it will expereince a vertical lifting force of 3649 N. This is less than the manufacuter rating.

B.6 Pulley Link Assembly

PARTS LIST			
ITEM	*QTY*	*PART NOMENCLATURE*	*LOAD BEARING*
a	*1*	*Eyebolt, Shouldered*	*X*
b	*1*	*Link, Pulley*	*X*
c	*1*	*Pulley, Side*	*X*
d	*1*	*Cable Crimp, Front*	*X*
e	*1*	*Hook, Front*	*X*
f	*1*	*Eyebolt, Shoulder*	*X*

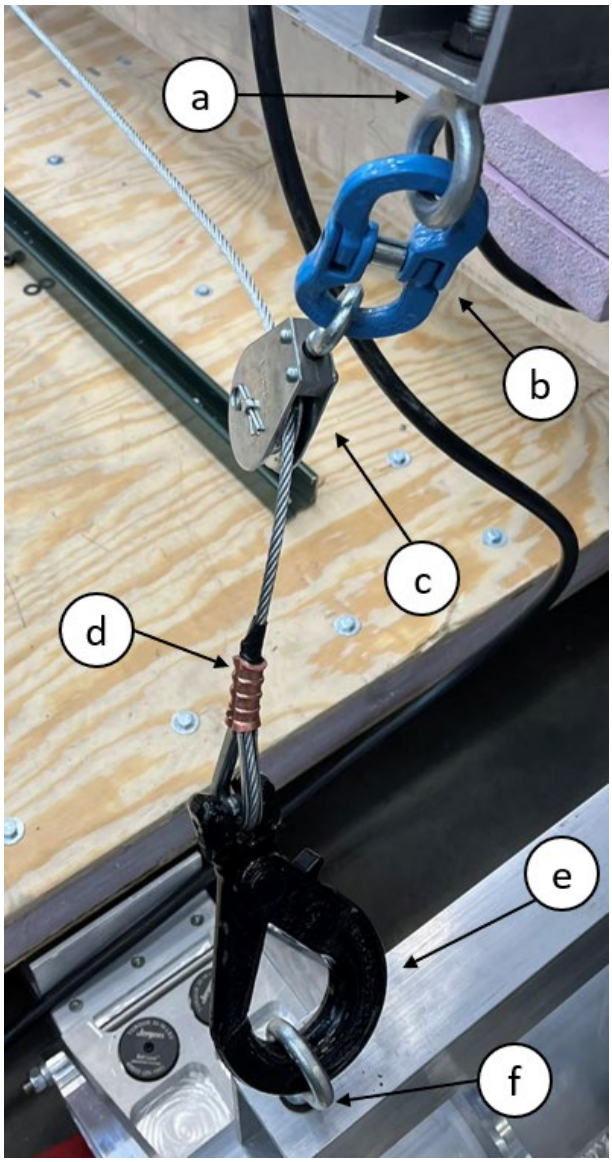

Figure 81: Individual Parts Breakdown for the Side Pulley Assembly

B.6.a- Back Shouldered Eyebolts

The back shoulder eyebolt has a manufacuter rating of 1300 lbs, or 5782 N. This eyebolt is where the pulley linkage connects to the spreader bars. The forces presented by the side cable will go through the linkage to the eyebolt, due to this the eyebolt will expereince a force of 1825 N. This is less than the manufacuter rating.

B.6.b Pulley connecting link

The manufacturer of the pulley connecting links claims the lifting capacity of them to be 5200 lbs, or 23.13 kN. The forces presented by the side cable will go through the pulley to the linkage and the eyebolt will expereince a force of 1825 N. This is less than the manufacuter rating.

B.6.c Side Pulley

The manufacturer of the side pulley connecting links indicates their lifting capacity to be 600 lbs, or 2669 N. The forces presented by the side cable will be expereinced by the pulley, due to this the pulley will expereince a force of 1825 N. This is less than the manufacuter rating.

B.6.d 3/16-inch Cable Crimp

The 3/26 cable crimps are rated for 100% of the rope's capacity per the manufacture. Because the cable has satisfed the requirements the crimps will as well.

B.6.e – Back Hooks

The back hook has a manufacuter rating of 3500 lbs, or 15.6 kN. This hook connects the side cables to the carrige. The forces presented by the side cable will go through to the hook, due to this the hook will expereince a force of 1825 N. This is less than the manufacuter rating.

B.6.f- Back Shouldered Eyebolts

The back shoulder eyebolt has a manufacuter rating of 1300 lbs, or 5782 N. This eyebolt is where the back hook connects the side cable to the carrige. The forces presented by the side cable will go through to the hook to the eyebolt, due to this the eyebolt will expereince a force of 1825 N. This is less than the manufacuter rating.

E. Block and Tackle Assembly

PARTS LIST			
ITEM	*QTY*	*PART NOMENCLATURE*	*LOAD BEARING*
1	*1*	*Pin, Large Pulley*	*X*
2	*1*	*Pulley, Large*	*X*
3	*2*	*Link, Pulley*	*X*
4	*1*	*Pin, Link*	*X*
5	*1*	*Connector, 1/4 inch Cable*	*X*
6	*2*	*Connector, 3/16 inch Cable*	*X*

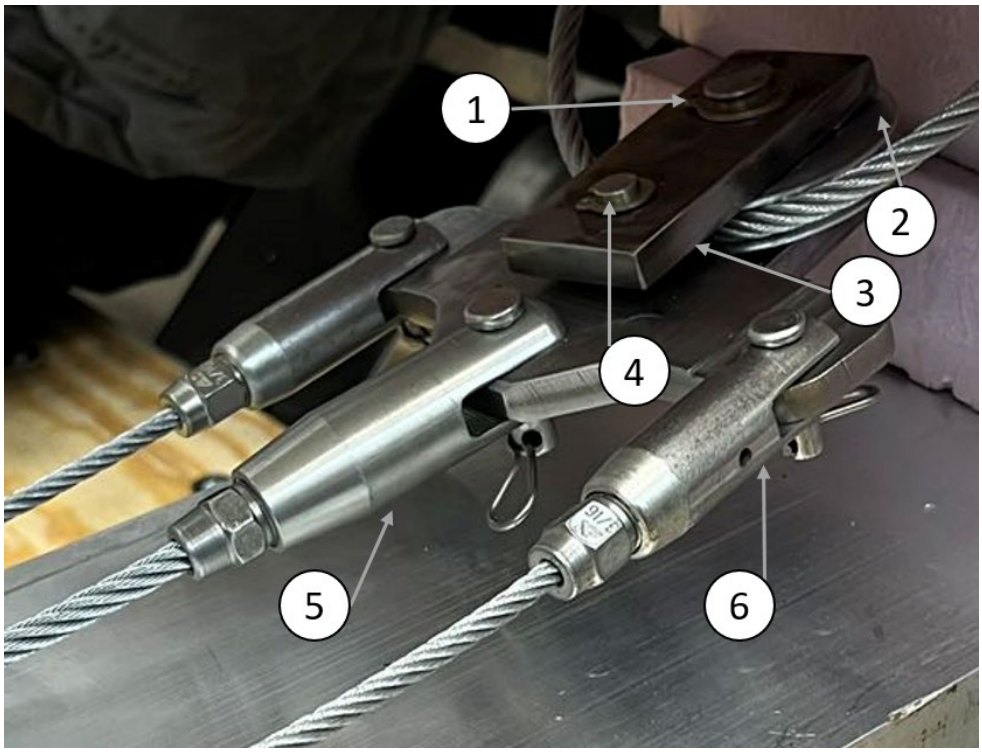

Figure 82: Individual Parts Breakdown for the Block and Tackle.

E.1- Large Pulley Pin

The large pulley pin is manufacuted from 5/8 inch 1566 carbon steel. The significant stress experienced by this pin will result from the force of the linkage acting in double shear. This will result in shear stress on this pin calculated to 43 MPa. When considering minimum yield strength of 1566 carbon steel, the saftey factor would be above 2 and would satisfy the requirement of ASME BTH-1-2017 para. 3-1.3.1.

E.2 Large Pulley

The manufacturer of the large pulley lists its lifting capacity as 1550 lbs, or 6894N. This pulley allows for the back cables to double back to the winch. This pulley will experince the resultant force from cable linkage, which would be 3649 N. This is less than the manufacuter rating.

E.3- Pully Link

The link pin is manufacuted from ½-inch 4140 hardened steel bar stock. When under operation the pully link will experince the entire weight of the system under the spreader bar. This will result in stress on this link calculated to 7.54 MPa. When considering minnimum yield strength of 4140 hardened steel, 415 MPa , the saftey factor would be above 2, and would satisfy the requirement of ASME BTH-1-2017 para. 3-1.3.1.

E.4- Link Pin

The link pin is manufacuted from 3/8 inch 1566 carbon steel. The significant stress experienced by this pin will result from the force of the linkage acting in double shear. This will result in shear stress on this pin calculated to 122 MPa. When considering minnimum yield strength of 1566 carbon steel, 517 MPa, the saftey factor would be above 2, and would satisfy the requirement of ASME BTH-1-2017 para. 3-1.3.1.

E.5 ¼-inch cable connectors

The ¼-inch cable connector have a manufacuter rating of 1300 lbs, or 5782 N. These connectors are where the front cable connects to the block and tackle, and the back cable attaches to the rear mounting point. These connectors will experice the force from the front cables, and rear cable, respectively. The front cable has a force of 3649 N and the rear cable will have a force of 1825 N. Both of these forces are less than the manufacuter rating.

E.6- 3/16-inch Cable Connectors

The ¼-inch cable connector have a manufacuter rating of 1300 lbs, or 5782 N. These connectors are where the front cable connects to the block and tackle. These connectors will experice the force from the side cables, which would be 1825 N. This is less than the manufacuter rating.

Tie Plate

The wire ropes and items E.1-E.6 all attach to a custom tie plate. The tie plate is made of hardened 4140 Chromoly alloy steel, properties given in Table 8. This steel has a high tensile yield strength of 685 MPa.

The tie plate was modeled using an elastic FEA model which meshed the plate with 139,900 tetrahedral elements. The model was loaded with 3825 N of force pulling on each of the link connections, see Figure 83. This puts 390 kg of weight load on each of the pins. The fourth pin, to which the pulley and winch side are connected, was modeled as a fixed support.

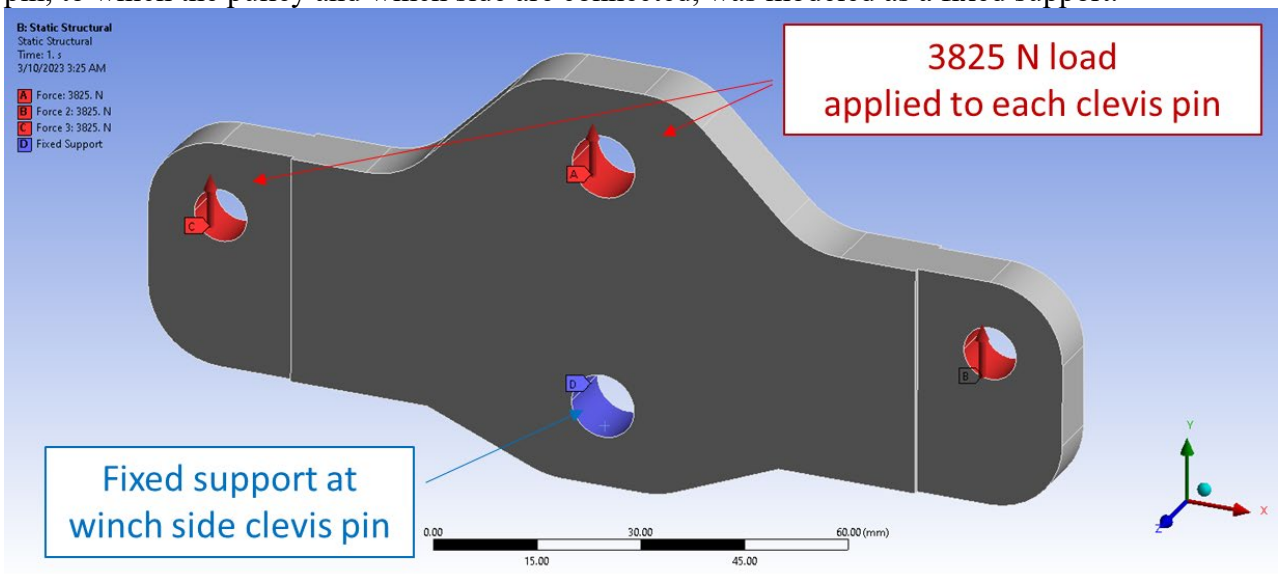

Figure 83: Loading of the tie plate in FEA model (rotated 180º compared to Figure 82)

Equivalent stress within the tie plate is 108 MPa at maximum, see Figure 84. This is far below the tensile yield strength of 685 MPa. This meets the 2.0 design factor required in ASME BTH-1-2017 para. 3-1.3.1.

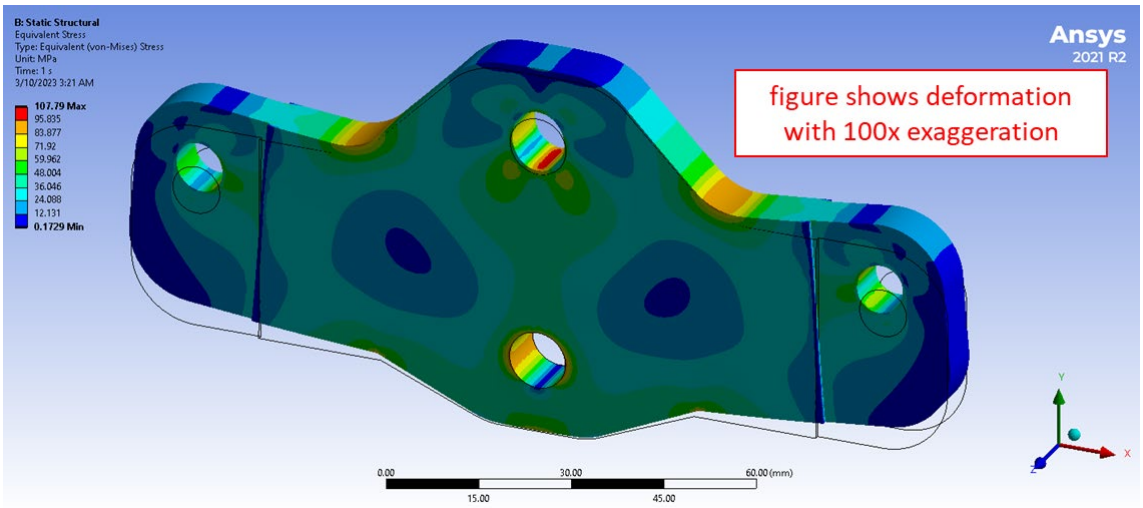

Figure 84: Equivalent stress within tie plate, maximum of 108 MPa at clevis pin hole.

10 Proof Load Tests

10.1 Mock CRP

A mock CRP was created to proof load test and function check the lifting device. The mock CRP is made from plywood and polystyrene insulation. Using these materials a semi-ridgid platform with the same dimensions as the CRP was manufactured. To add rigidity, steel unistrut was bolted to the surface. The resultant mass of the plywood, unistrut, and polystyrene is 135 kg.

10.2 Weights and Proof Load

To suppliment the mass that would be required to simulate a CRP steel weights were added to the mock CRP. Using an electronic scale the mass of each weight was verified. There were two size weights: large, with a mass of 45.7 kg, and small, with a mass of 10.5 kg. The goal for proof loading the device was to lift 150% of the mass of the CRP. The 150% configuration used 5 large and 2 small weights on the ridged platform to achieve a total mass of 384 kg. In Figure 85,Figure 85**Error! Reference source not found.** and Figure 86**Error! Reference source not found.** the lifitng device can be seen successfully lifting 150% of the mass of the CRP.

Figure 85: Proof load with 384.5 kg

Figure 86:Proof load with 384.5 kg

Appendix 4: Lifting Device Operational Procedures

CRP Lifting Procedures

Table of Contents

1 Introduction

The Deep Underground Neutrino Experiment (DUNE) utilizes Charge Readout Planes (CRP) to detect an electron train from a passing neutrino through a liquid argon medium. The CRP is extremely delicate and must be handled with care. The cryostat in which the CRP and liquid argon are to be housed utilizes a unique corrugated steel membrane. This membrane ensures that thermal contraction will not cause buckling or damage to the cryostat. Due to this congregation pattern, each CRP has a different orientation of supports, which requires the lifting device to have adjustability in the tine width. This congregation also limits the usable workspace under the CRP and the thickness of the tines, which requires the tines to be a limited thickness.

In the far detector, the cryostat door is a limited size. This requires the lifting device to be disassemble and limits the size of the crane. The lifting capacity of cranes that can enter the cryostat is relatively small. As such, the lifting device must be as light as possible. For the installation of CRPs 4 and 5 within NP02, a lightweight aluminium gantry crane with a 2000 kg capacity will be used. The crane for the far detector has yet to be chosen, but it will likely be some small form factor counter-weighted boom crane.

The engineering requirements of the lifting device require long thin tine made from relatively light material. This combination of traits results in significant bending when the CRP weight is applied. To ensure the CRP is installed correctly, the tines must have an adjustable incline to counter the bending in the tines.

A false floor will be installed during operations to protect the membrane floor. This false floor allows for a crane to operate on top of it. The installation of the CRP is below the level of the false floor. A tine system lowered into the hole of the false floor cannot retract its tines without removing the false floor. However, the false floor must be in place to move the lifting crane. This requires an installation system where the tine can be detached from the lifting device and crane. Once detached from the tines, the lifting device and crane can be moved once detached from the tines, and the false floor can be removed. After this, the tines can be removed as well.

The following sections will explain how to assemble the tine system.

2 Assembly

The purpose of this section is to illustrate and explain how to assemble the lifting device. The carriage boom, crossbeam, and tines supports are removable for easy transportation.

2.1 Installation of Crossbeam

The crossbeam is centered in the carriage boom using the crossbeam supports and mounting clamps. The cross beam has two tine supports, one on each side, that can be adjusted depending on the placement of the adaptor plates and tine guides. The tine supports utilized guide blocks and cam locking clamps to secure the cross beam. The tine supports also are held in place by cam locking clamps.

NOTE: For easier assembly, loosen the bolts attaching the crossbar guides.	 *Figure 87: Loosen bolts on the crossbeam guide to ease the installation of the crossbeam.*
NOTE: Do not install clamping handles or T nuts. Insertion of the crossbeam is significantly easier.	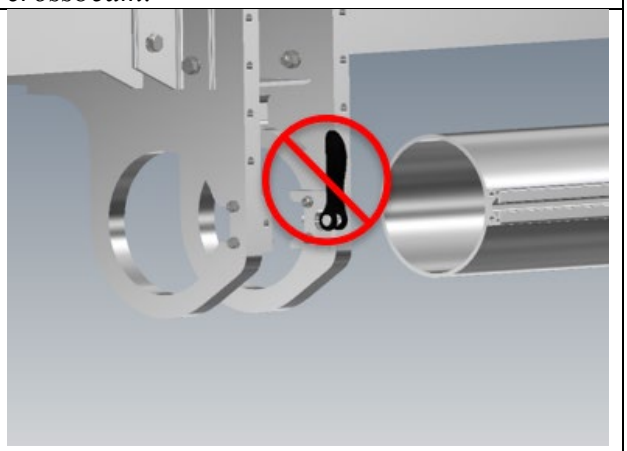 *Figure 88:Remove clamping handles and T-nuts. The crossbeam is challenging to slide with clamping handles and T-nuts inserted.*
2.1.1 Align the crossbeam with the crossbeam supports so the key stock and keyway align. 2.1.2 Insert crossbeam through both crossbeam supports.	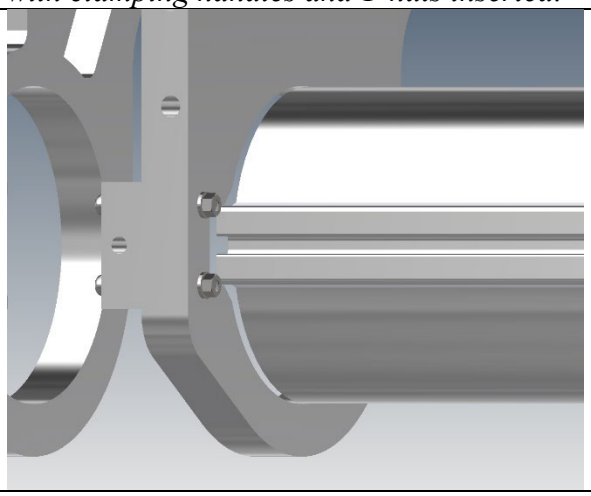

	Figure 89: Properly aligned crossbeam.
2.1.3 Center the crossbeam concerning the crossbeam supports. *NOTE: When measuring to align the crossbeam in the center of the carriage, use the edge of the cross beam as the center key stock is not perfectly centered.*	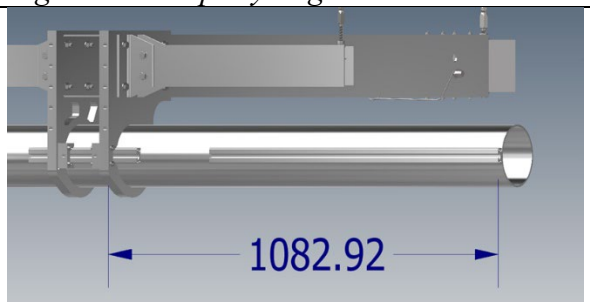 *Figure 90: Proper measurement location for centering of the crossbeam.*
2.1.4 Install and tighten handles. This requires the following hardware: 2 piece 5/16-18 thread weld nut 2 pieces 5/16-18 threaded cam locking handles	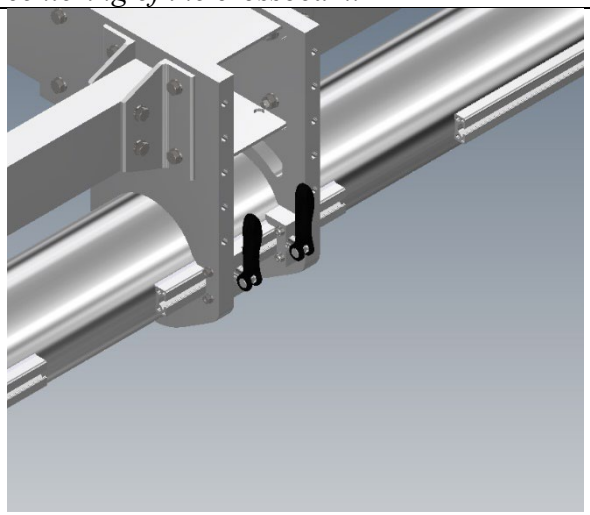 Figure 91: Example of the properly installed crossbeam
2.1.5 Position tine support so the large holes for ball locks are forward and the jacking screw is toward the back of the device. The alignment wheel should be facing outward for easy access.	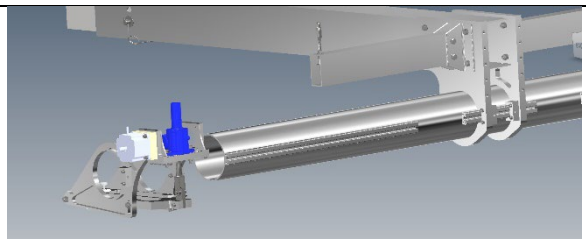 *Figure 92: The tine support in the correct position.*
2.1.6 Ensure that when tine support enters the tine support, the key stock is aligned with the keyway	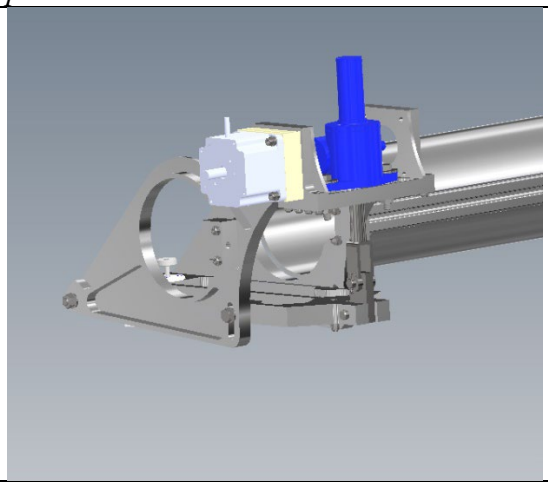

	Figure 93: Tine support aligned with the crossbeam.
2.1.7 Continue tine to slide tine support onto the crossbeam, ensuring that the second guide block properly aligns with the key stock.	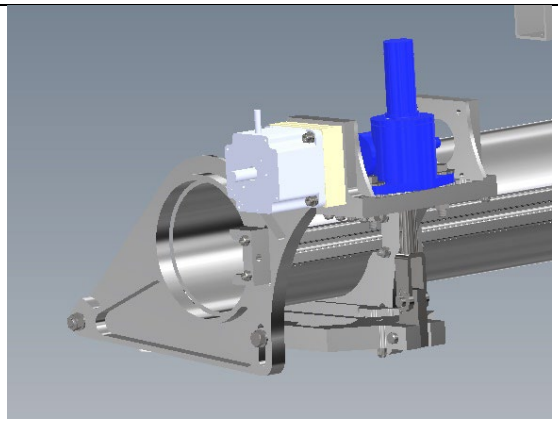 *Figure 94: Tine support with the crossbeam through both ends.*
2.1.8 Slide tine support to correct the position of the crossbeam support. 2.1.9 Insert clamping handles and T-nuts. Once inserted, clamp tine support into position. Each tine support requires the following hardware: 2 piece 5/16-18 thread weld nut 2 pieces 5/16-18 threaded cam locking handles	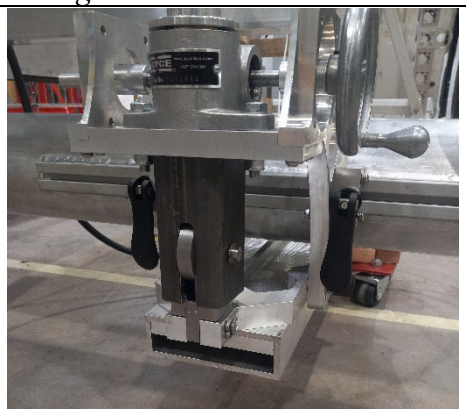 *Figure 95: Fully installed and correctly positioned tine support.*

2.2 Connecting Carriage boom

The spreader beam and carriage boom connect via cabling. The cabling is connected with hooks and eyebolts attached to the carriage boom.

2.2.1 Attach rear hooks to the rear eyebolt	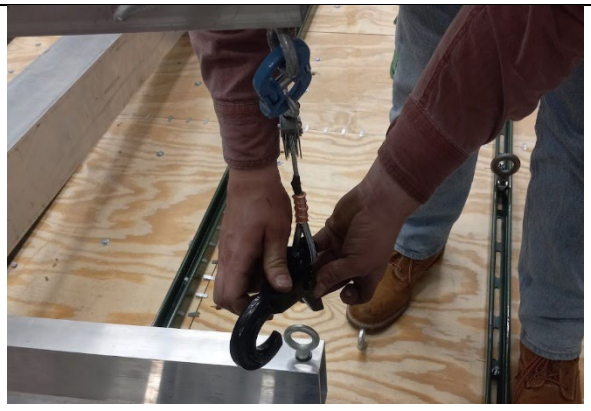 *Figure 96: Illustration of the back hook being attached to the eyebolt on the carriage.*

CAUTION: Ensure that the back lifting hooks are straight when attaching. Improperly attached hooks can potentially fail or damage to the lifting carriage.	 *Figure 97: (Left)Example of improperly installed rear hook.* *(Right) Example of properly installed rear hook.*
2.2.2 Attach the front hook to the front eyebolt on the carriage boom. *CAUTION: When lifting the device, ensure the front cable is positioned correctly in the front pulley. There is potential for the cable to come out of the pulley track if there is a significant force applied to the pulley when out of the track. Binding of the pulley and damage to the cable can occur if the cable is pulled out of its track.*	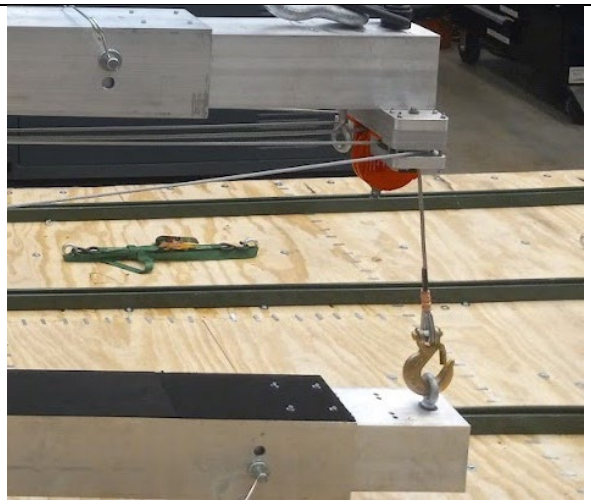 *Figure 98: Example of properly installed front hook.*
2.2.3 Verify that the front cable is correctly placed in the track of the front pulley when putting tension onto the carriage.	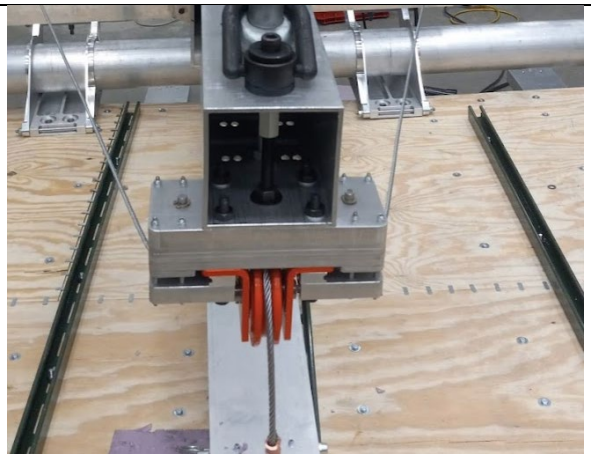 *Figure 99:Example of properly aligned front cable.*

Figure 100: Example of improperly aligned front cable.

3 Disassembly

Purpose: The purpose of this section is to illustrate and explain how to disassemble the lifting device. The carriage boom, crossbeam, and tines supports can be disassembled depending on the requirements of the lift.

3.1 Disassembly of the lifting device

The disassembly section is the reverse of the assembly.

4 Tine Installation

Purpose: The purpose of this section is to illustrate and explain how to install the tines. There are two tine removal scenarios, with tine guides and without. Both methods will be explained in this section.

CAUTION: Installing tines without a tine guide on the cryostat membrane floor could cause damage to the membrane floor. This operation requires the false floor to be installed to ensure the membrane floor's protection.

4.1 Installation of tines without Tine guides

The installation of the tines without the tine guides requires the use of tine carts which can be seen in Figure 101. These can only be used when there is a false floor is installed.

4.2 Installation of tines with Tine guides

Once the tine guides have been installed, the tine guide will be used. The tine guide prevents the tine from falling during the installation when no false floor is present.

CAUTION: Always handle tines with two workers. Due to the size of the tine, there is potential for injury and damage to equipment. 4.1.1 Install tine on tine carts.	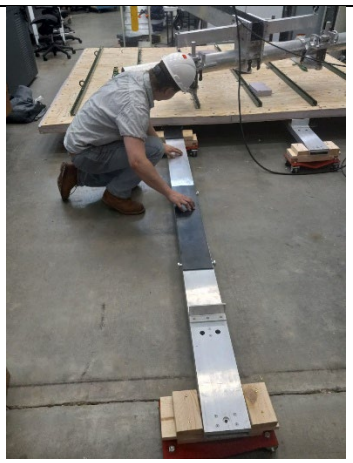 *Figure 101: Tines on roller carts.*
4.1.2 Slide tine under the CRP in a designated location.	 Figure 102: Tine being placed under CRP.
4.1.3 Verify that the tine is placed correctly in the designated location. For CRP4 and CRP5 the tines should be placed so as to contact the inside side of the adapter plates, thereby forming the narrowest spacing width that maintains full tine contact with the adapter plates.	 Figure 103: Verify alignment of tine in relationship to adapter plates.

CAUTION: With at least two workers. The tine has awkward geometry, and there is potential for a single person to hurt themselves or the equipment if attempted a lot. 4.2.1 Using the tine guides, carefully push tines into place.	 *Figure 104: Properly align tine into tine guides.*
NOTE: There is a gap in the tine guides around the start of the far adapter plate. Ensure the gap is crossed correctly when installing tines.	 *Figure 105: Under view of the tine guide properly functioning.*
4.2.2 Push the tine into place until fully seated.	 4.2.3 Figure 106:sample of adequately seated tine

4.3 Removing Tines without tine guides

Removing tines without tine guides is the exact reverse order of installation. The roller carts should be placed under the tines before the tines have been removed. Placement of the roller carts may need the assistance of a push stick when placed at the front of the tine.

CAUTION: Removing the tine guide on the cryostat membrane floor will cause damage to the membrane floor. This operation requires the false floor to be installed.

4.4 Removing Tines with tine guides

Removing tines with tine guides is the exact reverse order of installation.

5 Connecting/Disconnecting Tines

Purpose: The purpose of this section is to illustrate and explain how to connect the tines to the carriage via tine supports.

5.1 Connecting Tines to the carriage

To ensure that the tines can be installed under the CRP without injuring workers or damaging equipment, a connect/disconnect feature has been implemented. The tine supports utilized ball locking pins to create a clamping force great enough to hold the tines in place while a whole load is applied. To assist with placement, there is an alignment pin and guide hole.

5.1.1 After the tines have been installed, lower the carriage onto the tines.	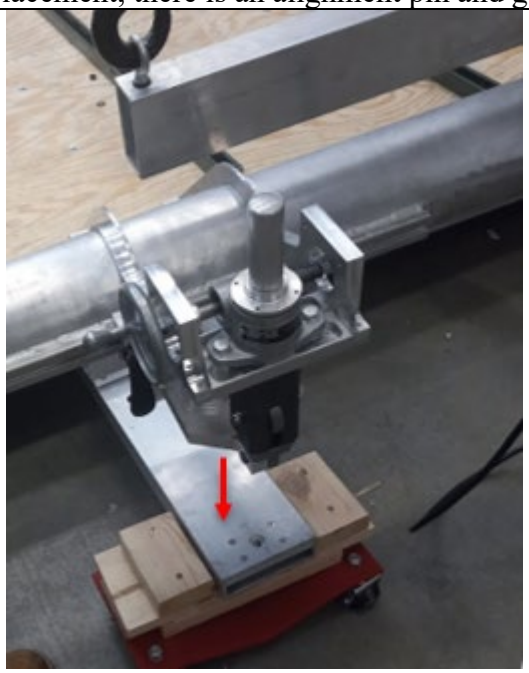 *Figure 107:Tine carriage suspended above the tines:*
5.1.2 When near the tines, use the alignment pin on the rear of the tine support.	 *Figure 108:The tine support alignment pin.*

5.1.3 Verify that there is proper seating of the tine support plate.	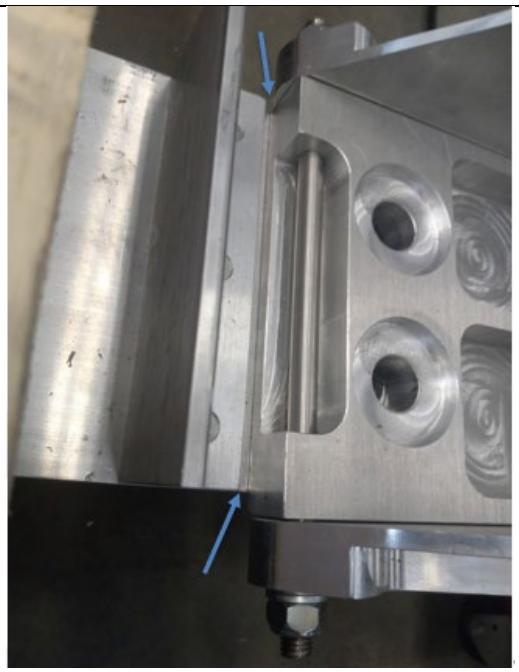 *Figure 109:Properly installed tine in tine support.*
CAUTION: The tines must be appropriately seated before attempting to lift. If not correctly seated, there is potential for damage to be done to the equipment. The ball locks require precise spacing, which will be affected by improper seatings.	 *Figure 110:Example of Improper seating of tine in tine support.*

5.1.4 Install ball locks. Drop ball locks into place through a hole in tine supports. They should require very little force to become seated.	 *Figure 111: Installation of the ball lock.*
WARNING: The ball locks must be properly installed and torqued. If the improper holding force is not achieved, the ball locks will allow the tines to disconnect. Disconnection could severely injure someone and probably will damage equipment. 5.1.5 Torque to ball lock to 35 lb-in. The torquing of the ball locks is critical due to potential failure if not properly torqued.	 *Figure 112: Example of the torquing ball locks.*

6 Raising and Lowering

Purpose: The purpose of this section is to illustrate and explain how to operate the. A winch is used to raise and lower the carriage allowing for controlled placement of the CRP.

CAUTION: The winch installed on the lifting device is designed to be operated with 110V. Do not use any voltage other than 110V.

WARNING: Ensure that you are familiar with the controls of the winch before operation. The wrong direction may cause severe injury or damage to equipment.	 *Figure 113: Controller pendant for winch.*

6.1 Raising the carriage using the winch

A winch and cable system is used to raise the carriage to ensure that the CRP can be appropriately positioned.

6.1.1 Using the winch controller, turn the selector knob counter clockwise to the "IN" position to raise the carriage.	 *Figure 114: Winch control pendent, raising the carriage.*
6.1.2 Hold the selector knob in the "IN" position until the carriage has been raised to the desired height.	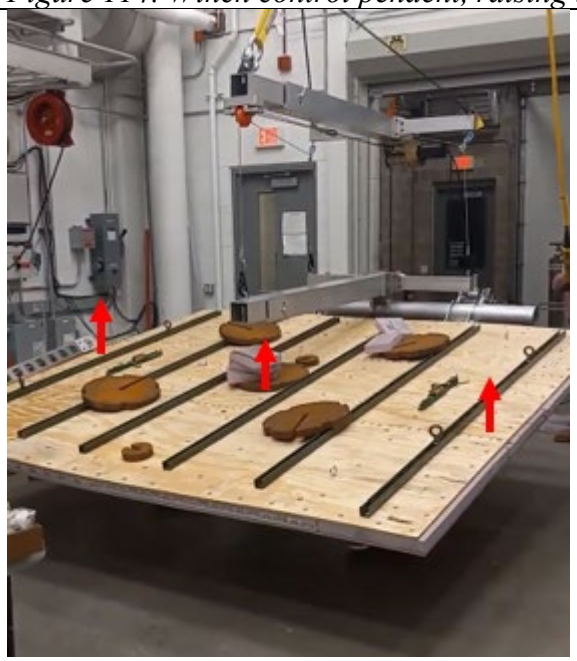 *Figure 115:The winch and cable system lifting CRP.*

6.2 Lowering the carriage using the winch

A winch and cable system are used to lower the carriage to ensure the CRP can be appropriately positioned.

6.2.1 Using the winch controller, turn the selector knob clockwise to the "OUT" position to lower the carriage.	 *Figure 116:Winch control pendent, lowering the carriage.*
6.2.2 Hold the selector knob in the "OUT" position until the carriage has been lowered to the desired height.	 *Figure 117:The winch and cable system lowering the CRP.*

7 Tine Angle Adjustment

Purpose: The purpose of this section is to illustrate and explain how to operate the tine angle adjustment. Using the tine angle adjustment, the bending of the tines can be corrected to ensure level placement of the CRP.

CAUTION: When lowering CRP onto the ground, adjust the tine angle to ensure the tines maintain equal pressure across the guides. If not done correctly, there is a potential for equipment to be damaged.

7.1 Utilize the tine adjustment wheel to raise or lower the angle of the tine.

To ensure that the CRP does not damage the other CRP and the floor, it is crucial to ensure that the CRP is parallel to the ground. As the CRP comes into contact with the floor, slight adjustments to position must be made. To accomplish this, the four feet must be able to be lowered into place at relatively the same time. It is also vital that their angle can be adjusted when relieving pressure from the tines. If the tine angle is not maintained correctly, then the weight of the lifting device could pull out the tine guide, potentially damaging equipment.

7.1.1 Using the hand crank turns, the jacking screw forward, as illustrated by the label, lowers the tine. 7.1.2 Inversely, rotating the wheel backward will raise the tines.	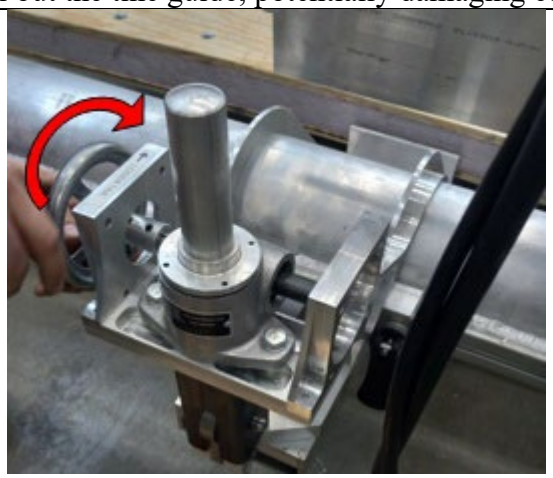 *Figure 118: Tine adjustment system lowering the tines.*
7.1.3 NOTE: Verify that the tine lock is correctly seated on the tine support plate.	 *Figure 119: Properly seated tine lock.*
7.1.4 Utilize bolts on tine support mounts as indicators of travel.	 *Figure 120:Tine mounting plate identification bolt.*

CAUTION: Ensure that if the bolt reaches the bottom of the slot, do not continue extending the jack screw as this may result in damage.	 *Figure 121: Tine mounting plate fully extended.*

7.2 Installing the tine support block

To ensure that the jacking screw does not receive excessive force while the crane system is moving the lifting device, a support block will be utilized, ensuring the proper angle is maintained.

7.2.1 Raise tines until the safety block securely fits into the cable between the tine lock and jacking screw support plate. 7.2.2 Once the block is installed, lower the tines until the stress is off the jacking screw.	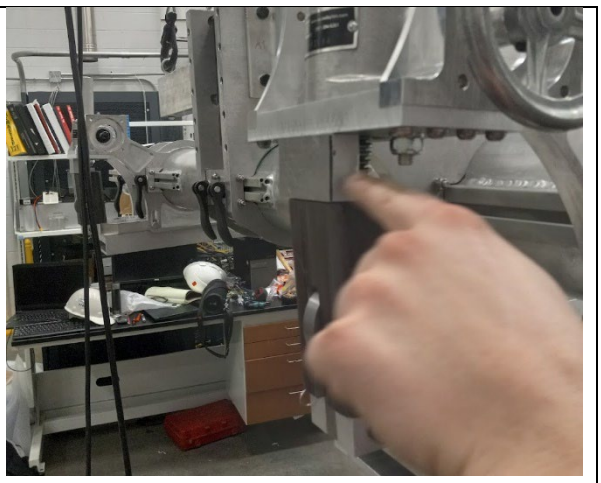 *Figure 122: Safety block in place.*